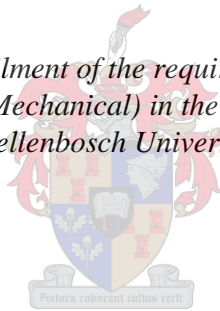


Computational Modelling Techniques to Determine Patellofemoral Joint Reaction Forces

by

Bruce de Jongh

*Thesis presented in fulfilment of the requirements for the degree of
Master of Engineering (Mechanical) in the Faculty of Engineering at
Stellenbosch University*



Supervisor: Dr. J.H. Müller

March 2016

Declaration

By submitting this thesis electronically, I declare that the entirety of the work contained therein is my own, original work, that I am the sole author thereof (save to the extent explicitly otherwise stated), that reproduction and publication thereof by Stellenbosch University will not infringe any third party rights and that I have not previously in its entirety or in part submitted it for obtaining any qualification.

March 2016

Copyright © 2016 Stellenbosch University

All rights reserved

Abstract

A computational modelling pipeline is introduced to determine knee muscle forces, knee kinematics, patellofemoral contact force and patella kinematics during stance phase of over ground level walking. By applying a computational method the underlying causative factors of anterior knee pain can be investigated and can be used to assist physicians in developing a treatment plan. Eleven subjects with anterior knee pain were tested pre- and post-physiotherapeutic intervention at the Central Analytical Facility Motion Analysis Clinic to record the kinematic and kinetic data of the body.

One force plate is available to measure ground reaction force (GRF) data; therefore the GRF on the foot not striking the force plate is estimated using two methods, which are compared. Within the method used in this project, an average GRF and centre of pressure (COP) is computed throughout stance phase using force plate data and is then superimposed onto the foot not striking the force plate. The knee muscle forces and joint kinematics are then computed in OpenSim, whereby a generic musculoskeletal model is scaled according to the subject's anthropometric data, where after the subjects kinematic and kinetic data, recorded in the motion laboratory, is applied to the model.

The muscle forces compare well to literature in terms of magnitude and their linear relationship, however, the division of the forces between the muscles of the quadriceps femoris does not agree with literature. This is as a result of the inaccurate hip adduction and rotation angles and the simplified knee joint. Furthermore, errors arise in the modelling pipeline as a result of the superimposition method. The difference in magnitude of the GRF measured on the different feet and between sessions, results in knee moments and muscle forces that differ in magnitude.

The computed muscle forces and knee kinematics are applied to a patient specific musculoskeletal model generated by segmenting an MRI scan of the affected knee. The patella kinematics and patellofemoral contact force were investigated during stance phase. The patella was situated more laterally when the knee was relaxed and when the knee begins to flex it moves medially until trochlear engagement, where after its lateral displacement remains constant. The initial medial displacement is caused by the medial patellofemoral ligament (MPFL) that applies considerable tension to the patella during trochlear engagement.

The patellofemoral contact force agrees with values published in literature and computes repeatable results within sessions. The small difference between sessions and the contact force in literature is due to the rectus femoris force applied to the patella. Knee and hip adduction and rotation effect the patella kinematics and therefore have an effect on the mediolateral contact force.

Due to limitations such as having one force plate and renovations being done on the Motion Analysis Clinic during this project, accurate results were not compared pre- and post-intervention. However, the modelling pipeline is validated as it produced repeatable results in the majority of the steps of the pipeline. If results were not repeatable, the cause could be attributed to the assumptions made in this project.

Uittreksel

Die gebruik van 'n numeriese modellerings tegniek word beskryf waarvolgens knie spier kragte, knie kinematika, patella-femorale kontak krag en knieskyf kinematika tydens die standsfase in normale loop beraam kan word. Toepassing van die tegniek bemoontlik die ondersoek na onderliggende faktore wat kan lei tot anterior kniepyn met die doel om dokters by te staan in die ontwikkeling van nuwe behandelingsplanne. Elf deelnemers met anterior kniepyn was getoets voor en na fisioterapeutiese behandeling by die Sentrum vir Analitiese Fasiliteite se bewegingsopname kliniek om kinematika en kinetika opnames van die lyf te neem.

Die grond reaksiekrag data van die voet wat nie die lassel tref nie is benader m.b.v. twee metodes wat teen mekaar opgeweeg word. Die metode wat in die modelleringspyplyn gebruik was behels die beraming van die gemiddelde grond reaksiekrag en drukmiddelpunt soos bereken vanaf die lassel data van die teenoorstaande voet stand fase. Die beraamde parameters word dan op die voet wat nie die lassel tref nie aangewend. Deur om die eksperimentele data vanaf die bewegingskliniek te gebruik, is 'n generiese OpenSim model geskaleer volgens die deelnemers se antropometries mates en is gebruik om die knie spierkragte en gewrig kinematika te bereken.

Die berekende spierkragte vergelyk goed met literatuur i.t.v. omvang sowel as tendens. Die onderverdeling van die kragte tussen die spiere stem egter nie ooreen met literatuur nie. Die krag verdeling tussen die kwadrisep spier is verkeerd en dit kan toegeskryf word aan die onakkurate heup adduksie en rotasie hoeke asook die vereenvoudigde een graad van vryheid knie. Foute sluip ook in a.g.v. die superponerings metode. Die verskil in omvang van die gemete en grond reaksiekrag tussen voete en sessies lei tot knie momente en spierkragte wat verskil in omvang.

Die berekende spierkragte en knie kinematika is ingespan in 'n pasiënt spesifieke spier-skelet model soos beraam vanaf gesegmenteerde MRI beelde van die geaffekteerde knie. Die knieskyf kinematika en patella-femorale kontak krag is ondersoek vir die standfase. Die knieskyf was in 'n laterale posisie by volle ekstensie waarna dit mediaal begin skuif aan die begin van fleksie tot en met trochlea interaksie. Die laterale verplasing bly daarna konstant. Die inisiële mediale verplasing kan toegeskryf word aan die mediale patellofemorale ligament wat noemenswaardige tensie op die knieskyf uitoefen voor trochlea interaksie.

Die patello-femorale kontak krag is soorgelyk aan waardes soos vervat in die literatuur en berekende waardes is herhaalbaar tussen sessies. Die klein verskille tussen sessies en die kontak krag in die literatuur is a.g.v. die krag wat deur die rectus femoris spier aangewend word. Knie en heup adduksie en rotasie beïnvloed knieskyf kinematika en daarom het dit ook 'n effek op die mediaal-laterale kragte.

A.g.v. beperkings, soos bv. een lassel en die feit dat verbeteringe aan die bewegingskliniek aangebring is tydens die uitvoering van die projek, kon akkurate vergelykings tussen die voor en nabehandeling nie geskied nie. Die herhaalbaarheid van die metode kon egter bewys en bevestig word vir meeste stappe in die modelleringspyplyn en waar daar verskille was, kon dit toegeskryf word aan die aannames wat gemaak is.

Acknowledgements

I would like to acknowledge and express my sincere thanks to the following people who have contributed to this project and kept me motivated throughout:

- My supervisor, Dr. Cobus Müller. Thank you for your invaluable insight and advice throughout the project and giving me the opportunity to do my Masters using such great facilities. Thank you for always making time for me and giving me a nudge or constructive criticism when it was necessary.
- To Dr. Quinette Louw, Dr. John Cockcroft and Dominique Leibbrandt at the Central Analytical Facility Motion Clinic. Thank you for allowing me to use your facilities and sharing your knowledge on the human body and human kinematics. To John, specifically, thank you for always being available to give me advice or discuss problems with my project. I appreciate all of your help and how accommodating you were to me.
- To my fellow BERG students. Thank you for creating such a happy and motivating work environment, and given me advice or different opinions when necessary. Thank you Debbie Lloyd for joining me in the office at night to work on our theses and motivate each other.
- Thank you to my family and friends for supporting me throughout these last two years and always giving that extra motivation when it was necessary. Specifically, thank you to my Mom, Dad and Brother for always being there for me and always pushing me on.
- To Amy Bradley and her wonderful family, thank you for the abundance of support and motivation throughout this thesis. It is greatly appreciated. Thank you Amy for being there with me every step of the way and ensuring it was a pleasant two years.

Contents

Declaration	i
Abstract	ii
Uittreksel	iv
Acknowledgements	vi
List of Figures	x
List of Tables	xii
Nomenclature	xiii
Variables.....	xiii
Abbreviations.....	xvi
1. Introduction	1
1.1 Background	1
1.2 Motivation.....	2
1.3 Aim.....	3
1.4 Thesis outline	3
2. Literature review	5
2.1 The lower limb	5
2.1.1 Anatomical definitions	5
2.1.2 The hip joint	5
2.1.3 The knee joint	6
2.1.4 The ankle joint.....	8
2.1.5 Human gait	9
2.2 Computational modelling of the musculoskeletal system.....	10
2.2.1 OpenSim	11
2.2.2 Contact modelling.....	19
3. Experimental procedure	21
3.1 Ethical consent	21
3.2 Subjects	21
3.3 Apparatus	22
3.3.1 Motion capturing	22

3.3.2	Ground reaction force measurements	24
3.3.3	Electromyography measurements	24
3.3.4	Portable lab	25
3.3.5	Magnetic resonance imaging	25
3.4	Data processing	25
3.5	Statistical methods	25
4.	Inclusion of the foot not striking the force plate	27
4.1	Introduction	27
4.2	Methods	27
4.2.1	FScan inclusion	27
4.2.2	Force plate superimposition	33
4.3	Results	34
4.3.1	Locating the centre of pressure results	35
4.3.2	Estimation of complete ground reaction force results	36
4.3.3	Resulting knee moment comparison	38
4.4	Discussion	38
4.4.1	Locating the centre of pressure	38
4.4.2	Estimation of complete ground reaction forces	39
4.4.3	Resulting knee moment comparison	40
5.	OpenSim analyses	42
5.1	Introduction	42
5.2	Methods	42
5.2.1	Step 1 – Scaling	44
5.2.2	Step 2 – Inverse kinematic analysis	44
5.2.3	Step 3 – Inverse Dynamic analysis	45
5.2.4	Step 4 – Residual Reduction Algorithm analysis	45
5.2.5	Step 5 – Computed Muscle Control analysis	46
5.3	Results	47
5.3.1	Scaling results	47
5.3.2	Comparison between torso and non-torso trials	47
5.3.3	Repeatability study	48
5.4	Discussion	59
5.4.1	Comparison between torso and non-torso trials	59
5.4.2	Comparison between filtered and unfiltered trials	59
5.4.3	Repeatability study	60
6.	Subject specific musculoskeletal patellofemoral joint model	67
6.1	Introduction	67
6.2	Methods	67
6.2.1	Segmentation procedure	68
6.2.2	Define bone axes	68
6.2.3	Computational technique	70

6.3	Results	74
6.3.1	Patellofemoral contact force	74
6.3.2	Lateral patella displacement	78
6.3.3	Patella tilt angle	79
6.4	Discussion	81
6.4.1	Patellofemoral contact force	81
6.4.2	Lateral patella displacement	84
6.4.3	Patella tilt angle	84
7.	Conclusion	86
7.1	Aims	86
7.2	Limitations	92
7.3	Future work	93
7.4	Contribution to the field	93
	References	94
	Appendix A: FScan and superimposition method results	102
	Appendix B: OpenSim results	118
	Appendix C: Adams results	134

List of Figures

Figure 1: Anatomical reference planes and rotations	5
Figure 2: The hip joint (adapted from www.dr.samsani.com) [80]	5
Figure 3: The knee joint (adapted from Christy Krames [97])	6
Figure 4: The ankle joint (Adapted from www.turbosquid.com [25])	8
Figure 5: Human gait cycle (Adapted from Dynamics of Human Gait [27])	9
Figure 6: Knee joint angle (a) and internal joint moment (b) during level ground walking [26]	10
Figure 7: Simplified OpenSim pipeline	11
Figure 9: Muscle-tendon actuator model [40]	12
Figure 8: Simplified joint model [43] and accompanying equations	12
Figure 10: Schematic of CMC algorithm [39]	17
Figure 11: Flow of data in the project	21
Figure 12: Anterior and posterior marker positions on a subject [51]	22
Figure 13: Capture volume and force plate layout in the motion laboratory	23
Figure 14: Vertical ground reaction force local maxima and minima	28
Figure 15: FScan co-ordinate axes (X'Y') relative to the capture volume co-ordinate axes (XY)	28
Figure 16: FScan force in the (a) mediolateral and (b) anteroposterior directions	31
Figure 17: Subject 1 trial 1 and Subject 2 trial 1 COP position comparisons for perimposed and FScan methods	35
Figure 18: Subject 1 trial 1 comparison of GRF estimation for superimposed and FScan methods	37
Figure 19: Knee moment comparisons for superimposed and FScan methods with statistical comparison	38
Figure 20: OpenSim modelling pipeline	42
Figure 21: Detailed OpenSim pipeline flow diagram	43
Figure 22: Marker placement on the subject and scaled model	44
Figure 23: Comparison of filtered and raw ground reaction forces	49
Figure 24: Resulting knee moment using unfiltered and filtered GRF data	49
Figure 25: Subject 1 knee angle comparison during stance phase	51
Figure 26: Subject 1 left hip angles comparison during stance phase	51
Figure 27: Subject 5 intra-session knee moment comparison	53
Figure 28: Normalised session 1 right leg extensor muscle forces	56
Figure 29: Right leg extensor muscle force comparison between sessions	58
Figure 30: Computational modelling pipeline flowchart	67
Figure 31: Segmentation procedure	68
Figure 32: Femur local axes definition	69
Figure 33: Tibia local axes definition	69
Figure 34: Define the tibia knee centre	70
Figure 35: Insertion points of the extensor muscles on the patella	72
Figure 36: MPFL insertion points	73

Figure 37: Lines used for the bisect offset and patella tilt measurement	73
Figure 38: Intra-session comparison of computed contact force	74
Figure 39: Inter-session contact force comparison	76
Figure 40: Mediolateral patellofemoral contact force	76
Figure 41: Patellofemoral contact force and quadriceps force ratios in flexion....	77
Figure 42: Medial patellofemoral ligament (MPFL) tension during flexion.....	78
Figure 43: Bisect offset measured in each trial.....	78
Figure 44: Inter-session bisect offset comparison	79
Figure 45: Intra-session patella tilt angle comparison	80
Figure 46: Inter-session comparison of patella tilt angle.....	81

List of Tables

Table 1: Muscles responsible for hip joint movement [17]	6
Table 2: Muscles responsible for knee joint movement [17].....	7
Table 3: Knee joint muscle parameters [40]	13
Table 4: Estimated COP position comparison between the FScan and superimposition methods	35
Table 5: FScan and superimposition complete GRF estimation comparison.....	36
Table 6: Scaling marker errors for six random subjects	47
Table 7: Comparison between the measured joint angles and knee moment for a model with and without a torso	48
Table 8: RRA results using unfiltered and filtered GRF data.....	50
Table 9: Knee angle comparison between OpenSim and Plug-In Gait models...	50
Table 10: Hip angles comparison for OpenSim and PiG models	51
Table 11: Hip angle RMS errors and maximum errors percentages.....	52
Table 12: Intra-session knee moment comparison	53
Table 13: Mean RRA results for each foot in each session	54
Table 14: Session 1 left and right foot maximum knee moment and GRF data....	54
Table 15: Mean CMC results for each foot in each session	55
Table 16: Intra-session comparison of muscle forces.....	56
Table 17: Inter-session muscle force comparison.....	57
Table 18: Maximum residual forces and moments and extensor muscle forces ...	58
Table 19: Physical measurements of subject	67
Table 20: Stiffness properties of the model ligaments and tendons	72
Table 21: Mechanical properties of patella and femur cartilage	73
Table 22: Intra-session contact force comparison	75
Table 23: Intra- and inter-session comparison of knee flexion angles	75
Table 24: Average contact force to muscle force ratios	77
Table 25: Intra-session bisect offset comparison.....	79
Table 26: Intra-session comparison between patella tilt angles	80

Nomenclature

Variables

B_c	Damping coefficient
$C(q, \dot{q})$	Coriolis and centrifugal force vector
C_j	Equality constraint
COP_{FSG}	FScan COP in global axis system
COP_{FSL}	FScan COP in local axis system
COP_{SI}	Superimposed COP
F_c	Contact force
F_{FP}	Force measured by force plate
F_{FS}	Force measured by FScan
F_{FSG}	GRF computed from FScan in the global frame
F_{FSL}	FScan force in the local frame
F_{grf}	Ground reaction forces
F^l	Ligament force
F^M	Muscle force
F_O^M	Maximum isometric muscle force
F^{MT}	Muscle-tendon force
FP_x	Force plate COP x-value
FP_y	Force plate COP y-value
F_{res}	Residual forces
F_{SI}	Superimposed force
F_{st}	Ligament/tendon force
FS_x	FScan COP x-value
FS_y	FScan COP y-value
$G(q)$	Gravitational force vector
H_m	Heel marker position
H_{m_other}	Heel marker of foot not striking the force plate
J	Static optimization performance criterion
L	Ligament/tendon length
L_0	Zero-load length

L_O^M	Optimal muscle fiber length
L_O^T	Tendon slack length
MA	Moment arm of a muscle
$M(q)$	System mass matrix
M_y	Rotational moment on force plate
O_{FSG}	FScan origin in the global axis system
P	Co-ordinates to define muscle paths
R	Correlation coefficient
R^2	Coefficient of determination
R_m	Rotation matrix
RT	Total rotation matrix
RT_{actual}	Actual total rotation matrix
$RT_{computed}$	Computed total rotation matrix
T_m	Toe marker position
T_{m_other}	Toe marker of foot not striking the force plate
T_{ZFP}	Free moment
T_{ZSI}	Superimposed free moment
\vec{V}	Varying muscle segment
a_x	Distance between COP and force plate centre in x-direction
a_y	Distance between COP and force plate centre in y-direction
exp_c	Force exponent
d_{AP}	Difference between anteroposterior marker foot angles and actual foot angle
d_H	Force plate COP and heel marker relationship
$d_{H_{SI}}$	Superimposed heel marker relationship
d_{ML}	Difference between mediolateral marker foot angles and actual foot angle
d_{OG}	Difference between the toe marker and FScan origin in the global frame
d_{OL}	Difference between the toe marker and FScan origin in the local frame
d_T	Force plate COP and toe marker relationship

dT_{SI}	Superimposed toe marker relationship
k	Stiffness
k_c	Contact stiffness
k_p	Position feedback error gain
k_v	Velocity feedback error gain
l^M	Muscle length
l^{MT}	Muscle-tendon length
l^T	Tendon length
q	Generalised position
\dot{q}	Generalised velocity
\ddot{q}	Generalised acceleration
q_j	Virtual co-ordinate value
q_j^{exp}	Experimental co-ordinate value
w_i	Marker weight
x_i^{exp}	Experimental marker position
$x_i(q)$	Virtual marker position
δ	Interpenetration depth
ε	Strain
ε_l	Non-linear strain level parameter
θ	Local axes angle
θ_{AP}	Anteroposterior marker foot angle
$\theta_{AP,a}$	Actual anteroposterior foot angle
$\theta_{AP,c}$	Computed anteroposterior foot angle
θ_F	Foot angle in the XY plane
θ_{ML}	Mediolateral marker foot angle
$\theta_{ML,a}$	Actual mediolateral foot angle
$\theta_{ML,c}$	Computed mediolateral foot angle
σ	Standard deviation
τ	Generalised forces
ϕ_i	Actuator controls
ϕ_O^M	Pennation angle at optimal length
ω_j	Co-ordinate weight

Abbreviations

AC	Ankle Centre
AP	Anteroposterior
CAF	Central Analytical Facility
CMC	Computed Muscle Control
COD	Coefficient of Determination
COM	Centre of Mass
COP	Centre of Pressure
CF	Contact Force
CT	Computerised Tomography
EMG	Electromyography
FE	Flexion-Extension
FKC	Femur Knee Centre
FLCC	Femur Lateral Condylar Centre
FMCC	Femur Medial Condylar Centre
GRF	Ground Reaction Force
HJC	Hip Joint Centre
ID	Inverse Dynamics
IK	Inverse Kinematics
LPFL	Lateral Patellofemoral Ligament
ML	Mediolateral
MPFL	Medial Patellofemoral Ligament
MPML	Medial Patellomeniscal Ligament
MTP	Metatarsophalangeal
PD	Proportional-derivative control
PiG	Plug-In Gait
PT	Patella Tendon
QF	Quadriceps Force
RF	Rectus Femoris
RMS	Root Mean Square
RRA	Residual Reduction Algorithm
TKC	Tibia Knee Centre

TLCC	Tibia Lateral Condylar Centre
TMCC	Tibia Medial Condylar Centre
VI	Vastus Intermedius
VL	Vastus Lateralis
VM	Vastus Medialis
WLS	Weighted Least Squares

Chapter 1

Introduction

1.1 Background

Anterior knee pain, or patellofemoral pain, is one of the most frequently seen lower extremity conditions in orthopaedic practice [1]. In the Western Cape 70 % of clients visiting health care centres are affected by musculoskeletal problems, of which a majority are experiencing knee pain [2]. This alarming occurrence of knee problems is associated with moderate to high levels of disability [2], which will affect one's ability to perform daily activities such as stair ambulation, walking and running.

Anterior knee pain typically affects adolescents and young adults [3]. Most individuals (74 %) who suffer from anterior knee pain decrease their level of physical activity for up to five years after the onset of the condition [4]. Therefore, it can potentially have serious implications on the development of chronic lifestyle diseases. Appropriate management of anterior knee pain is crucial to facilitate physically active lifestyles among South Africans.

Physiotherapy is the mainstay management of anterior knee pain as surgical and pharmacological management appear to be inadequate [5]. Due to limited health resources in South Africa and an expected increased burden of chronic musculoskeletal conditions, cost effective evidence based approaches are crucial. To develop these approaches practitioners require up to date clinical evidence as well as laboratory based evidence to understand the effect of the intervention on the underlying contributing factors.

To make an optimal management decision, an understanding of the aetiological factors of a condition is necessary. Despite the prevalence and impact of anterior knee pain, its aetiology remains elusive [6]. Because of this, anterior knee pain is often a diagnosis of exclusion [7]. Factors that are believed to contribute to the pain include lower limb strength, flexibility, muscle imbalances, malalignment and patellofemoral joint mechanics [8]. A common, yet relatively under-researched intrinsic aetiological predisposing factor includes patellofemoral interface loads and pressures. In order to investigate these interface loads and pressures, one can make use of computational methods.

Computational musculoskeletal models and finite element analyses find wide application in the field of biomechanics, especially to investigate joint reaction forces, joint contact pressure and muscle forces [9], [10]. Therefore, computational modelling can be used to measure possible risk factors associated with anterior knee pain such as the stress distribution within the patellofemoral joint. Besier *et al.* [9] introduced a modelling pipeline with which patellofemoral posture and pressure distribution can be simulated accurately. Using this approach, they compared the

effect of internal and external rotation of the femur on patellofemoral pressure [11], and implied that patients suffering from patellofemoral pain will present with greater patellofemoral peak shear stresses than pain-free controls [12].

1.2 Motivation

Practitioners require up to date clinical evidence as well as laboratory based evidence to understand the effect of an intervention on the underlying causative factors of an injury or disability. A recent study on anterior knee pain highlighted that physiotherapy yields a meaningful improvement in pain [5], however it is unclear what has led to this. Therefore, in order to justify an intervention one must understand the effect of said intervention on the underlying biomechanical mechanisms of the patellofemoral joint.

In previous studies the researches assumed a relationship between higher patellofemoral stresses and pain, despite confounding inter-subject variability such as anatomy, physiology and psychology between subjects [10], [12]. By allowing each subject to act as his/her own control, one can eliminate inter-subject variability. It is, therefore, necessary to repeat the measurement and analysis pre and post intervention in order to quantify intra-subject variability and measurement variability. Valid insight into the association between pain and the proposed underlying mechanisms can thus be drawn.

This project makes up a part of a larger study that aims to unlock scientific evidence about the aetiology of patellofemoral pain and likely effect of interventions on the underlying mechanisms. More specifically, this project will apply a modelling pipeline using measured kinematic and kinetic data to predict the muscle forces around the patellofemoral joint. These forces can then be used to determine the patellofemoral joint reaction forces and patella kinematics.

Previous studies have been conducted that made use of computational musculoskeletal models to determine patellofemoral joint biomechanics [9], [10], [13]–[15]. A study performed by Besier *et al.* successfully determined the stresses and strains in the patellofemoral cartilage using finite element methods [9]. Within this study the subject's joint geometry, acquired from Magnetic Resonance Imaging (MRI), was used to create subject specific musculoskeletal models, and muscle forces were estimated from an Electromyography (EMG) driven musculoskeletal model. Elias *et al.* performed an *in vitro* study where cadaver knees were loaded and analysed using computational modelling to determine the patellofemoral contact pressures [16]. Within the study the force and pressure distribution in the knee is recorded with a pressure sensor.

Both studies mentioned successfully determine the patellofemoral joint stresses. However, Elias *et al.* performed a more invasive *in vitro* study and Besier *et al.* is comparing different subjects to one another which can lead to inter-subject variability. This study is non-invasive and eliminates inter-subject variability by

using each subject as his/her own control. This project aims to determine the muscle forces applied to the knee using the body kinematics and ground reaction forces as inputs, whereas Besier *et al.* made use of EMG measurements to determine muscle forces.

The experimental data for this project is obtained at the Central Analytic Facility (CAF) Movement Analysis Laboratory at Stellenbosch University's Tygerberg Campus. This project is the first project being done at this laboratory that will be combining the various measurement devices that will be discussed later. Therefore, methods must be developed to successfully incorporate and synchronise the devices being used. This project will propose a computational modelling pipeline to successfully use the experimental data to obtain the muscle forces at the knee joint and determine the patellofemoral contact force and patella kinematics during stance phase of walking.

1.3 Aim

This project forms part of a prospective study on anterior knee pain for which the aim is to assess the effect of a physiotherapeutic intervention on patellofemoral risk factors and clinical outcomes in subjects with anterior knee pain during functional movement. This project aims to predict the muscle forces and contact load in the patellofemoral joint and track patella kinematics using a computational modelling pipeline. To achieve the project aim, the following objectives have been defined:

- Measure joint geometry, kinematic and kinetic drivers for the musculoskeletal model during above ground level walking and stair descent.
- Estimate the position of the centre of pressure (COP) of the foot not striking the force plate during stance phase.
- Estimate the complete ground reaction force (GRF) of the foot not striking the force plate during stance phase.
- Apply a modelling pipeline in OpenSim (OpenSim V3.2, <https://simtk.org/home/opensim>) to determine the muscle forces during stance phase of the muscles responsible for movement of the knee joint.
- The development of a subject specific musculoskeletal model using Adams View software (Adams 2015, MSC Software, Santa Ana, California), to measure the patellofemoral contact force and track the patella kinematics.
- Validate each step in the modelling pipeline by testing the intra-subject variability and repeatability.

1.4 Thesis outline

The thesis will cover the following headings:

- **Chapter Two:** A literature study is conducted on the human lower extremity, with particular focus on the knee joint and patellofemoral joint thereof. The principle of biomechanics is introduced where after human gait and the measures thereof are discussed. Finally, modelling techniques used to model the human musculoskeletal system are introduced and explained. Specifically, modelling in OpenSim and contact modelling are discussed in detail; where after previous studies done using similar techniques are discussed.
- **Chapter Three:** The apparatus and methods used to obtain experimental data are discussed in detail, as well as the statistical methods used in this project. Limitations of the available apparatus are also briefly discussed.
- **Chapter Four:** Two methods used to incorporate the ground reaction force and centre of pressure on the foot not striking the force plate are discussed and compared to experimental data. These methods are then compared to one another, where after a method is chosen to use in this projects computational modelling pipeline.
- **Chapter Five:** The modelling pipeline applied using OpenSim software is discussed. The kinematic and kinetic results are compared inter-session and intra-session as well as to literature sources that report on the same outputs.
- **Chapter Six:** The modelling approach used to develop a subject specific musculoskeletal patellofemoral joint model is discussed. The full modelling pipeline is applied to one subject's data and the results thereof are discussed.
- **Chapter Seven:** The final conclusions, limitations and future work are discussed.

Chapter 2

Literature review

2.1 The lower limb

The human lower limb is designed for weight-bearing, locomotion and maintaining an upright posture [17]. Within this section the three main joints of the lower limb will be discussed as per Palastanga *et al.* [17], namely the hip, knee and ankle joint. These joints play an important role during human gait.

2.1.1 Anatomical definitions

Throughout this work specific terms are used to describe anatomical reference directions and planes. These terms are shown in Figure 1.

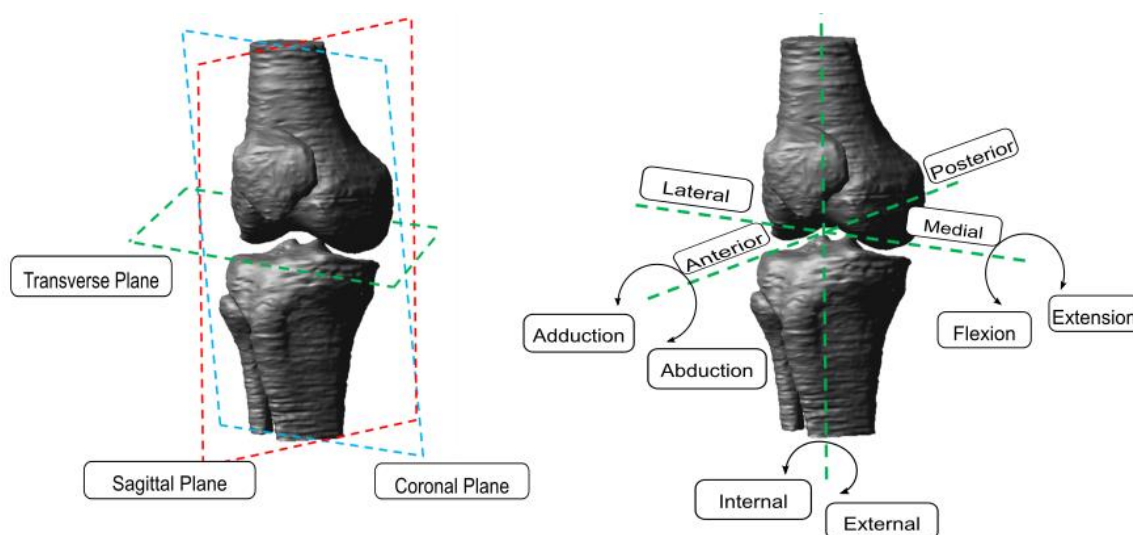


Figure 1: Anatomical reference planes and rotations

2.1.2 The hip joint

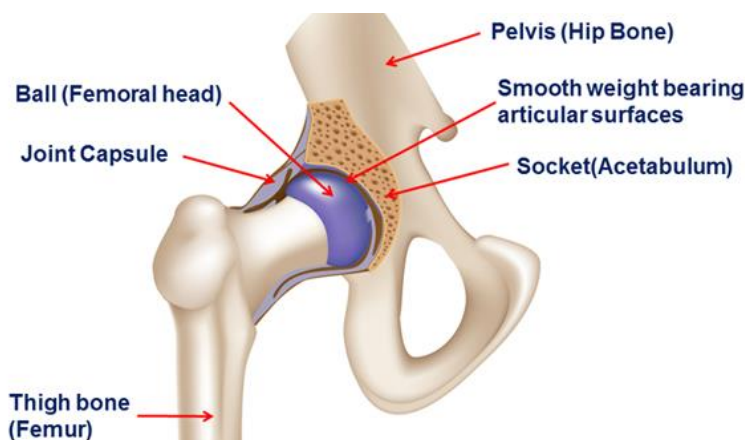


Figure 2: The hip joint (adapted from www.dr.samsani.com) [80]

The hip joint (Figure 2) is a ball and socket joint that connects the lower limb to the trunk, and as such it is capable of supporting the entire weight of the body and successfully transferring weight during activities such as walking or running. To perform such activities the hip joint has three degrees of freedom, namely flexion/extension, abduction/adduction, and internal/external rotation. Articulation of the hip joint occurs between the femoral head and acetabulum of the pelvis.

To support the weight of the body, the hip joint must possess a large amount of strength and stability. The capsular ligaments of the hip stabilise it, as well as limit and control the movement of the hip. These are the iliofemoral, pubofemoral, and ischiofemoral ligaments. The hip joint is strengthened by the muscles crossing it, shown in Table 1.

Table 1: Muscles responsible for hip joint movement [17]

Movement	Muscle
Flexion	Psoas major, iliacus, pectineus, rectus femoris, and sartorius
Extension	Gluteus maximus and hamstrings (semitendinosus, semimembranosus and bicep femoris)
Abduction	Gluteus maximus, medius and minimus, and tensor fascia lata
Adduction	Adductor magnus, longus and brevis, gracilis, and pectineus
Internal rotation	Gluteus medius and minimus, tensor fascia lata, psoas major, and iliacus
External rotation	Gluteus maximus, piriformis, obturator internus, gemellus superior and inferior, quadrates femoris, and obturator externus

2.1.3 The knee joint

❖ Functional anatomy

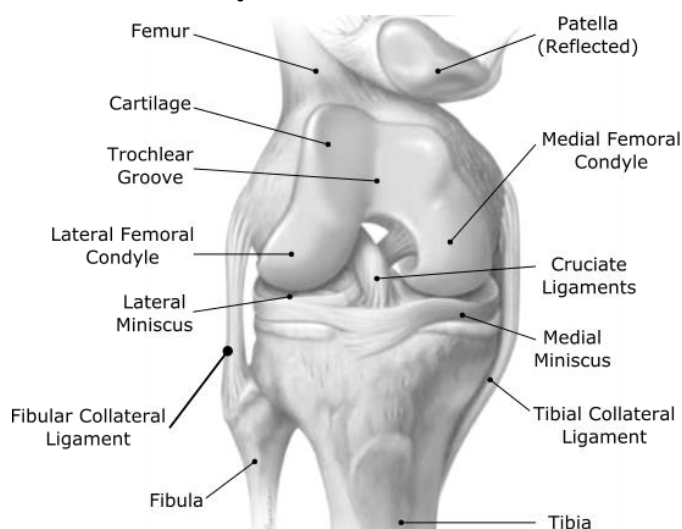


Figure 3: The knee joint (adapted from Christy Krames [99])

The knee joint (shown in Figure 3) is known as one of the largest and most complex joints in the human body [17]. It is made up of the patellofemoral joint (patella and anterior femur), the tibiofemoral joint (proximal tibia and distal femur), and the fibulotibial joint (fibula and proximal tibia).

The knee is a six degree of freedom joint that allows for flexion-extension, abduction-adduction and a small degree of rotation, yet provides complete stability and control under a large range of loading conditions [18]. The knee can achieve both mobility and stability together due to the interaction of ligaments and muscles, as well as gliding and rolling movements at the articular surfaces [17].

As well as supporting the weight of the body, the knee joint also plays an important role in locomotion. To do this the knee joint has a number of favourable features: the weight bearing surfaces of the femur and tibia, known as condyles, are expanded; it has strong collateral and intracapsular ligaments; and tendons help to reinforce the knee. Locomotion is achieved when the knee's powerful muscles work with the ankle joint to propel the body forward. The various muscles responsible for the movement of the knee joint are shown in Table 2.

Table 2: Muscles responsible for knee joint movement [17]

Movement	Muscle
Flexion	Hamstrings (semitendinosus, semimembranosus and bicep femoris), gastrocnemius, gracilis, sartorius, and popliteus.
Extension	Quadriceps femoris (rectus femoris, vastus lateralis, vastus medialis and vastus intermedius), and tensor fascia lata.
Lateral rotation	Bicep femoris
Medial rotation	semitendinosus, semimembranosus, gracilis, Sartorius, and popliteus

The ligaments and tendons surrounding the knee provide the joint capsule with the necessary strength and control that is required to perform its functions. The collateral and cruciate ligaments also provide further stability to the knee joint together with the muscles crossing the joint. The joint capsule of the knee is lined with a synovial membrane that aids in lubrication of the knee [17].

During movement of the knee two articulations are considered: between the tibia and femur (tibiofemoral joint) that controls the lengthening and shortening of the lower limb, and that between the femur and patella (patellofemoral joint) that acts as a pulley for the quadriceps tendon and changes its line of action. These articulating surfaces are lined with hyaline cartilage that provides a smooth surface for movement and acts as a shock absorber.

Within the patellofemoral joint, the main function of the patella is to increase the lever arm of the quadriceps muscle to improve its efficiency and aid in knee extension or resist knee flexion [19]. The patella also centralises different forces

coming from the four muscles of the quadriceps and transmits tension around the femur to the patella tendon as the patella engages the trochlea of the femur [20]. When the knee is extended, the angle formed between the resultant quadriceps force and patella tendon is known as the quadriceps angle (Q-angle) [21]. This angle results in a force that laterally displaces the patella and counters external (lateral) rotation of the patella [22].

The patella is positioned proximal and lateral to the trochlea at full extension. As the knee flexes the patella moves medially into the trochlea where after it moves laterally until 90° of flexion [21], [23]. While this is happening the patella tilts medially (internally) until it engages with the trochlea at 30°, after which it's tilt is determined by the lateral trochlear facet's slope angle [21]. This internal rotation results in a reduced Q-angle, which decreases the lateral forces on the patella. Therefore, the patella is most vulnerable to dislocation at 30° flexion when the Q-angle is the largest and the patella is not as secure in the trochlear groove [21].

The primary restraint to lateral displacement of the patella at 30° to 40° flexion is the medial patellofemoral ligament (MPFL), which also controls the tilt. After this, the lateral facet of the trochlea restrains the lateral displacement with the help of the medial ligamentous structures and lateral retinaculum [21], [24].

2.1.4 The ankle joint

The ankle joint, a synovial hinge joint, only allows for one degree of freedom of movement resulting in dorsiflexion (flexion) or plantarflexion (extension) in the sagittal plane. It adjusts the line of gravity during standing and keeps the body in equilibrium during gait by providing restraint and propulsion during each step. The ankle, subtalar and midtarsal joints, supported by axial rotation of the knee, are equivalent to one joint with three degrees of freedom. On the other hand, unlike a single joint, they provide a large amount of stability without sacrificing mobility. The ankle joint is shown in Figure 4.



Figure 4: The ankle joint (Adapted from www.turbosquid.com [25])

Articulation in the ankle joint occurs between the distal end of the tibia and fibula and the superior surface of the talus. The trochlear surfaces of the tibia and talus are responsible for weight-bearing, while the medial and lateral malleoli, that grip the talus, are responsible for stabilization of the joint [17]. Articulation between the metatarsals and phalanges occur at the Metatarsophalangeal (MTP) joint.

2.1.5 Human gait

Biomechanics is the study of biological systems using mechanical engineering methods. In this paper biomechanics is used to study human gait, thus this section will give an introduction into the biomechanics of the knee during gait.

Normal gait is a broad term used to describe a standard against which a patient's gait can be compared. It is important to note that all people are different and if a person's gait differs it doesn't necessarily mean the results are incorrect, but it could indicate that the person is compensating for some problem. A gait cycle is defined by Whittle as the time period between two consecutive occurrences of one of the repetitive events of walking [26]. The gait cycle is shown in Figure 5.

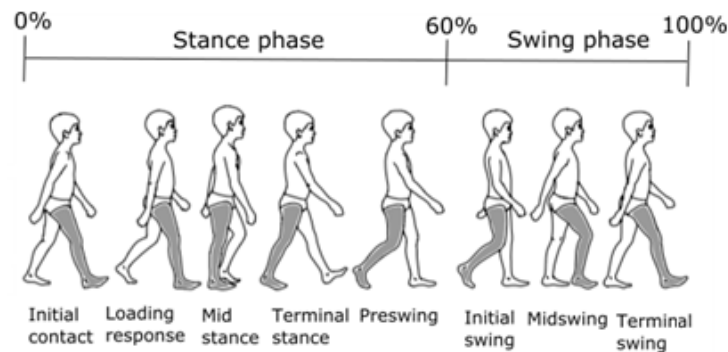


Figure 5: Human gait cycle (Adapted from Dynamics of Human Gait [27])

Stance phase occurs during the first 60 % of the gait cycle where after swing phase occurs in the remaining 40 % of the cycle. Stance phase occurs as follows [27]:

- Initial contact/heel strike (0 %)
- Loading response (0-10 %)
- Midstance (10 – 30 %)
- Terminal stance/heel off (30-50 %)
- Preswing/toe off (50-60 %)

During the full gait cycle the angle of the knee and torque around the knee varies. Figure 6 shows an example of the knee flexion-extension (FE) joint angle and joint moment during a single gait cycle. The joint moment is shown in Nm/kg so that the joint moment of subjects with different body masses is comparable to one another.

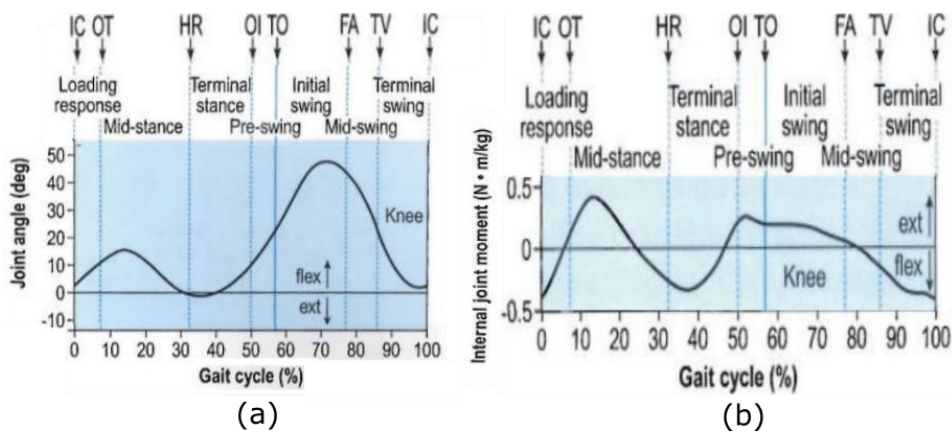


Figure 6: Knee joint angle in degrees (a) and internal joint moment in Nm/kg (b) during level ground walking [26]

In the field of biomechanics, to determine the moment occurring on the knee joint and resulting muscle forces, one must record the reaction forces between the ground and the subject being tested. When using measuring equipment with a fast enough response time, one can identify the heel strike transient in the vertical ground reaction force of certain individuals at initial contact [26]. The heel strike transient is a result of the transfer of momentum from the moving leg to the ground and is recognized as an impulsive event in the vertical ground reaction force occurring roughly at 10 % of the stance phase [28]. The heel strike transient is often filtered out of force plate data if a low cut off frequency filter is used.

2.2 Computational modelling of the musculoskeletal system

Engineers can potentially assist physicians in diagnosing patients with the use of computational modelling by using computer simulations to understand muscle and joint function. This enables engineers to not only assess the kinematic behaviour of the joint, but the kinetic behaviour too. Through doing this one can determine various parameters relating to joints, for example: irregular loads within a joint, irregular muscle activation times, and the force applied by muscles.

Muscle-tendon units enable movement by generating and transmitting a force to the skeleton, thereby acting as the primary contributors to joint loading. The force applied by the muscles over a joint result in joint reaction forces. Therefore, knowing the muscle forces, and geometrical coordination, the joint reaction forces can be computed [29]. Previous studies have determined the joint reaction forces and muscle forces using both *in-vitro* [30]–[34] and *in-vivo* methods [35]–[38] .

Kinetic and kinematic data can be applied to musculoskeletal models to reproduce motions performed by actual subjects and the forces experienced by their bodies. Methods used to achieve this are discussed here after.

2.2.1 OpenSim

OpenSim (OpenSim V3.2, <https://simtk.org/home/opensim>) is an open-source software used to perform analyses on the musculoskeletal system and create dynamic simulations of movement. This subsection gives an explanation of the OpenSim tools used in this project to determine the muscle forces acting on the knee joint. The modelling pipeline applied to determine the muscle forces is shown in Figure 7. All the information provided is adapted from the OpenSim User's Guide [39], unless otherwise specified.

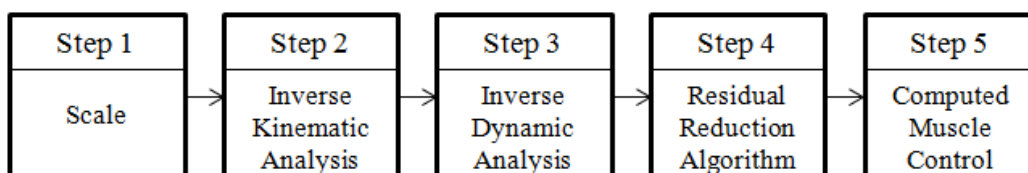


Figure 7: Simplified OpenSim pipeline

❖ The model

The generic musculoskeletal model used in this project is developed and described by Delp *et al.* [40]. The model consists of the lower extremity and simplified upper extremity. The simplified upper extremity is seen as one rigid body segment and consists of the spine, rib cage, sternum and skull. The lower extremity was originally modelled as seven rigid body segments, including the pelvis, femur, patella, tibia/fibula, talus, foot (comprising the calcaneus, navicular, cuboid, cuneiforms, and metatarsals), and toes. However, the patella was removed to eliminate kinematic constraints.

The line of action (paths) of musculotendon actuators, represented by a series of line segments, are defined according to anatomical landmarks of the bone surface models. The landmarks used were the origin and insertion of the muscle tendons. In certain cases these points are sufficient to describe the muscle path, but if the muscle wraps over bone, additional landmarks are used to represent the muscle path more precisely. For example, when the knee is flexed greater than 90° the quadriceps tendon wraps over the distal femur. Therefore, additional landmarks known as wrapping points are introduced to enable wrapping of the quadriceps tendon over the distal femur instead of passing through it.

Models of the hip, knee, ankle, subtalar and MTP joints define the relative motion of the body segments. The hip is characterised as a ball and socket joint and is therefore able to rotate about three orthogonal axes fixed in the femoral head. The knee is modelled as a hinge joint, thus it has one degree of freedom. The simplified knee joint accounts for the kinematics of both the patellofemoral and tibiofemoral joints in the sagittal plane, as well as the patellar levering mechanism. The ankle, subtalar and MTP joints are modelled as frictionless revolute joints.

To calculate the moment arm and muscle-tendon length of a muscle, all muscle coordinates are transformed to a common reference frame (Figure 8). P_1 to P_n are coordinates that define the muscle path, where P_1 to P_m are fixed to segment A and P_{m+1} to P_n are fixed to segment B. Consequently \vec{V} is the only muscle segment that changes in length during joint motion defined by the angle θ_1 .

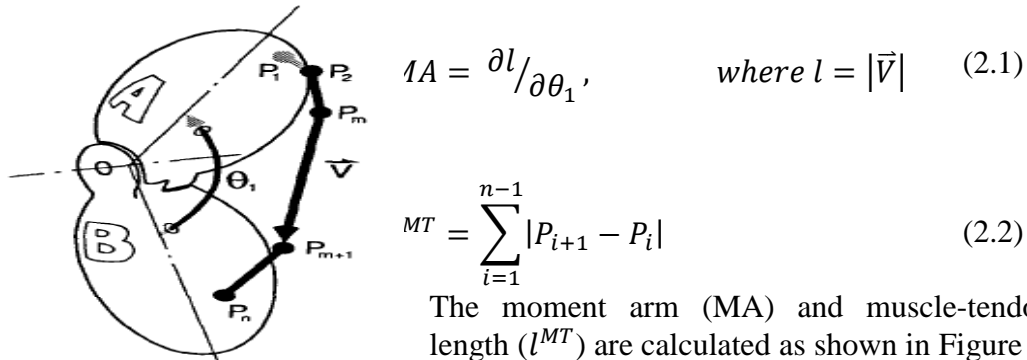


Figure 8: Simplified joint model [43] and accompanying equations

where ∂l is the change in length of the muscle segment, and $\partial \theta_1$ is the consequent change in the joint angle.

The muscle-tendon force is computed as a function of muscle-tendon length by formulating a specific model for each musculotendon actuator. Each muscle is adapted from a generic model, shown in Figure 9, which accounts for the static properties of the muscle and tendon. The isometric properties of the muscle are represented in Figure 9 by an active contractile element (seen as CE) in parallel with a passive elastic element (seen as a spring). The total isometric muscle force is assumed to be the sum of the passive (inactive) and active muscle forces. As can be seen, the muscle is in series with a tendon (seen as a spring).

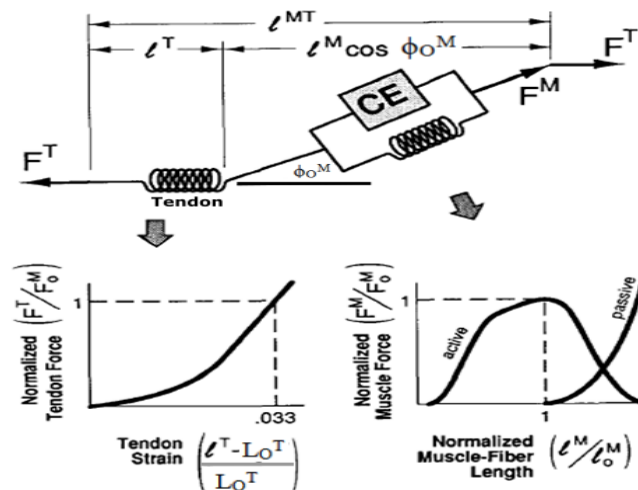


Figure 9: Muscle-tendon actuator model [40]

The pennation angle (ϕ_o^M) indicates the direction of the force relative to the tendon. The forces in the muscle (F^M) and tendon (F^T) are normalised by the maximum isometric force (F_o^M). The tendon length (l^T) and muscle fiber length (l^M) are normalised by the optimal muscle fiber length (L_o^M). Using the model in Figure 9 and values in Table 3, the following equations are developed to calculate the muscle-tendon length and muscle-tendon force:

$$l^{MT} = l^T + l^M \cos(\phi_o^M) \quad (2.3)$$

$$F^{MT} = F^T = F^M \cos(\phi_o^M) \quad (2.4)$$

Table 3: Knee joint muscle parameters [40]

Muscle	F_o^M (N)	L_o^M (m)	L_o^T (m)	ϕ_o^M (degrees)
Semitendinosus	410	0.201	0.264	5
Semimembranosus	1288	0.082	0.369	15
Bicep femoris long head	896	0.1121	0.3352	0
Bicep femoris short head	804	0.1786	0.0919	23
Medial gastrocnemius	1558	0.0657	0.4269	17
Lateral gastrocnemius	683	0.0701	0.4160	8
Gracilis	162	0.3634	0.1301	3
Sartorius	156	0.5335	0.1026	0
Rectus femoris	1169	0.1160	0.3153	5
Vastus lateralis	1871	0.0856	0.1600	5
Vastus medialis	1294	0.0906	0.1283	5
Vastus intermedius	1365	0.0884	0.1382	3

❖ Scaling

The scaling tool is used to alter the anthropometry of a musculoskeletal model to match a specific subject as closely as possible. It achieves this by comparing experimental marker data from motion capturing to virtual markers on the model. One can also use the scale tool to adjust virtual marker positions to better match experimental markers.

To scale a model one must place virtual markers on a model in the same anatomical positions that they were placed on the subject in the laboratory. The experimental marker locations used for scaling are captured during a static trial where the subject stands upright and doesn't move. Each body segment (bone) is scaled according to a scale factor that is calculated by comparing the relative distance between a pair of experimental markers on the body segment to the corresponding virtual marker locations on the model [41]. Thus, after scaling, the distance between the virtual markers will match the distance between the same experimental markers.

During scaling the inertial and geometrical properties of the body segments are altered. The muscle actuators and ligaments attached to the body segments are also scaled. The joint frame locations, mass centre location, force application points, and muscle attachment points are all part of a specific body frame; therefore these positions are scaled according to the scale factor applied to the corresponding body segment. One can choose to preserve the mass distribution of the body segments during scaling or scale the mass of each body segment according to its scale factor. The former is encouraged since it ensures that the model will have the mass of the subject specified in the scaling tool.

After scaling the model, the scaling tool also adjusts the virtual markers position to better match the position of the experimental markers. This is done by solving a weighted least-squares (WLS) problem, which is discussed in the next subsection.

❖ Inverse kinematic analysis

To perform an inverse kinematic (IK) analysis experimental marker trajectories during gait are imported into OpenSim. The IK tool goes through each time step of motion and computes generalized coordinate values that position the generic model according to the position of experimental markers and coordinate values for that time step. This is done by solving a WLS problem (shown in equation 2.5) that minimizes both marker and co-ordinate errors. A co-ordinate error is the difference between an experimental joint angle and the value computed by IK.

$$\min_q \left[\sum_{i \in \text{markers}} w_i \|x_i^{\text{exp}} - x_i(q)\|^2 + \sum_{j \in \text{unprescribed coords}} \omega_j (q_j^{\text{exp}} - q_j)^2 \right] \quad (2.5)$$

q = Vector of generalised co-ordinates

x_i^{exp} = Position of experimental marker i

$x_i(q)$ = Position of the corresponding virtual marker

q_j^{exp} = Experimental value for co-ordinate j

The marker weights (w_i) and co-ordinate weights (ω_j) are specified by the user. If the user has not input measured joint angles, then the co-ordinate values are known as unprescribed co-ordinates. Unprescribed co-ordinate's values are computed using IK. If prescribed co-ordinates are used, the experimental co-ordinate values (q_j^{exp}) equal the virtual co-ordinate values (q_j).

❖ Inverse dynamic analysis

The Inverse Dynamics (ID) tool is used to calculate the generalised forces (net forces and torques) at each joint that result in a given movement. The joint angles determined using the IK tool are used as an input for the kinematics of the model in order to describe the model's motion. The kinetics (ground reaction force) applied to the model are another input into the ID tool. The ID tool solves Newton's

Second Law of motion (equation 2.6) to yield the net forces and torques at each joint that will produce the movement from the IK analysis.

$$M(q)\ddot{q} + C(q, \dot{q}) + G(q) = \tau \quad (2.6)$$

where q , \dot{q} and $\ddot{q} \in \mathbb{R}^N$ are vectors of generalised positions, velocities, and accelerations, respectively, for N number of degrees of freedom. The known input parameters are: the system mass matrix ($M(q) \in \mathbb{R}^{N \times N}$), the vector of Coriolis and centrifugal forces ($C(q, \dot{q}) \in \mathbb{R}^N$), and the vector of gravitational forces ($G(q) \in \mathbb{R}^N$). The unknown vector of generalised forces ($\tau \in \mathbb{R}^N$) is solved using the known motion of the model from the IK tool to solve the equations of motion.

❖ Residual reduction algorithm

As a result of experimental error and modelling assumptions, the measured ground reaction forces (GRF) and moments are often dynamically inconsistent with the model's kinematics [41]. The Residual Reduction Algorithm (RRA) tool minimises the effect of modelling and marker data processing errors that cumulate and result in nonphysical compensatory forces on the pelvis known as residuals.

Residual reduction, a form of forward dynamics simulation, uses a tracking controller to follow a model's kinematics determined from the IK tool. According to Thelen *et al.*, a forward dynamic simulation is performed by integrating differential equations that describe the properties of the subject's musculoskeletal system and its interactions with the environment [42]. These equations include first-order equations for muscle activation dynamics and musculotendon contraction dynamics, and second-order equations of motion for the body [42].

The OpenSim model used in this project has 23 degrees of freedom (DOF) across its body segments. Seventeen of these represent joint angles for the joints relating the body segments to one another. Each of these generalised co-ordinates is actuated by a single joint actuator. The remaining six DOF represent the three translations and three rotations between the model's pelvis and the ground.

To simulate gait, one must characterize how the model propels itself forward relative to the ground. This is done by combining the six aforementioned DOF to form one joint between the pelvis and ground. Each of the six DOF is actuated by its own torque actuator, known as a residual actuator. These are the residual forces (F_x , F_y and F_z) responsible for translation of the pelvis relative to the ground, and the residual moments (M_x , M_y and M_z) responsible for the rotation of the pelvis.

Dynamic inconsistencies arise due to modelling assumptions, such as having a model with no arms, or due to the fact that the markers are not actually fixed to the body, but can move with the skin during walking. In essence the ground reaction forces and accelerations estimated using the marker trajectories during gait do not satisfy Newton's Second Law. Therefore, the six residual actuators account for the

inconsistencies and balance out the equation of motion as shown in equation 2.7. The sum of the GRF (F_{grf}) and the residual forces (F_{res}) are equal to the force generated by the acceleration (a_i) of each body segment's mass (m_i).

$$F_{grf} + F_{res} = \sum_{i=1}^{body\ segments} m_i a_i \quad (2.7)$$

The RRA tool performs two main functions. It computes forces that must be applied by the actuators to produce accelerations that resemble those produced by the IK tool. Secondly, it adjusts the mass centre of the model's torso and recommends mass adjustments to be made to the individual body segments so that the model's kinematics are more consistent with the measured GRF.

The RRA begins by placing the model in the starting configuration by setting the joint angles of the model to those calculated by the IK tool at the user defined initial time. At different time intervals, the RRA tool then computes forces for all the model's actuators to make the model move from its current position to the position desired at the end of the step. The actuator forces are calculated by solving a weighted minimisation problem shown in equation 2.8.

$$\min_{\phi} = \sum_{i=1}^{n\phi} \phi_i^2 + \sum_{j=1}^{nq} w_j (\ddot{q}_j^* - \ddot{q}_j) \quad (2.8)$$

ϕ_i^2 = Actuator controls being solved for

\ddot{q}_j = Accelerations calculated by the IK tool

The desired model body segment accelerations (\ddot{q}_j^*) are solved using an iterative process by solving the equation of motion for the RRA model shown in equation 2.7 and the equation shown above.

The average value for each residual actuator is calculated after the RRA simulation has run. The average value for the residual moment in the coronal (M_x) and sagittal (M_z) planes are used to adjust the mass centre of the model's torso to correct any excessive leaning caused by inaccuracies in the mass distribution and geometry of the torso. A new model, with the adjusted torso mass centre, is generated.

The average vertical residual force (F_y) is used to compute recommended mass changes for all the body segments. The user can then make the recommended mass changes to the body segments to better match the vertical ground reaction force applied to the model. Once the simulation has been run, a modified model with an adjusted torso has been generated, and the body segment's masses have been adjusted, the whole process is repeated with the new model. Through repeating the problem, smaller residual forces are computed.

Minimum and maximum values are applied to the residual actuators to reduce the need for residual forces and moments to the minimum that is necessary follow the desired kinematics. Through doing this, the motion is generated purely by internal joint moments.

❖ Computed muscle control

Computed Muscle Control (CMC) is used to calculate a set of muscle excitations (or actuator controls) that result in a co-ordinated muscle-driven simulation of the subject's movement in the presence of applied external forces [41]. The actuator controls aim to drive the model's generalised co-ordinates (joint angles) to resemble the kinematics produced by the RRA tool. The CMC tool achieves this by using a combination of proportional-derivative (PD) control and static optimization, as seen in Figure 10.

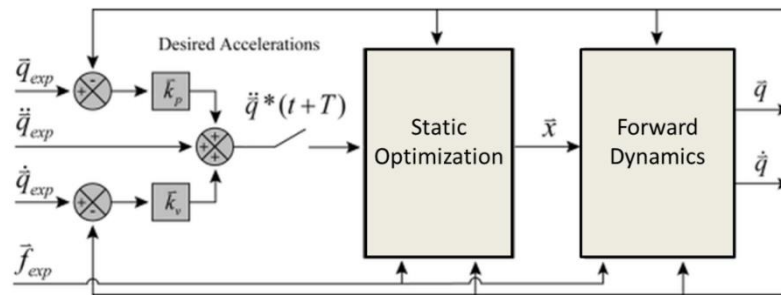


Figure 10: Schematic of CMC algorithm [39]

First the model's initial states are computed. These states are the joint angles, angular velocities, and any muscle states (e.g. muscle activation levels and fiber lengths). The initial values for the joint angles and joint angular velocities are taken from the desired kinematics, which is either the kinematics computed by the IK or RRA analysis. The initial muscle states are unknown; therefore muscle states are computed by the CMC tool in the first 0.03 seconds.

Once the initial states are specified, a set of desired accelerations ($\ddot{\vec{q}}^*$) must be computed so that the model's co-ordinates (\vec{q}) are driven to resemble the experimental co-ordinates (\vec{q}_{exp}). These accelerations are calculated using the following PD control law:

$$\ddot{\vec{q}}^*(t+T) = \ddot{\vec{q}}_{exp}(t+T) + \vec{k}_v[\dot{\vec{q}}_{exp} - \dot{\vec{q}}(t)] + \vec{k}_p[\vec{q}_{exp} - \vec{q}(t)] \quad (2.9)$$

where \vec{k}_v and \vec{k}_p are velocity and position feedback error gains. The forces applied by muscles cannot change instantaneously, thus the desired accelerations are determined for some small time T in the future. This period is short enough to allow acceptable control, but long enough to allow muscle forces to change.

Errors between the model co-ordinates and experimental co-ordinates are driven to zero if the desired accelerations are achieved. To reduce the errors in a critically damped manner (i.e. without over-shooting or over-damping), the velocity gain is chosen using the relation in equation 2.10.

$$\vec{k}_v = 2\sqrt{\vec{k}_p} \quad (2.10)$$

Next the CMC tool determines actuator controls (ϕ_i) that will achieve the desired acceleration ($\ddot{q}_{exp}(t + T)$). The actuator controls are predominately muscle excitations, but any kind of actuator can be used (e.g. idealised joint moments). Static optimization allocates the loads across synergistic actuators. It is referred to as static optimization because the performance criterion (i.e. the cost index) is confined to quantities that can be calculated at any point in time in the simulation. Therefore, one cannot use criteria like the total metabolic energy over a gait cycle, because it requires information from the whole gait cycle.

CMC can formulate the static optimization problem in two ways, namely slow target or fast target static optimization. The slow target consists of a performance criterion (J) that is formulated as shown in equation 2.11.

$$J = \sum_{i=1}^{n\phi} \phi_i^2 + \sum_{j=1}^{nq} w_j (\ddot{q}_j^* - \ddot{q}_j) \quad (2.11)$$

The first summation above distributes loads across actuators and the second summation drives the acceleration of the model (\ddot{q}_j) towards the desired acceleration (\ddot{q}_j^*). This equation is the same one used by the RRA tool.

The fast target is the sum of square controls that are increased by a set of equality constraints ($C_j=0$). The equality constraints need the desired acceleration to be achieved within the tolerance set for the optimizer. The fast target performance criterion is computed in equation 2.12.

$$J = \sum_{i=1}^{n\phi} \phi_i^2; \quad C_j = \ddot{q}_j^* - \ddot{q}_j \forall_j \quad (2.12)$$

The fast target is faster and produces better tracking. On the other hand, if the desired constraints cannot be met, the fast target will fail. This could be due to the musculoskeletal model not being strong enough for the applied external forces. To prevent fast target failure, reserve actuators are added to the model that makes up for strength deficiencies in muscles if encountered. These reserve actuators have a low optimal force; hence they require very high excitations to apply a substantial load to the model. Thus, use of reserve actuators is highly penalized in both the fast

and slow formulations. If the muscles are strong enough to propel the model, the reserve actuator forces and moments should be small.

Finally the CMC algorithm uses computed controls to conduct a forward dynamic simulation that advances in time by steps T . Within each step the desired accelerations are calculated, the static optimization is run, and the forward dynamics simulation is conducted. These steps are repeated until the model has reached the end of the desired movement and all muscle forces are computed.

2.2.2 Contact modelling

Subject specific skeletal geometry can be generated from Magnetic Resonance Imaging (MRI) images [43], [44] and Computerized Tomography (CT) scan data [45]. Through these methods subject specific representations of the skeletal geometry are generated. Musculoskeletal models can then be generated by applying the muscle forces to this subject specific skeletal model using Adams View software (Adams 2015, MSC Software, Santa Ana, California) at insertion points acquired from literature or scans.

When modelling the patellofemoral joint it is necessary to model the soft tissues that oppose the muscle forces applied to the patella. According to a method introduced by Blankevoort *et al.* [46], these soft tissues can be modelled as idealised tension-only parallel spring damper elements. Within this method the ligaments and tendons are described by a number of line elements that are assumed to be elastic. Therefore, the forces of the soft tissues are a function of their lengths. The force (F_{st}) of the ligaments and tendons are computed using equation 2.13, where the force is assumed to be non-linear for low strains and linear for strains above a certain level [46].

$$F_{st} = \begin{cases} \frac{k\varepsilon^2}{4\varepsilon_l}; & 0 \leq \varepsilon \leq 2\varepsilon_l \\ k(\varepsilon - \varepsilon_l); & \varepsilon < \varepsilon_l \\ 0; & \varepsilon < 0 \end{cases} \quad (2.13)$$

k = Stiffness (N)

ε_l = Non-linear strain level parameter [$\varepsilon_l = 0.03$]

$$\varepsilon = \text{strain} = \frac{L - L_0}{L_0} \quad (2.14)$$

L = Ligament/tendon length (mm)

L_0 = Zero-load length (mm)

The zero-load length is taken at the point when the knee joint is at maximum extension. The stiffness coefficient (k) is computed in units of Newton below:

$$\sigma = E\varepsilon \rightarrow \frac{F}{A} = E\varepsilon \rightarrow F = AE\varepsilon \rightarrow F = k\varepsilon \quad (2.15)$$

$$\therefore k = AE$$

σ = Stress (MPa)

E = Elastic modulus (MPa)

A = Ligament/tendon cross-sectional area (mm²)

Once the muscles, ligaments and tendons of the patellofemoral joint have been defined, one must model the contact between the cartilages of the distal head of the femur and the patella to predict the patellofemoral reaction forces (contact force). The contact force is measured using the Adams built in contact function. The contact model used by Adams is based on the Hertz's contact model with a damper added to allow for energy dissipation [47]:

$$F_c = k_c \delta^{exp_c} + B_c(\delta) \dot{\delta} \quad (2.16)$$

k_c = contact stiffness (N/mm)

δ = interpenetration depth (mm)

exp_c = force exponent

B_c = damping coefficient (Ns/mm)

The subject specific musculoskeletal model can also be used to track patella kinematics during gait. Various sources in literature have employed different methods to predict the patellofemoral contact force and track patella kinematics. Besier *et al.* developed a geometrically accurate subject specific model from MRI images [9] onto which he applies quadriceps muscle forces estimated from an EMG-driven model of the knee [48]. The EMG driven model uses raw EMG and lower limb kinematics as an input into a modified Hill-type muscle model developed by scaling a generic model developed by Delp *et al.* [40].

Lin *et al.* developed a patient specific model of the knee using CT scan data and determined the relative origin and insertions points of the muscles and ligaments using the scans [49]. Kinematic and kinetic data captured in a motion lab was used to perform an inverse dynamic analysis which outputted the net forces and torques on the knee, where after the muscle and contact forces were computed simultaneously using a two level optimization approach.

Mesfar and Shirazi-Adl applied an approach where by a predefined constant force is applied by the quadriceps muscle at incremental flexion angles from 0° to 90° [50]. The patellofemoral contact force is then measured under different quadriceps forces and flexion angles. Applying a similar approach on cadaver knees, Powers *et al.* applied a force to the quadriceps muscle and measured the contact force within the patellofemoral joint at different intervals of knee flexion [15]. The measured forces were then compared to forces computed using a computational model that was based on co-ordinates obtained from the cadaveric knees.

Chapter 3

Experimental procedure

This chapter discusses the experimental setup and procedures followed to obtain the input data for the musculoskeletal computational models. The experiments for this project were performed at the Central Analytic Facility (CAF) Motion Clinic (from here on referred to as motion laboratory) at Stellenbosch University's Tygerberg Medical Campus. Figure 11 shows the flow of data in the project.

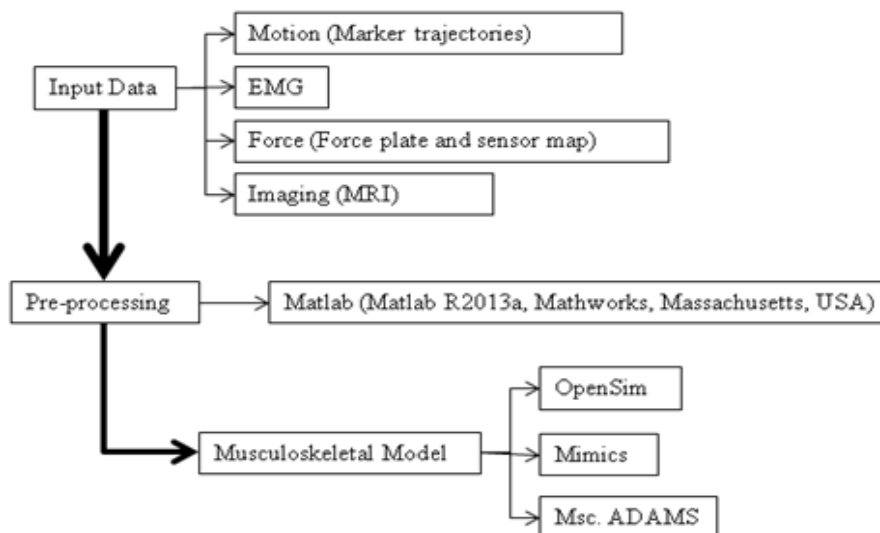


Figure 11: Flow of data in the project

3.1 Ethical consent

Ethical approval for this study has been obtained from the Health Research Council of the Stellenbosch University (Ref: N13/05/078).

3.2 Subjects

The subject population for this study comprises of males and females between the ages of 14 and 40 years that suffer from anterior knee pain. Subjects included in the study first fill in a screening questionnaire to indicate whether they exhibit symptoms of anterior knee pain during at least two of the following activities: prolonged sitting, stair ascent and descent, squatting, running, kneeling, lunging and jumping.

After completing the initial screening, potential participants undergo a clinical assessment conducted by an experienced physiotherapist. The subjects are excluded from the study under one or more of the following circumstances:

- had previous surgery involving the lower extremity of the affected limb.
- have history of patella dislocation or subluxation.
- require foot orthosis due to pes planus (flat footed) or cavus (high instep).
- have possible underlying degeneration and instability of the knee joint.
- received any conservative treatment from the onset of pain, including physiotherapy, non-steroidal anti-inflammatory drugs or corticosteroids.
- had previous traumatic injuries to the menisci, cruciate or collateral ligaments in the asymptomatic or symptomatic limb.
- have any signs of inflammation.

For this project, eleven subjects with anterior knee pain are used to obtain input data. The procedure is as follows: screening questionnaire and clinical assessment, the subject is tested in the motion capture laboratory, an MRI is taken of the affected limb, the subject undergoes a physiotherapeutic intervention, and finally the subject is tested in the motion capture laboratory again.

3.3 Apparatus

3.3.1 Motion capturing

The motion of the subject and his/her relative body segments is captured at 200 Hz using a Vicon Motion Analysis (Ltd) (Oxford, UK) system (from here on referred to as Vicon) with Nexus software (© Vicon Motion Systems Ltd., Oxford UK). In order to record the kinematics of the subject's body, markers are attached to body landmarks on the subject by a trained physiotherapist in order to track body segments (Figure 12).

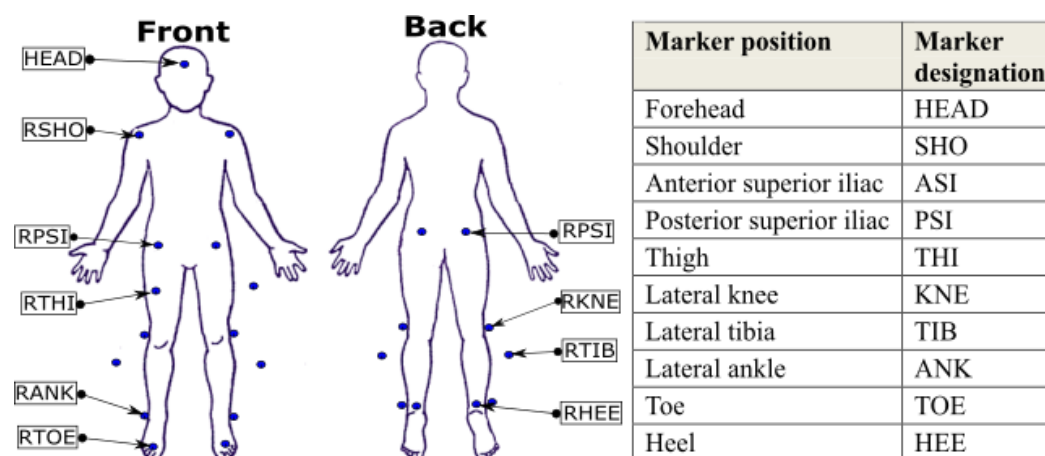


Figure 12: Anterior and posterior marker positions on a subject [51]

Eight cameras are used to capture the motion of the subject in what is termed the capture volume (shown in Figure 13). These cameras are positioned in a way that at any time each marker is visible to at least three cameras. This is necessary to successfully track the three dimensional displacement of each marker.

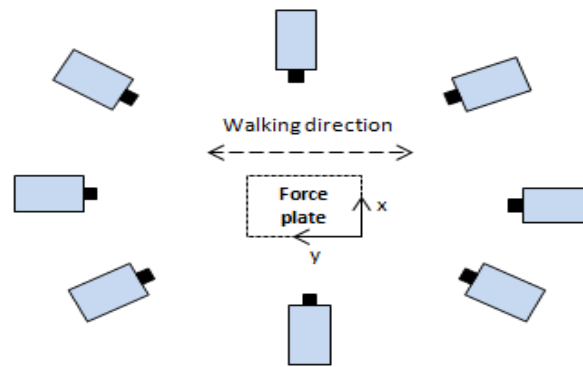


Figure 13: Capture volume and force plate layout in the motion laboratory

During motion capturing the subjects perform various activities. First a static calibration is performed, where the subject stands up right in a static pose and the marker positions are recorded. After the static trial the subject performs six trials of each of the following: over ground level walking (from here on referred to as walking), stair ascent and descent, squatting, and a single leg stance. The six trials for the walking and stair ascent and descent are divided into three right foot and three left foot strikes on the force plate. A standard full body Plug-In Gait (PiG) model is used in the Nexus software to output the joint angles produced by the relevant movements. These joint angles are later compared to the joint angles calculated using OpenSim. The PiG model is made up of rigid segments that represent the bones of the subject. These segments are defined using the measured marker trajectories and subject anthropometric measurements [52]. These measurements include the subject's mass, height, leg lengths, knee widths, and ankle widths.

As this project is the first project at the CAF Motion Clinic combining the measuring equipment being used, the project has continually developed and has evolved throughout the course of its existence. One such development is the positions of markers on the subject. Initially there were no markers attached to the upper extremity of the subject, but later in the project it was clear that the upper extremity kinematics must be tracked to successfully complete a RRA and CMC analysis in OpenSim. This observation was made later in the project, therefore many of the trials do not track the upper extremity kinematics (i.e. do not have the shoulder and head markers).

Due to the evolution of the project two different rounds were identified in which different subjects were analysed. In Round 1 subjects wore running shoes and FScan pressure measurement insoles and only the lower extremity kinematics were recorded for the subjects. In Round 2 the subjects were tested barefoot and only the lower extremity kinematics were measured for five out of the six subjects tested in session 1 of Round 2. The sixth subject's full body kinematics were recorded. The data captured for this sixth subject during both sessions is used for the full computational modelling pipeline in this project since it contains the upper extremity kinematics in both sessions.

Since the methods used in the full modelling pipeline must be validated, only subjects who were captured in round two (barefoot) are used in the repeatability analysis in Chapter 5, since they were tested under the same conditions.

3.3.2 Ground reaction force measurements

The motion laboratory only has one force plate, Bertec FP6090-15 (Bertec Corporation, Columbus, OH, USA), to measure the ground reaction force (GRF) between the subject and laboratory floor. The force plate measures the GRF at a frequency of 3000 Hz, where after it is resampled by the motion Analysis Clinic to 200 Hz to match the motion capture data. It is resampled using Matlab software by only recording every fifteenth sample of the GRF data.

In this project the patellofemoral contact force and patella kinematics will only be computed during stance phase when the force plate is struck, however it is necessary to know the GRF acting on both feet to perform a successful gait analysis. Tekscan F-Scan pressure insoles (Tekscan Incorporated, Boston, MA, USA) are worn by the subjects to record the normal force on the non-striking foot at 200 Hz.

Insole pressure measurement devices are thin wireless in-shoe sensors that capture the pressure, pressure distribution, force, COP, and timing information of each foot during gait. These devices are predominantly used to record the pressure distribution on the foot during movement, but are increasingly being used to measure the force and COP thereof on the foot [53]–[57].

Two major differences exist between the force plate and FScan system. The FScan system only records the force normal to the insole, whereas the force plate records a three-dimensional GRF between the subject and the ground. The FScan insole records the normal force and COP in a local co-ordinate system, compared to the force plate that records the GRF, COP and resulting moment on the force plate in the global co-ordinate system of the capture volume. Chapter 4 introduces a method to overcome these problems whereby the FScan data is converted into the global co-ordinate system using numerical optimization and the angle of the foot obtained from the foot markers. An alternative approach is also introduced in Chapter 4 where an average COP and GRF obtained from force plate data is superimposed onto the non-striking foot. These methods will be discussed in depth and compared later.

3.3.3 Electromyography measurements

When skeletal muscle is activated, an electrical impulse is produced that stimulates the production of an action potential in the muscle. A wireless electromyography (EMG) system with surface electrodes is used to measure the action potentials of predetermined muscles. These action potentials provide an indication of when the muscle is activated and to what extent. A telemyo, 12 channel, Noraxon-10-channel, wireless EMG system with surface electrodes is used to collect data from the

quadriceps, medial and lateral hamstrings, tibialis anterior and medial and lateral gastrocnemius muscles.

3.3.4 Portable lab

Due to renovations being done on the CAF Motion Clinic, the second session of tests done during Round 2 were performed in a portable lab setup in a Gymnasium at the Tygerberg medical Campus. All of the same equipment is used, except a Bertec FP4060-05-PT force plate is used. This force plate is not mounted to the foundations of the building.

3.3.5 Magnetic resonance imaging

For each subject a magnetic resonance image (MRI) is captured of the affected knee to attain the bone and cartilage geometries. The MRI (Siemens Symphony, 1.5 Tesla) is taken of the knee when the leg is in a relaxed position.

3.4 Data processing

The data from motion capturing (a collective term describing the process of measuring the body kinematics, GRF and muscle activation) has to be processed before it can be used for computational modelling. The following processes are undertaken to use the experimental data:

- The marker trajectory data obtained from the motion capture system is filtered at 6 Hz using a fourth order low-pass Butterworth filter (zero-lag).
- The GRF data is resampled from 3000 Hz to 200 Hz.
- Unfiltered GRF data is used as well as GRF data that has been filtered using a fourth order low-pass Butterworth filter with a cut-off frequency of 10 Hz. A comparison is shown later in the report.
- In-house Matlab (Matlab R2013a, Mathworks, Massachusetts, USA) functions are used with the measured data to generate the required input files to be used in the OpenSim software.

3.5 Statistical methods

The statistical methods used in this project are standard deviation, correlation coefficient, coefficient of determination and root mean square (RMS) error. The standard deviation indicates the amount of variability either between the numbers in the data set or between different data sets [58]. The standard deviation is calculated using equation 3.17.

$$\sigma = \sqrt{\sum \frac{(x - \bar{x})^2}{n - 1}} \quad (3.17)$$

In equation 3.17, the standard deviation (σ) is calculated using the values in the data

set (x), the mean of the data sets being compared at a specified time (\bar{x}) and the number of data sets being compared to one another.

The correlation coefficient is a measure of how strong the linear relationship is between two variables or datasets [59]. Equation 3.18 shows how to compute the correlation coefficient [59]:

$$R = \frac{\sum(x_i - \bar{x})(y_i - \bar{y})}{\sqrt{\sum(x_i - \bar{x})^2(y_i - \bar{y})^2}} \quad (3.18)$$

where R is the correlation coefficient, x_i is the value in one data set at step i , \bar{x} is the mean of said data set, y_i is the value in the data set being compared to at step i , and \bar{y} is the mean of the aforementioned data set. The value of the correlation can occur in the following range:

$$-1 \leq R \leq 1 \quad (3.19)$$

A positive correlation coefficient ($R \sim 1$) indicates that when the values for one data set increases, the values of the other data set will also increase. A negative value indicates that when the values of one data set increase, the values of the other data set decrease. [60]

The correlation coefficient indicates how similar the pattern of two results are, however the coefficient of determination (COD) indicates the portion of variation in one set of results that is predictable in the other set of results, i.e. the percent of data from one result that fits (is the same as) the other results [60]. The COD is the correlation coefficient squared (R^2). A COD of 1 indicates that 100 % of the results are the same and a COD of 0 indicates that the results are completely different.

The RMS error is measured using the predicted value (\hat{x}_i) and observed value (x_i) for n number of predictions as seen in the equation below:

$$RMS\ error = \sqrt{\frac{\sum_{i=1}^n (\hat{x}_i - x_i)^2}{n}} \quad (3.20)$$

Chapter 4

Inclusion of the foot not striking the force plate

4.1 Introduction

Although the muscle forces and patellofemoral loads will be determined during stance phase only, the kinematic and kinetic data of the foot not striking the force plate is still required to perform a full computational gait analysis. Chapter 3 discusses the Tekscan F-Scan insole pressure measurement device used in this project. The FScan devices are made up of 960 sensor elements (sensors) in a thin insole which measure the normal force of the foot and COP thereof. The F-Scan system has three limitations: it only measures the normal force on the foot, it measures the force in a local co-ordinate system reference frame, and it begins measuring at a varying delayed time when compared to the other measuring equipment used.

Chapter 4 introduces a method to include the data measured by the FScan system in the global capturing volume and overcome the aforementioned drawbacks. A different method is also put forward to approximate the GRF on the non-striking foot, whereby average GRF and COP data measured with a force plate is superimposed onto the non-striking foot. The results of each method are compared, where after one method is chosen and used in the modelling pipeline.

4.2 Methods

4.2.1 FScan inclusion

To include the FScan data in the computational analysis, first the timing of the FScan must be synchronised with the recording time of the other measuring equipment, where after the COP and normal force measured by the FScan insole must be converted from its local axis system to the global co-ordinate system of the capture volume. This subsection introduces data processing techniques to include the FScan data in the modelling pipeline.

❖ Time synchronisation:

The FScan insole pressure measurement system's measured data is not recorded through the Nexus software like the force plate and motion capture system. Therefore the recorded data from the two systems need to be synchronised. To ensure that the FScan data is compared to force plate data in real time, a Matlab function is written that matches the normal force recorded by the FScan to the vertical force recorded by the force plate. This is achieved by either matching the first peak, second peak, or midstance of the force data (Figure 14).

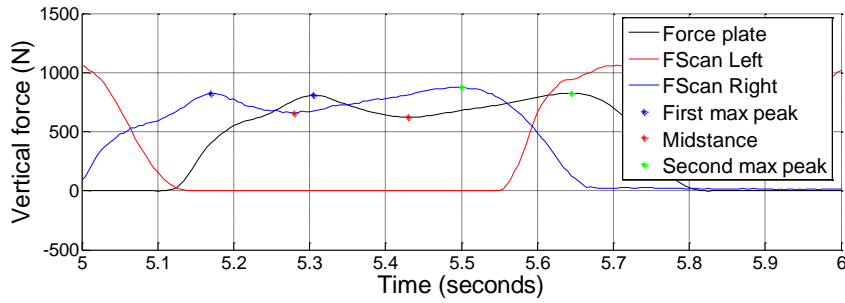


Figure 14: Vertical ground reaction force local maxima and minima

This method is repeated for all trials to determine the time delay and ensure that the FScan data occurs at the same real time as the other measuring equipment.

❖ Transform the FScan centre of pressure

The data captured in the local axis system of the FScan insole must be transformed into and located in the global capture volume.

Figure 15 shows an error between the FScan and force plate COPs. The aim is to minimize this error to match the COPs as closely as possible in the x- and y-directions. A rigid foot model is assumed because the COP is measured at a point on the foot where it is in contact with the ground.

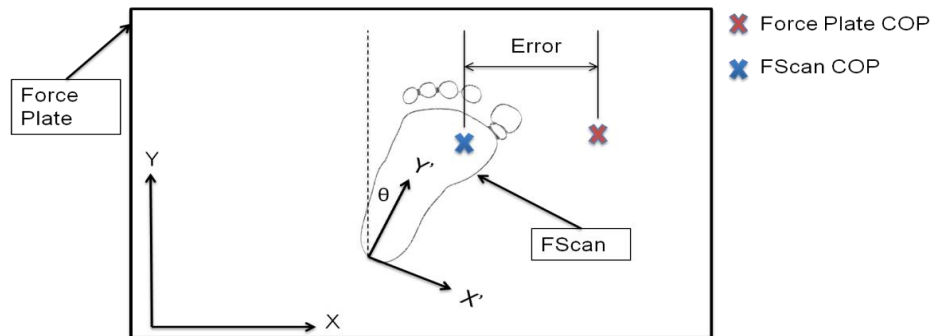


Figure 15: FScan co-ordinate axes (X'Y') relative to the capture volume co-ordinate axes (XY)

To determine the orientation of the local axis system and the position of the FScan in the capture volume, a numerical optimization (*fminsearch*, Matlab) is used that minimizes the error between the force plate COP and the FScan COP that has been transformed in the global frame.

$$Error = \sum_{t_i}^{t_f} (FP_x - FS_x)^2 + (FP_y - FS_y)^2 \quad (4.21)$$

The least square error is calculated by squaring the error in the x- and y-direction between the force plate COP (FP_x , FP_y) and FScan COP (FS_x , FS_y). Minimizing this

error will produce a value for the insole origin and angle of the local axes that successfully transforms the FScan into the global reference frame.

Equation 4.22 is used to calculate the FScan COP in the global reference frame (COP_{FSG}) using the COP measured by the FScan in the local reference frame (COP_{FSL}) and a rotation matrix, R_m .

$$COP_{FSG} = O_{FSG} + COP_{FSL} \times \begin{bmatrix} \cos(\theta) & -\sin(\theta) & 0 \\ \sin(\theta) & \cos(\theta) & 0 \\ 0 & 0 & 1 \end{bmatrix} \quad (4.22)$$

θ = angle between the local and global co-ordinate frames (local axes angle)

Within the numerical optimization used to minimize the least square error, different values are assigned to the origin of the FScan in the global reference frame (O_{FSG}) and the local axes angle used in the rotation matrix (R_m).

After determining the position of the FScan's origin and the local axes angle, the FScan must be tracked throughout stance phase to incorporate the complete GRF and COP of the foot not striking the force plate. Various methods were applied to track the FScan origin and the local axes angle using the trajectories of the heel and toe markers on the feet. The method that produced the best results is discussed here. The lessons learnt that led to the final method are:

- One cannot assume that the local axes angle at midstance is constant throughout the stance phase i.e. the angle of the foot does not remain constant during stance phase.
- The relationship between the heel marker and FScan origin and toe marker and FScan origin, continuously changes during stance phase because of the insole bending and slipping in the shoe.
- The origin of the FScan is located at the top left corner of the insole, therefore the toe marker is closer to the origin and bending of the insole during walking has a greater effect on the relationship between the heel marker and insole origin. Therefore, the origin is related to the toe marker.

To incorporate the FScan COP into the global axis system it is assumed that the foot angle is equal to the angle of the FScan insole (local axes angle). The foot angle is the angle between the global axis system and a vector between the heel marker and toe marker in the XY plane (or plane parallel to the ground). Thus in equation 4.22, theta is equal to the foot angle.

To determine the origin of the insole of the non-striking foot, three trials are used where the foot being investigated strikes the force plate. Using the method that will be explained, an average of the output of these three trials will be used to determine the position and orientation of the insole in a different trial (referred to as trial 2). The foot in trial 2 is not striking the force plate, thus the insole position and angle is unknown and cannot be solved for using a numerical optimization.

The method used to determine the FScan COP in the global axis system for a foot (referred to as the foot being investigated) not striking the force plate is summarized below. Steps 1 to 3 that follow are repeated for three trials where the foot being investigated strikes the force plate. For simplicity the method will be explained for one trial referred to as trial 1.

- A numerical optimization is applied in Matlab that minimizes the least square error (equation 4.21) and determines the origin of the FScan in the global axis system (equation 4.22) in trial 1. The optimization is applied throughout the stance phase at specified time steps, so that the origin position is known for the whole stance phase. The rotation matrix used at each time step is calculated using the foot angle of trial 1 (θ_{F1}).

$$\theta_{F1} = \tan^{-1} \left(\frac{T_{m,y1} - H_{m,y1}}{T_{m,x1} - H_{m,x1}} \right) \quad (4.23)$$

- The global FScan origin (O_{FSG}) position is related to the position of the toe marker (T_m) at each time step during stance phase in trial 1:

$$d_{OG,1} = T_{m,1} - O_{FSG,1} \quad (4.24)$$

- This relationship (d_{OG}) is then transformed into the local co-ordinate system (d_{OL}) using the same rotation matrix applied before:

$$d_{OL} = d_{OG,1} / \begin{bmatrix} \cos(\theta_{F1}) & -\sin(\theta_{F1}) & 0 \\ \sin(\theta_{F1}) & \cos(\theta_{F1}) & 0 \\ 0 & 0 & 1 \end{bmatrix} \quad (4.25)$$

- The procedure followed in steps 1 to 3 is repeated for two more trials in the same session for the same foot, where after an average value is calculated for the relationship between the origin and toe marker in the local reference frame. This average is used with data measured during trial 2 and is transformed into the global axis system using the foot angle (θ_{F2}). The foot angle for trial 2 is calculated using equation 4.23.

$$d_{OG,2} = d_{OL} \times \begin{bmatrix} \cos(\theta_{F2}) & -\sin(\theta_{F2}) & 0 \\ \sin(\theta_{F2}) & \cos(\theta_{F2}) & 0 \\ 0 & 0 & 1 \end{bmatrix} \quad (4.26)$$

- This relationship is used with the trajectory of the toe marker in trial 2 ($T_{m,2}$) in stance phase to calculate the position of the FScan origin in global co-ordinates:

$$O_{FSG,2} = T_{m,2} - d_{OG,2} \quad (4.27)$$

- Finally, the calculated origin and FScan COP measured during trial 2 are used to calculate the FScan COP in the global axis system.

$$COP_{FSG,2} = O_{FSG,2} + COP_{FSL,2} \times \begin{bmatrix} \cos(\theta_{F2}) & -\sin(\theta_{F2}) & 0 \\ \sin(\theta_{F2}) & \cos(\theta_{F2}) & 0 \\ 0 & 0 & 1 \end{bmatrix} \quad (4.28)$$

❖ Estimate the complete ground reaction force with FScan data

The FScan insole pressure measurement system only measures a force normal to the foot. Therefore, the mediolateral (ML) and anteroposterior (AP) friction forces between the foot and ground are not measured. Figure 16 (a) and (b) show exaggerated images of how the normal force measured by the FScan can be broken up into the ML and AP directions in the global capture volume.

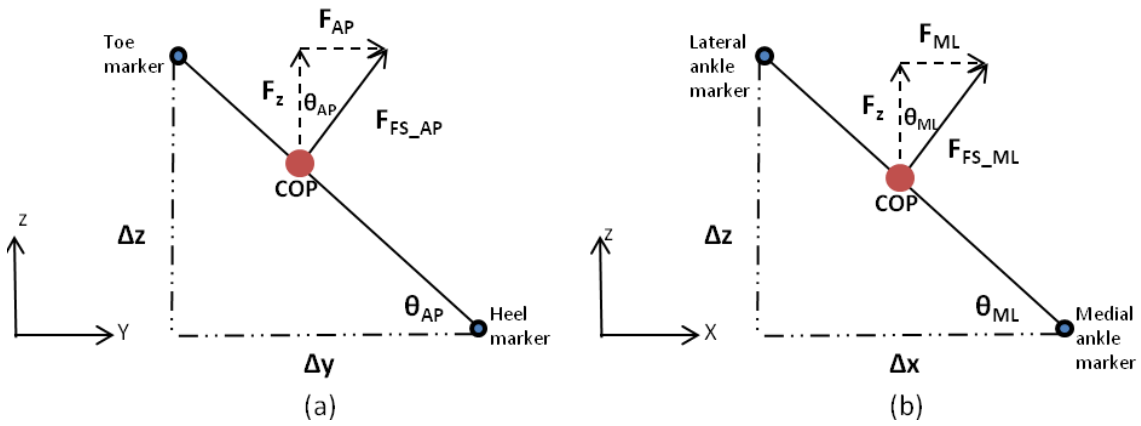


Figure 16: FScan force in the (a) mediolateral and (b) anteroposterior directions

The heel and toe markers (H_m and T_m) are used to determine the angle of the foot relative to the x- and z-axis, while the medial and lateral ankle markers (A_M and A_L) are used to determine the angle of the foot relative to the y-axis (Figure 16). The anteroposterior foot angle/flexion-extension angle (θ_{AP}), and mediolateral foot angle/tilt angle (θ_{ML}) are calculated as shown below.

$$\theta_{AP} = \tan^{-1} \left(\frac{T_{m,z} - H_{m,z}}{T_{m,y} - H_{m,y}} \right) \quad (4.29)$$

$$\theta_{ML} = \tan^{-1} \left(\frac{A_{L,z} - A_{M,z}}{A_{L,x} - A_{M,x}} \right) \quad (4.30)$$

These angles are used in the rotation matrix shown in equations 4.31, to rotate the normal force vector in such a way that the force is broken up into the global reference frame directions to match the forces measured by the force plate.

$$RT = \begin{bmatrix} \cos(\theta_{ML}) & 0 & \sin(\theta_{ML}) \\ 0 & 1 & 0 \\ -\sin(\theta_{ML}) & 0 & \cos(\theta_{ML}) \end{bmatrix} \times \begin{bmatrix} 1 & 0 & 0 \\ 0 & \cos(\theta_{AP}) & -\sin(\theta_{AP}) \\ 0 & \sin(\theta_{AP}) & \cos(\theta_{AP}) \end{bmatrix} \quad (4.31)$$

A similar approach as is applied to the FScan COP is applied to the FScan reaction force. In this method the anteroposterior and mediolateral foot angles are related to the actual mediolateral and anteroposterior foot angles ($\theta_{ML,a}$ and $\theta_{AP,a}$), respectively. The actual angles are computed using a numerical optimization (*fminsearch*, Matlab) where a least square sum is minimized as shown in equation 4.32. To perform the optimization, a trial is used where the foot being investigated strikes the force plate (this trial is referred to as trial 1). The force measured by the force plate ($F_{FP,1}$) is compared to the GRF computed from the FScan data ($F_{FSG,1}$) throughout the duration of the stance phase in trial 1.

$$\min \left(\sum_{t_i}^{t_f} (F_{FP,1} - F_{FSG,1})^2 \right) \quad (4.32)$$

, where

$$F_{FSG,1} = \begin{bmatrix} 0 \\ 0 \\ F_{FSL,1} \end{bmatrix} \times RT_{actual} \quad (4.33)$$

In equation 4.33 the normal force measured by the FScan (F_{FSL}) is multiplied by the actual total rotation matrix (RT_{actual}), which is computed using equation 4.31 and the actual foot angles. The actual angles are then related to the original foot angles from trial 1 that are determined using equation 4.29-30.

$$d_{ML} = \theta_{ML,1} - \theta_{ML,a} \quad (4.34)$$

$$d_{AP} = \theta_{AP,1} - \theta_{AP,a} \quad (4.35)$$

The relationships shown in equations 4.34-35 are computed throughout stance phase. These variables are then used in a trial (trial 2) where the same foot is not striking the force plate, and hence its force has to be included in the analysis. The computed mediolateral and anteroposterior foot angles ($\theta_{ML,c}$ and $\theta_{AP,c}$) are calculated using the difference in angles calculated in equations 4.34-35 and the foot angles computed using the markers in trial 2 (equations 4.29-30).

$$\theta_{ML,c} = d_{ML} - \theta_{ML,2} \quad (4.36)$$

$$\theta_{AP,c} = d_{AP} - \theta_{AP,2} \quad (4.37)$$

The foot angles are computed using two more trials where the foot being investigated strikes the force plate. Averages of the computed foot angles for the three trials are used in a computed total rotation matrix ($RT_{computed}$) using equation 4.31 to determine the complete GRF ($F_{FSG,2}$) calculated using the FScan force.

$$F_{FSG,2} = \begin{bmatrix} 0 \\ 0 \\ F_{FSL,2} \end{bmatrix} \times RT_{computed} \quad (4.38)$$

4.2.2 Force plate superimposition

An alternative to using the FScan pressure measurement insoles is to superimpose an average force and COP onto the foot not striking the force plate. These average values are computed using trials where the foot being investigated struck the force plate, i.e. if GRF data is superimposed onto the right foot, the average force and COP are computed using the trials where the right foot struck the force plate.

Before computing average GRF and COP values for each foot, the free moment (or frictional torque) applied to the foot as a result of the ground reaction forces must be computed. The free moment (T_{ZFP}) is computed using the rotational moment on the force plate (M_Z) caused by the frictional forces on the force plate in the mediolateral ($F_{FP,x}$) and anteroposterior ($F_{FP,y}$) directions.

$$T_{ZFP} = M_Z - F_{FP,y} \times a_x + F_{FP,x} \times a_y \quad (4.39)$$

The variables a_x and a_y are the distances from the COP to the centre of the force plate in the x- and y-directions, respectively. Once the free moment has been calculated for each trial, the superimposition method can be applied.

For the superimposition method the trials where the left foot strikes the force plate (from here on referred to as left foot trials) are grouped together and the trials where the right foot strikes the force plate (from here on referred to as right foot trials) are grouped together. An average GRF, free moment and COP is calculated for each foot of each subject using the data from the specific subject where the foot being superimposed struck the force plate. The following method is applied to the recorded data of each subject to superimpose the COP, GRF and free moment on the foot not striking the force plate during stance phase (assume the method is being applied to the right foot):

- Trials where subject A's right foot strikes the force plate are identified.
- The measurement data obtained during stance phase for each trial is interpolated so that all of the trial's data are contained in vectors of equal lengths. This includes the motion capture and force plate data.
- To determine where the forces and free moment are acting, the average COP is first determined. The position of the COP measured in each trial at stance phase is related to the toe (T_m) and heel markers (H_m) of that trial in the same time period as shown in equations 4.40-41.

$$dT = T_m - COP_{FP} \quad (4.40)$$

$$dH = H_m - COP_{FP} \quad (4.41)$$

- The average of these relationships for the right foot trials is then computed (assume there are three right foot trials).

$$dT_{SI} = [mean(dT_{x1 \rightarrow 3}) \quad mean(dT_{y1 \rightarrow 3}) \quad mean(dT_{z1 \rightarrow 3})]' \quad (4.42)$$

$$dH_{SI} = [mean(dH_{x1 \rightarrow 3}) \quad mean(dH_{y1 \rightarrow 3}) \quad mean(dH_{z1 \rightarrow 3})]' \quad (4.43)$$

- Once the average toe and heel marker relationships (dT_{SI} and dH_{SI}) are calculated, the average GRF (F_{SI}) and free moment (Tz_{SI}) applied to the right foot in the three trials during stance phase is computed as shown in equations 4.44-45.

$$F_{SI} = [mean(F_{FP,x1 \rightarrow 3}) \quad mean(F_{FP,y1 \rightarrow 3}) \quad mean(F_{FP,z1 \rightarrow 3})]' \quad (4.44)$$

$$Tz_{SI} = mean(Tz_{FP,1 \rightarrow 3}) \quad (4.45)$$

- The mean relationships, forces and moment calculated in steps four and five are superimposed onto a right foot that is not striking the force plate during a left foot trial. The heel strike and toe off events of the foot not striking the force plate are determined using a PiG model in Nexus software.
- The foot is not rigid during stance phase. Therefore the mean heel marker relationship (dH_{SI}) is used to compute the COP from heel strike to midstance together with the heel marker of the foot not striking the force plate (H_{m_other}). The mean toe marker relationship (dT_{SI}) is used to compute the COP from midstance to toe off together with the toe marker of the foot not striking the force plate (T_{m_other}).

$$COP_{SI_{HS \rightarrow MS}} = H_{m_other_{HS \rightarrow MS}} - dH_{SI_{HS \rightarrow MS}} \quad (4.46)$$

$$COP_{SI_{MS \rightarrow TO}} = T_{m_other_{MS \rightarrow TO}} - dT_{SI_{MS \rightarrow TO}} \quad (4.47)$$

- After the average COP (COP_{SI}) is superimposed onto the foot not striking the force plate, the average force (F_{SI}) and free moment (Tz_{SI}) can be applied at these positions during stance phase.

4.3 Results

To compare the FScan and superimposition methods put forward, they will be applied to the foot striking the force plate and the results will be compared to the actual measured GRF data measured by the force plate. Experimental data is used from two subject's three left foot trials. For each trial, the other two trials are used to generate the averages used to determine the COP and GRF, where after the resulting COP and GRF is compared to the actual experimental data.

4.3.1 Locating the centre of pressure results

The results for the first trial of three for subject one and subject two are shown in Figure 17. The remaining trials COP comparisons are shown in Appendix A.

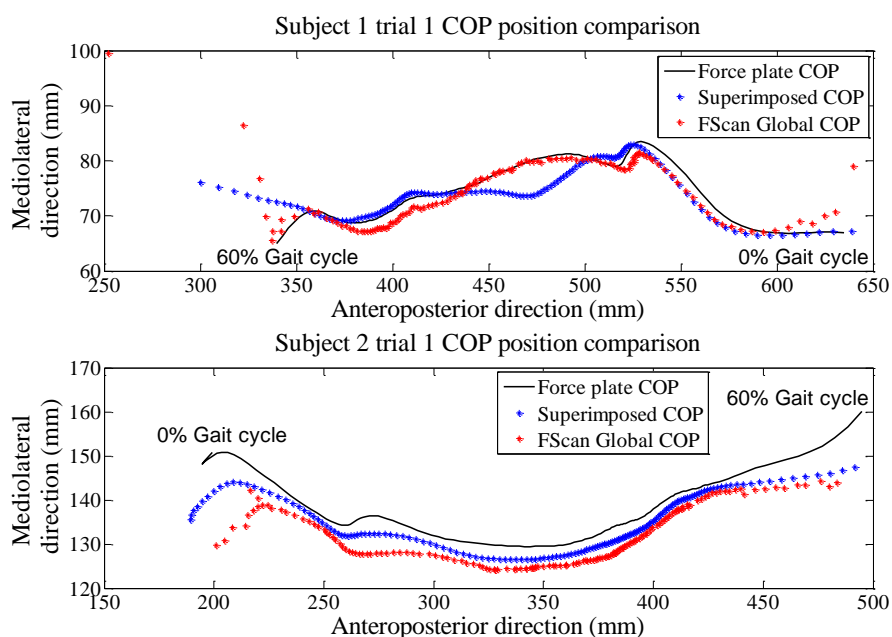


Figure 17: Subject 1 trial 1 and Subject 2 trial 1 COP position comparisons for superimposed and FScan methods

When inspecting Figure 17 visually, one can see that both methods struggle to correlate well with the force plate measurement from heel strike to the end of the loading response (0-10 % of gait cycle) and from terminal stance to toe off (50-60 % of gait cycle). Table 4 compares the average correlation coefficient, COD (R^2) and RMS errors in the mediolateral (ML) and anteroposterior (AP) directions for two subject's data on which both methods are applied to three trials.

Table 4: Estimated COP position comparison between the FScan and superimposition methods

Subject	Direction	Method	Correlation coefficient, R [R^2]	RMS error (mm)	RMSE % of length
1	ML	FScan	0.781 [0.624]	3.98 - 9.41	17.8 - 42
		Superimpose	0.487 [0.352]	2.55 - 10.93	11.4 - 48.8
	AP	FScan	0.992 [0.984]	7.13 - 10.78	2.4 - 3.6
		Superimpose	0.992 [0.985]	7.44 - 13.39	2.5 - 4.5
2	ML	FScan	0.794 [0.641]	5.77 - 8.58	18.2 - 27.1
		Superimpose	0.928 [0.862]	2.96 - 5.06	9.3 - 16
	AP	FScan	0.994 [0.989]	8.43 - 17.27	2.7 - 5.5
		Superimpose	0.998 [0.99]	2.33 - 6.86	0.7 - 2.2

For subject one the COD in the mediolateral direction for the both methods indicates that the methods produce a COP that is on average 62.4 % and 35.2 % similar to the measured COP. In comparison, in the anteroposterior direction the FScan and superimposition methods produce a COP that is 98.4 % and 98.5 % similar, respectively. For subject two the superimposition method produces a COP that on average correlates strongly with the measured COP in both the mediolateral (0.928) and anteroposterior (0.998) directions. In comparison, the FScan method doesn't correlate as strongly in the mediolateral direction (0.794), but correlates well in the anteroposterior direction (0.994).

The RMS errors in the mediolateral direction for both subjects using both methods are less than that of the anteroposterior direction. However one must look at this relatively as the COP in the mediolateral direction spans over an average length of 22.4mm for subject one and 31.7mm for subject two. Whereas it spans over a length of 298.7mm and 312.6mm for subject one and two in the anteroposterior direction. Therefore, the mean RMS error is 31.3 % and 30.5 % of the total length covered in the mediolateral direction for subject one using the FScan and superimposition methods, respectively. In comparison, in the anteroposterior direction, the mean RMS error is 3 % and 3.4 % of the total length covered in the anteroposterior direction for the FScan and superimposition methods respectively.

4.3.2 Estimation of complete ground reaction force results

The GRF for subject one estimated using both the FScan and superimposition methods is shown in Figure 18 and compared statistically in Table 5.

Table 5: FScan and superimposition complete GRF estimation comparison

Subject	Measure	Method	Correlation coefficient, R [R ²]	RMS error
1	ML force	FScan	0.853 [0.738]	15.42 – 29.96 N
		Superimpose	0.979 [0.959]	3.97 – 8.06 N
	AP force	FScan	0.977 [0.954]	12.12 – 41.99 N
		Superimpose	0.996 [0.992]	9.429 – 10.17 N
	Vertical force	FScan	0.973 [0.946]	56.33 – 82.95 N
		Superimpose	0.988 [0.977]	31.69 – 43.04 N
Free moment	Superimpose	0.731 [0.535]	1.27 – 2.57 Nm	
2	ML force	FScan	0.468 [0.222]	29.97 – 167.6 N
		Superimpose	0.903 [0.817]	7.25 – 11.84 N
	AP force	FScan	0.992 [0.984]	17.04 – 22.18 N
		Superimpose	0.997 [0.993]	8.26 – 15.07 N
	Vertical force	FScan	0.952 [0.906]	90.37 - 123 N
		Superimpose	0.993 [0.985]	30.42 – 54.5 N
	Free moment	Superimpose	0.828 [0.696]	0.96 – 2.65 Nm

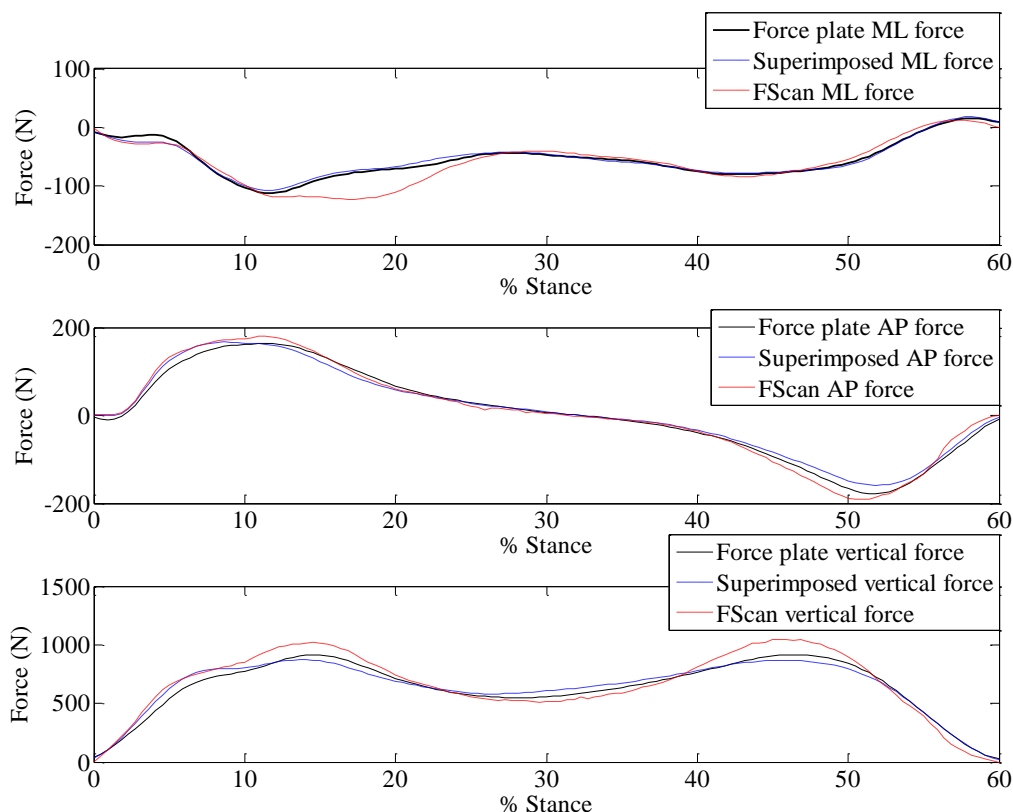


Figure 18: Subject 1 trial 1 comparison of GRF estimation for superimposed and FScan methods

The estimated GRF computed using the superimposition method correlated well with the measured GRF for both subject one and subject two as shown in Table 5. The lowest mean correlation coefficient is 0.979 ($R^2 = 0.959$) for subject one and 0.903 ($R^2 = 0.817$) for subject two both in the mediolateral direction. In contrast, the FScan method produced a GRF that does not correlate as well with the measured GRF. The lowest mean correlation coefficient achieved using the FScan method also occurs in the mediolateral direction, and is 0.853 ($R^2 = 0.738$) for subject one and 0.468 ($R^2 = 0.222$) for subject two.

For both subjects the FScan method produces mean RMS errors, which are in all cases except one, more than double those produced by the superimposition method (Table 5). However, the GRF calculated using the FScan method correlates well with the measured GRF in both the AP and vertical directions ($R > 0.9$), but the superimposition produces a GRF that correlates better in each case.

The free moment computed using the superimposition method achieves a mean correlation coefficient of 0.731 ($R^2 = 0.535$) using subjects one data and 0.828 ($R^2 = 0.696$) for subject two when compared to the actual free moment (Figure A.10 to Figure A.14).

4.3.3 Resulting knee moment comparison

The GRF and COP estimated using the FScan and superimposition methods are used in an ID analysis to compute the knee moment shown in Figure 19.

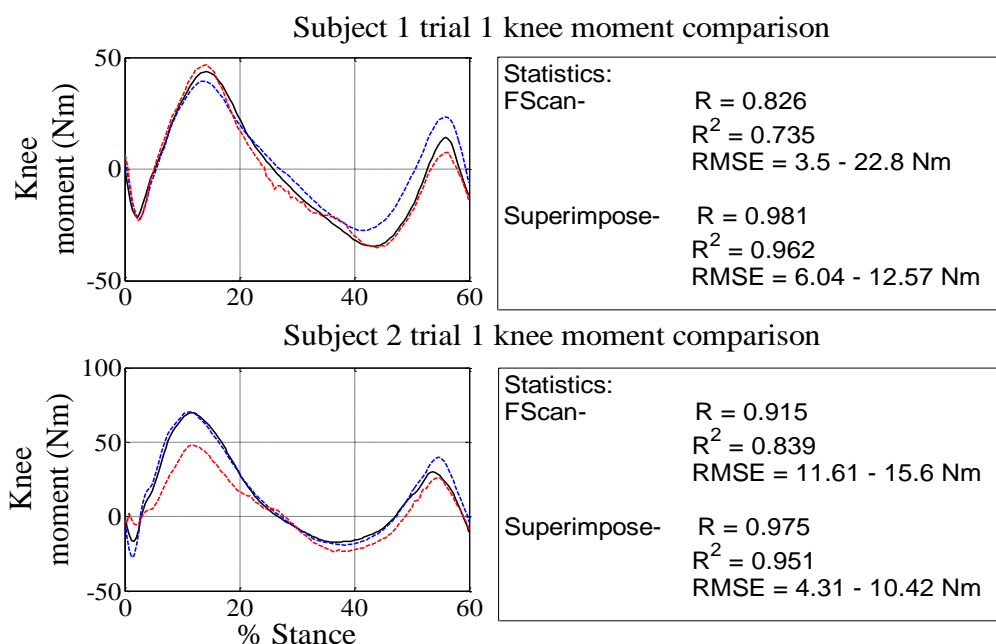


Figure 19: Knee moment comparisons for superimposed and FScan methods with statistical comparison (Force plate moment = solid black line, Superimposed moment = dotted blue line, FScan moment = dotted red line)

The resulting knee moment produced from the ID analysis using the FScan method and superimposition method is compared to the knee moment generated using the measured GRF data. The mean correlation coefficient for both subjects using the superimposition method is 0.978 ($R^2 = 0.957$), whereas using the FScan method the mean coefficients are 0.871 ($R^2 = 0.787$). The RMS error is on average 5.18 to 11.5 Nm for the superimposition method and 7.56 to 19.2 N using the FScan method.

4.4 Discussion

4.4.1 Locating the centre of pressure

For both the superimposition and FScan methods the foot is approximated to be a rigid foot model, meaning no bending or twisting of the foot is accounted for. Through doing this, larger errors are introduced for the first 10 % of the gait cycle (heel strike to the end of loading response) and during 50 to 60 % of the gait cycle (terminal stance to toe off). The reason for this is due to the foot bending in these stages of stance phase, and the COP is calculated in both methods using the position of the heel and toe marker which are not on the ground during toe off and heel strike, respectively. Therefore, the COP is no longer just a function of the difference

in the mediolateral and anteroposterior directions, but is also dependant on the difference in the vertical direction. This will introduce more errors.

For the remaining duration of stance phase (10 to 50 % of gait cycle) the foot is relatively flat on the ground and a rigid foot model approximation is more accurate. This is evident in Figure 17 where both methods produce a COP that visually better approximates the measured COP. The accuracy parameters in Table 4 show that the COP is estimated more accurately in the anteroposterior direction in comparison to the mediolateral direction. This is due to the variability between trials in the shape of the curve that the COP follows in the mediolateral direction compared to the anteroposterior direction. Meaning, in stance phase the weight of the foot is transferred from the posterior side of the foot to the anterior side of the foot without changing direction. However, the same cannot be said about the mediolateral direction as during stance phase the weight often shifts from the medial side of the foot to the lateral side of the foot and *vice versa*. This makes it more difficult to follow the path of the COP in the mediolateral direction.

Similar approaches were applied by Chumanov *et al.* [61] and Forner-Cordero *et al.* [54] using insole pressure measurement devices. Chumanov and Forner-Cordero both assume a rigid foot model and make use of a numerical optimization to minimize the least square error between the insole and force plate COP. Chumanov *et al.* uses a piecewise cubic spline interpolation to define 100 virtual markers from ten motion capture markers around the periphery of the foot. The position of the insole sensel (individual pressure sensors that make up the insole) is related to three virtual markers around it and is tracked using the position of the virtual markers. The COP location during each frame of the motion trial is computed using the position of the sensel in the global reference frame and the measured pressure [61].

Chumanov *et al.* reports COP RMS errors less than 8 mm in the mediolateral direction and less than 12 mm in the anteroposterior direction for 10 to 80 % of stance phase. Forner-Cordero achieves mean COP RMS errors of 15 mm ($R = 0.949$) and 11 mm ($R = 0.491$) in the anteroposterior and mediolateral directions, respectively. Both Chumanov and Forner-Cordero found that the errors were larger during heel contact and prior to toe off. Using an average of both subject's results for the FScan and superimposition methods, this project achieved COP RMS errors of 7.07 mm ($R = 0.7875$) and 5.43 mm ($R = 0.7075$) in the mediolateral direction, and 11.31 mm ($R = 0.993$) and 7.725 mm ($R = 0.995$) in the anteroposterior direction. It is clear that the superimposition method estimates the COP more closely and is in the same range as results reported in literature, but the results are for the whole of stance phase. The FScan method is still able to produce results that are within the same range as those reported in literature.

4.4.2 Estimation of complete ground reaction forces

Once the COP of the force on the foot is estimated, the complete GRF must be calculated. Table 5 and the accompanying figures show that the superimposition

method approximates the complete GRF more accurately than the FScan method. The FScan method produces GRF RMS errors that are more than double that of the superimposition method. It is important to note that the RMS errors in each direction must be analysed relative to the maximum forces measured in each direction, i.e. the largest RMS error occurs in the vertical direction, but the largest forces are also experienced in the vertical direction.

Amongst others, studies conducted by Fong *et al.* [62] and Forner Cordero *et al.* [54] put forward methods to estimate the complete GRF on the foot using measurements from pressure insoles. Fong *et al.* makes use of a stepwise linear regression method to reconstruct the value of the normal GRF measured by each sensel, to match the three-dimensional GRF measured by the force plate [62]. Fong *et al.* achieved GRF RMS errors of 11.71 N (R = 0.719), 27.41 N (R = 0.928), and 45.79 N (R = 0.989) in the mediolateral, anteroposterior, and vertical directions respectively.

Forner Cordero *et al.* applied a less statistical approach. The total COP is calculated using the individual COP measured by the left and right foot respectively [53]. An inverse dynamic analysis is done on the whole body using motion data to determine the total reaction forces. It is assumed that the total vertical force measured by the left and right insole combined determined the total COP. The distance from the total COP to the COP of the left and right foot is then computed in the x-, y- and z-direction. These distances together with the total reaction forces obtained with the inverse dynamic analysis are used to compute the three-dimensional GRF on each foot in the trial. The GRF RMS errors obtained in this study are 7.3-7.51 N (R = 0.778-0.818), 7.53-9.15 N (R = 0.977-0.979), and 27.84-30.13 N (R = 0.995-0.997) in the mediolateral, anteroposterior, and vertical directions respectively.

Although the FScan method applied in this project is not able to generate the GRF as accurately as the studies mentioned, the superimposition method is able to and one can calculate the free moment on the foot using this method. A disadvantage when using the FScan pressure measurement system is that it does not measure the moment on the insole, therefore one cannot calculate the free moment occurring on the foot. The correlation between the superimposed free moment and actual free moment isn't as strong as the correlation between the forces (Table 5). This is due to the fact that the free moment is calculated using the estimated COP position as well as the estimated GRF. Therefore, errors accumulate and lead to a lower correlation coefficient.

4.4.3 Resulting knee moment comparison

It is important that an accurate knee moment is replicated since this will later be used to determine the muscle forces acting on the knee and will reduce the errors during the RRA and CMC analyses in OpenSim (this will be discussed later). Figure 19 shows that the superimposition method more accurately calculates the knee moment when comparing to the knee moment computed using the actual GRF data.

Besides methodical and computational errors, other factors contribute to errors in the FScan method. The insole can slip in the shoe which results in crinkling. This crinkling effects both the COP and force measurement as it activates the load cells in the insole sensor. The damping caused by the sole of the shoe is not taken into consideration, as well as the different thickness of the subject's shoes. This can have an effect on the force measured by the pressure insole. It is also important to note that the insole only measures a normal force which comprises of frictional and vertical forces.

The superimposition method assumes that the GRF data measured during each trial of the same subject is repeatable. This is not always the case as sometimes a subject will walk slower or strike the ground with a larger force. This results in a different COP and GRF. However, the superimposition method produces more accurate results when comparing to the actual GRF data measured by the force plate and compares well to methods put forward in literature. Therefore, the superimposition method is applied to the foot not striking the force plate in the computational pipeline put forward in this project.

Chapter 5

OpenSim analyses

5.1 Introduction

Chapter 3 and 4 describe how kinetic and kinematic data is obtained that can be used to propel a musculoskeletal model in order to replicate the movement performed by a subject in a motion lab. The steps followed to determine the force that needs to be generated by the muscles surrounding the knee joint to produce said motion, are explained in chapter 5. These steps are performed using the OpenSim tools and are executed as shown in Figure 20.

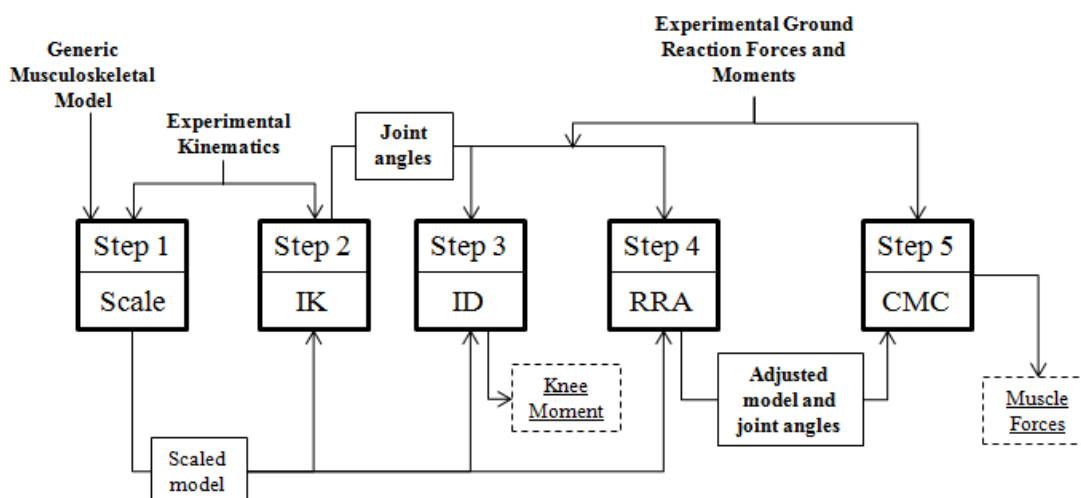


Figure 20: OpenSim modelling pipeline

5.2 Methods

This section explains the full OpenSim modelling pipeline used in this project with the aid of a flow diagram shown in Figure 21. Section 2.2.1 explains how each OpenSim tool used in this project works and the function thereof, therefore this section focuses on how the tool is used to compute the desired outputs.

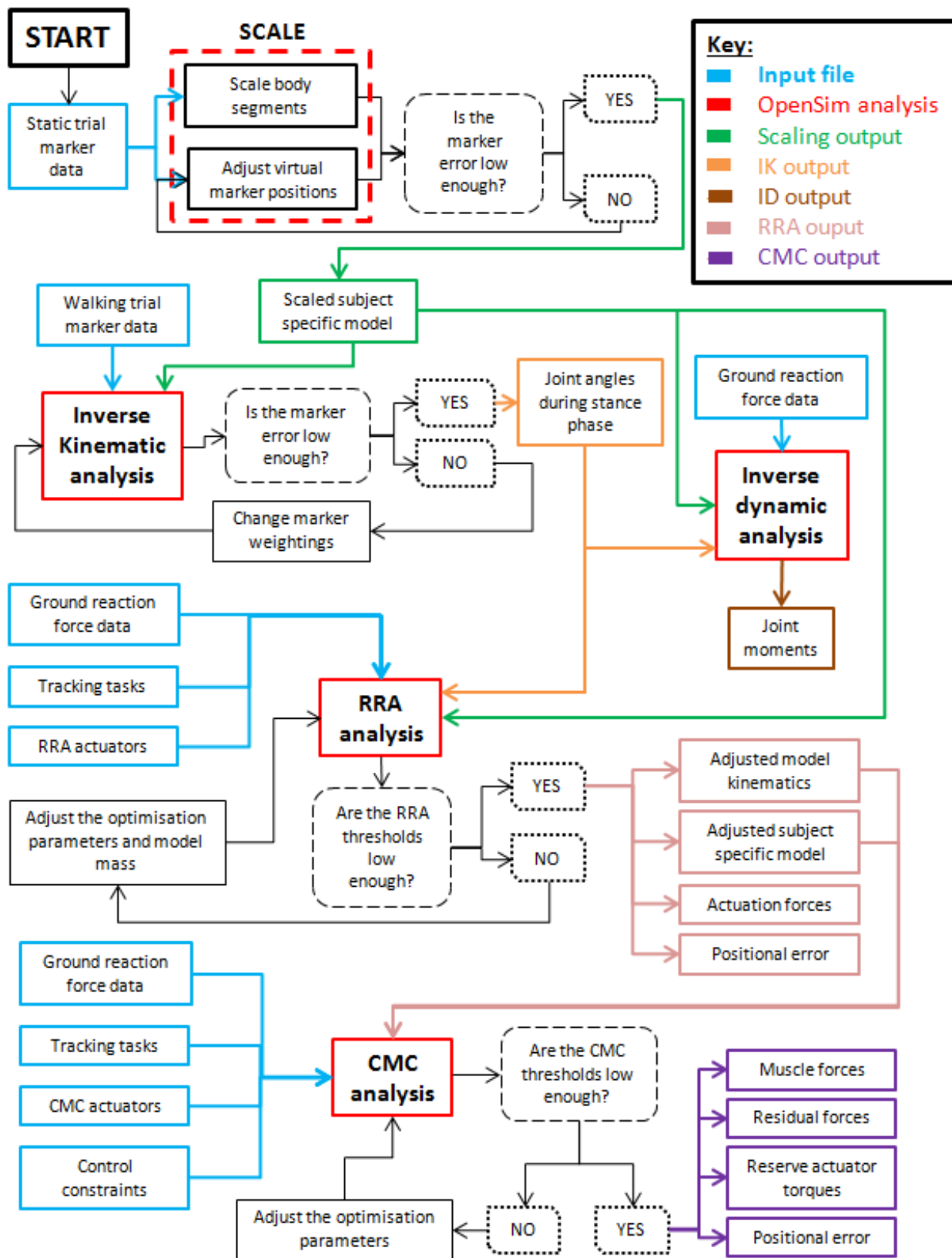


Figure 21: Detailed OpenSim pipeline flow diagram

5.2.1 Step 1 – Scaling

The aim of the scaling tool is to use motion capture data to scale a generic model to match the anthropometric properties of the subject being tested and to reduce the difference in position between the experimental and virtual markers. Using the scale tool, a subject specific model is created for each subject with the aid of photographs taken in the laboratory (Figure 22).



Figure 22: Marker placement on the subject and scaled model

To scale the generic model, markers on bony landmarks are given higher weightings, as you are more certain of their position. The remaining markers are manually adjusted in an iterative manner until the marker error is satisfactory. One can choose to preview the adjusted marker positions and ensure that they agree with the picture before applying the adjustment.

After scaling the model, OpenSim displays maximum and RMS marker errors for the marker with the largest positional difference between the virtual and experimental markers. OpenSim advises that one obtain a RMS marker error under 1 cm, and a maximum marker error for bony landmarks less than 2 cm. The marker positions are adjusted until the marker errors are below these values.

5.2.2 Step 2 – Inverse kinematic analysis

The Inverse Kinematic (IK) tool determines joint angles during each time frame to match the virtual marker positions to the experimental marker positions so that the model follows the same movement as the subject in the laboratory. The joint angles as a function of time are the output results from the IK tool using the scaled musculoskeletal model from scaling and marker trajectories captured during walking trials as inputs.

As is with the scaling tool, the error between the experimental and virtual marker positions must be minimized to ensure the trajectories are followed as closely as possible. According to OpenSim the RMS and maximum marker errors must be less than 2 cm and 4 cm, respectively.

The knee flexion-extension angle (referred to as knee angle) and hip flexion, adduction and rotation angles resulting from the IK analysis are compared to the same angles measured using a full body Nexus Plug-In Gait (PiG) model in the motion laboratory. The angles measured with the PiG model are the gold standard for this project. There are four differences between the PiG and OpenSim models:

- The OpenSim model is scaled to match the anthropometric properties of the subject, whereas the PiG model is constructed using the actual marker measurements and measured anthropometric properties of the subject.
- The OpenSim model approximates the knee as a one degree of freedom hinge joint, whereas the PiG model has three degrees of freedom (flexion-extension, adduction-abduction and rotation).
- There is an angular offset between the OpenSim hip flexion angle and the PiG model hip flexion angle.
- The OpenSim model used in this project has locked subtalar and MTP joints for both legs.

Because of the offset between the OpenSim and PiG model hip flexion angle; the results are compared to each other by comparing the difference between the left and right hip flexion angles of each model during stance phase. Within the results this difference is referred to as the hip flexion angle.

5.2.3 Step 3 – Inverse Dynamic analysis

The ID tool is applied to the scaled model after the joint angles have been determined for each time step in the trial. The ID tool is used to compute the net torques at each joint that are a result of the specific movement of the model and the GRF applied to the model. The movement of the model is determined using joint angles obtained with the IK tool.

A superimposition method is used to apply an average GRF to the foot not striking the force plate. However, for the non-torso trials that are only used for the OpenSim modelling steps up to and including the ID analysis, it is not necessary to superimpose a force onto the non-striking foot since the moment at the knee is calculated from the ground up and is not affected by the force on the other leg. Therefore, the superimposition method is only used with subject data that contains the torso kinematics. The computed knee flexion-extension moment (from here on referred to as knee moment) is used in an in-house muscle model that makes use of EMG measurements to determine muscle forces in the knee. The joint moment is also used in the RRA and CMC analyses in trials that contain torso kinematics.

5.2.4 Step 4 – Residual Reduction Algorithm analysis

The RRA tool is used to minimize the effects of modelling and marker errors that accumulate and lead to large nonphysical forces on the pelvis known as residual forces. These forces compensate for the aforementioned errors. More specifically

the tool alters the mass centre of the model's torso and allows the kinematics of the model to vary in order to be more dynamically consistent with the GRF data.

The inputs for the RRA tool are the scaled subject specific model, the model kinematics obtained using the IK tool, the measured GRF data, RRA tracking tasks and RRA actuators. The tracking task file indicates which joint angles from the model kinematics file must be tracked and how 'closely' that joint angle must be tracked using a weighting. Within the tracking task file position and velocity feedback error gains (k_p and k_v) are also specified for each muscle. These optimization parameters are used by the RRA tool to ensure that when the errors between model and experimental parameters are reducing to zero, this is done in a critically damped manner (i.e. without over-shooting or over-damping).

The RRA actuator input file contains the ideal joint actuators used to replace the model's muscles. Within this file the residual and reserve actuators which are to be applied and their parameters are specified. The specified parameters include the maximum and minimum force, and location of each actuator. The RRA tool determines what force each actuator must apply to enable the model to reproduce the subjects' kinematics. The residual forces determined using the RRA tool are applied to the centre of mass (COM) of the pelvis. These forces compensate for model assumptions such as the upper extremity of the model not having arms.

Once the RRA is run, the COM of the torso is adjusted and OpenSim provides the user with suggested mass adjustments for each body segment of the model. These adjustments will ensure that the model is more dynamically consistent with the GRF data. The outputs of the RRA analysis are the adjusted model kinematics, an adjusted subject specific model, the residual forces, and the positional error between the input kinematics and the resulting adjusted model kinematics.

The reason for wanting low residual forces is to ensure that the model motion is generated by internal joint moments and not the residual forces. Low positional errors indicate that the adjusted kinematics produced by the RRA tool follow the kinematics produced by the IK tool more closely. If the RRA results are not within the limits, the optimisation parameters are altered and the mass adjustments suggested by OpenSim are made, where after the RRA analysis is run again.

5.2.5 Step 5 – Computed Muscle Control analysis

The final step in the OpenSim pipeline is the CMC analysis. It is used to compute a set of muscle excitations that will drive the subject specific musculoskeletal model to track the kinematics from the RRA analysis in the presence of the GRF data measured in the motion lab. Hence, the muscle forces that are responsible for the subject's movement in the motion lab are computed.

Other inputs into the CMC tool are CMC tracking tasks, CMC actuators, and control constraints. As is with the RRA tool, the CMC tracking tasks file specifies which

joint angles must be tracked in the adjusted model kinematics file and how strongly these co-ordinates must be tracked according to a tracking weight. The CMC actuator file performs the same function as the RRA actuator file does for the RRA tool. It contains the residual and reserve actuators and their parameters.

The control constraints file comprises of the limits on model actuators, which include muscles, residual and reserve actuators. The maximum and minimum muscle excitation for each muscle is specified within this file. Furthermore, the CMC tool computes reserve actuator torques for each joint of the model. The reserve actuator torques are moments that act around each joint to assist the muscle forces, enabling the simulation to run. These torques are activated when the muscle cannot produce the force to produce the movement at a specific time.

The main aim of the CMC tool is to calculate the muscle forces that result when the desired kinematics are applied to the subject specific musculoskeletal model. Other outputs include residual forces and moments acting on the pelvis and the positional error between the applied kinematic data and the resulting kinematics of the CMC tool. One aims to minimize the residual and reserve torques so that the model's motion is a result of the muscle actuation. It is also important to keep the positional error as low as possible so that the motion of the model resembles the motion of the subject in the lab as closely as possible.

5.3 Results

5.3.1 Scaling results

All subjects' musculoskeletal models were scaled successfully and achieved RMS and maximum errors under 1 cm and 2 cm, respectively, as shown in Table 6.

Table 6: Scaling marker errors for six random subjects

Subject	RMS error (cm)	Maximum error (cm)
1	0.58	1.10
2	0.45	0.72
3	0.68	1.40
4	0.84	1.54
5	0.70	1.17
6	0.71	1.37

5.3.2 Comparison between torso and non-torso trials

The majority of the subjects tested in the motion lab were tested without markers on the upper extremity. It is important to prove that the knee moment computed using a model without a torso is still accurate when compared to a model with a torso. This subsection provides a comparison between the joint angles and knee moment achieved using three left foot and three right foot trials of the same

subject's data used with a model with and without a torso. The results show the average values for the three trials of each foot.

The comparison between the calculated joint angles and knee moment for a model with and without a torso is shown in Table 7.

Table 7: Comparison between the measured joint angles and knee moment for a model with and without a torso

Foot	Measure	COD (R^2)	RMS error (degrees)
Left	Knee flexion	0.9998	0.2 – 0.23 degrees
	Hip flexion	0.9999	0.26 – 0.69 degrees
	Hip adduction	0.9925	0.32 – 0.5 degrees
	Hip rotation	0.9987	0.39 – 0.46 degrees
	Knee moment	0.9996	0.62 - 0.74 Nm
Right	Knee flexion	0.9999	0.19 – 0.25 degrees
	Hip flexion	0.9998	0.49 – 0.94 degrees
	Hip adduction	0.9962	0.26 – 0.45 degrees
	Hip rotation	0.9993	0.48 – 0.54 degrees
	Knee moment	0.9996	0.62 - 0.74 Nm

All joint angles computed using a model without a torso match the joint angles computed using a model with a torso with an accuracy of 99 % (Figure B.1 and Figure B.2). The average RMS errors further enforce this point, as the largest RMS error is 0.937° for the right hip flexion angle. When comparing the computed knee moment for both the left and the right foot, a COD of over 0.999 is achieved for all trials. The largest knee moment RMS error is 0.74 Nm.

5.3.3 Repeatability study

An intra-subject repeatability study is completed to determine whether data measured for the same subject produces repeatable results when used in the OpenSim modelling pipeline. The study is done using three successful trials from either the left or right foot for six random subjects in either session one or two of testing. Unfortunately, there were not always three successful trials recorded for each subject for each foot striking the force plate. This is why six random subjects are chosen for which three successful trials are captured. For the same reason, this is an intra-session repeatability study, as often subjects do not have enough successful trials in one of the sessions to compare results between two sessions.

❖ Filtering the ground reaction force data

When analysing the subject's GRF data for session one and two, a clear artefact is present in the first 8 % of the gait cycle in all directions for both the force (Figure 23) and COP .

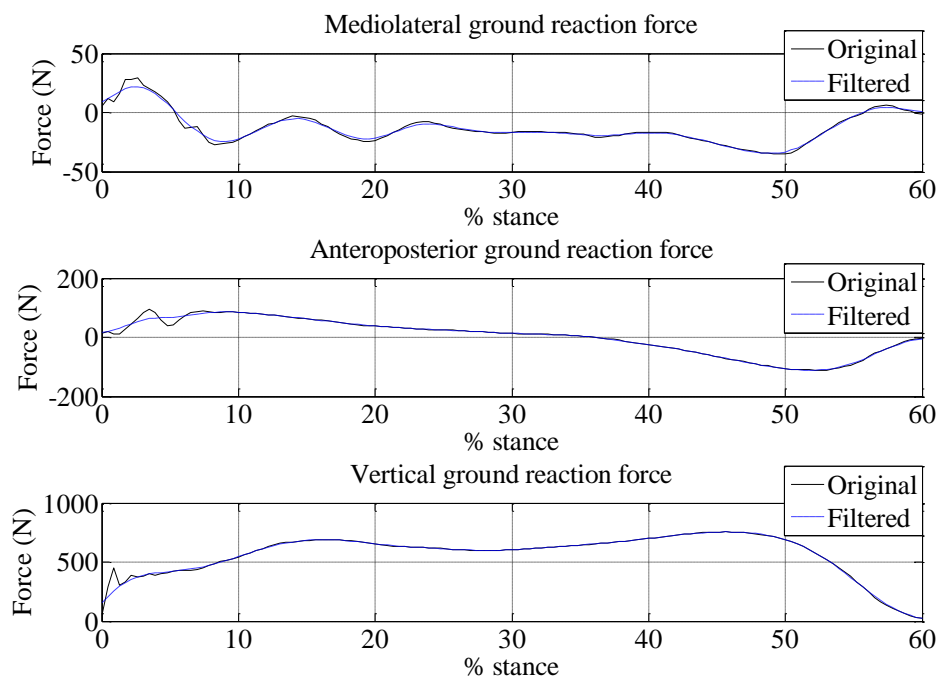


Figure 23: Comparison of filtered and raw ground reaction forces

The measured GRF and filtered GRF are compared in Figure 23. A heel strike transient is a common artefact in the vertical GRF that has been measured using a force plate. However, this artefact is present in all directions of the force (Figure 23) and COP. A comparison between the computed knee moment using filtered and unfiltered data is shown in Figure 24, where after the outputs of the RRA analysis is shown in Table 8 for both feet.

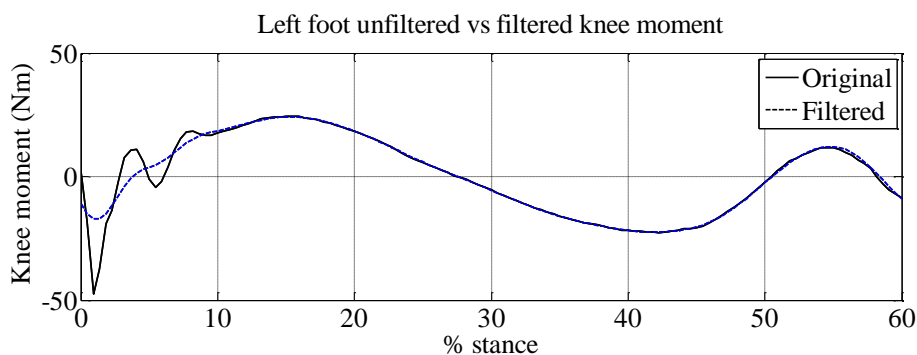


Figure 24: Resulting knee moment using unfiltered and filtered GRF data

From Figure 24 it is evident that filtering the GRF also removes an artefact from the resulting knee moment in the first 8 % of the gait cycle. Throughout the rest of stance phase, both sets of data produce a very similar knee moment. Although a slight difference in knee moment occurs in the last 5 % of stance phase.

Table 8: RRA results using unfiltered and filtered GRF data

Measurement	Original		Filtered	
	Left	Right	Left	Right
Max Residual Force (N)	-25.72	-21.71	-18.98	-17.98
RMS Residual Force (N)	11.83	8.89	12.23	7.75
Max Residual Moment (Nm)	-72.49	-74.53	-34.27	25.87
RMS Residual Moment (Nm)	20.29	20.35	14.93	15.09
Max positional error (translation, cm)	-4.42	-4.73	-4.25	-4.62
RMS positional error (translation, cm)	3.13	3.54	2.99	3.41
Max positional error (rotation, degrees)	0.24	0.843	0.24	0.87
RMS positional error (rotation, degrees)	0.24	0.53	0.23	0.55

*Green = Good (well in range), Orange = Okay, Red = Bad (out of range)

The RRA results in Table 8 show that filtering the GRF data results in lower threshold values for the RRA outputs. The actual results are not elaborated on in this section, just the comparison between using filtered and raw data.

❖ Joint angles comparison

All of the subjects maximum and RMS marker errors during the IK analysis are less than 4 cm and 2 cm, respectively. Therefore, the results can be analysed further.

The comparison between the OpenSim and PiG model knee angles during stance phase are shown in Table 9.

Table 9: Knee angle comparison between OpenSim and Plug-In Gait models

Subject	Session	Foot	R ²	RMS error (degrees)	% Max error
1	1	Left	0.992	0.66 – 0.77	3.4 – 3.8
2	2		0.990	1.36 – 1.41	7.8 – 8
3	2		0.987	1.38 – 1.61	6.7 – 7.4
4	1	Right	0.973	1.34 – 2.23	4.9 – 5.4
5	1		0.989	1.23 – 1.30	6 – 6.8
6	2		0.990	0.99 – 2.70	0.2 – 3.6

The COD is well over 0.9 for all the subject's knee angle comparisons. The maximum error between the OpenSim and PiG model knee angle at any point in stance phase is computed as a percentage of the maximum flexion angle during the trial in which it occurs. From Table 9 one can see that all the maximum errors are less than 10 % of the maximum flexion angle in stance phase. Figure 25 further shows the strong correlation between the OpenSim and PiG knee angles. The knee angle comparisons for the other subjects are shown in Appendix B.

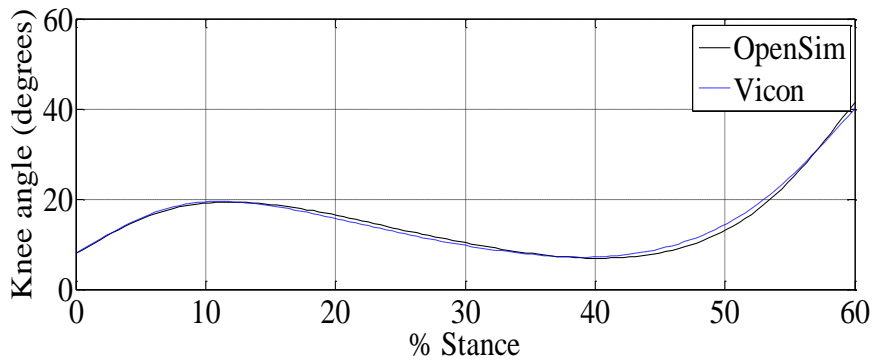


Figure 25: Subject 1 knee angle comparison during stance phase

The computed hip angles are also compared to the angles produced by the Plug-In Gait model. Figure 26 and Table 10 shows the comparisons between the hip flexion difference for each model as well as the hip adduction and rotation.

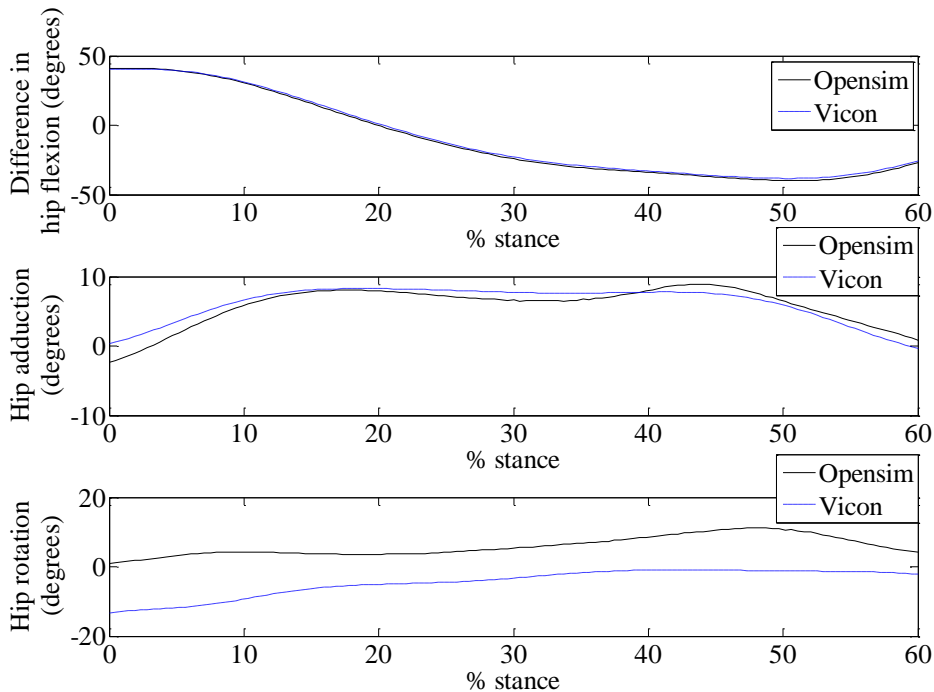


Figure 26: Subject 1 left hip angles comparison during stance phase

Table 10: Hip angles comparison for OpenSim and PiG models

Subject	Session	Foot	Correlation coefficient, R [R2]		
			Flexion	Adduction	Rotation
1	1	Left	0.999 [0.999]	0.920 [0.847]	0.774 [0.600]
2	2		0.999 [0.999]	0.874 [0.765]	0.917 [0.841]
3	2		0.999 [0.999]	0.858 [0.736]	0.952 [0.906]
4	1	Right	0.999 [0.999]	0.862 [0.744]	0.823 [0.678]
5	1		0.999 [0.999]	0.967 [0.934]	0.738 [0.544]
6	2		0.999 [0.999]	0.914 [0.835]	0.940 [0.883]

The difference between the left and right hip flexion angles during stance phase measured using OpenSim and the PiG model correlate accurately (>0.9) with one another. Although the hip adduction and rotation angles measured using both models correlate well with one another, they do not have the same magnitude. This is evident in Table 11 where the maximum errors as a percentage of the maximum angles in stance phase are shown along with the hip angle's RMS errors.

Table 11: Hip angle RMS errors and maximum errors percentages

Subject	Foot	RMS error, degrees [% Maximum error]		
		Flexion	Adduction	Rotation
1	Left	0.92 – 1.55 [3.5 – 6.8]	1.00 – 1.31 [29.2 – 36.2]	10.08 – 11.39 [438.6 – 539.9]
2		1.91 – 2.26 [1.3 – 3.3]	4.8 – 5.06 [54.1 – 57.1]	4.08 – 4.63 [193.4 – 208.8]
3		1.67 – 1.92 [6.8 – 7.3]	2.35 – 2.85 [57.6 – 67.6]	1.99 – 2.60 [141.8 – 202.4]
4	Right	2.23 – 2.72 [7 – 9.2]	2.78 – 3.20 [18.6 – 32.5]	7.31 – 10.34 [120.4 – 151.0]
5		2.09 – 2.35 [0.1 – 2.0]	1.44 – 1.67 [107.6 – 133.4]	14.41 – 15.78 [555.8 – 738.4]
6		3.38 – 4.34 [6.4 – 8.3]	1.64 – 2.12 [61.6 – 200.0]	8.82 – 13.64 [393.7 – 1019.4]

All of the subject's differences in hip flexion angles computed using OpenSim produce a maximum error that is less than 10 % of the maximum hip flexion difference measured using the PiG model. However, the maximum hip adduction angle errors are over 10 % with the minimum error percentage of 18.6 % for subject four and a maximum error percentage of 133.4 % for subject five. The hip rotation angle error percentage for the OpenSim results are all over 100 %. Figure 26 shows that the PiG hip rotation angle is much larger than that of OpenSim for subject one. However, subject four, five and six's hip rotation angle computed in OpenSim is larger than the PiG hip rotation angle. The largest flexion RMS error is 4.34° for subject six, the largest adduction RMS error is 5.06° for subject two, and the largest rotation RMS error is 15.78° for subject five.

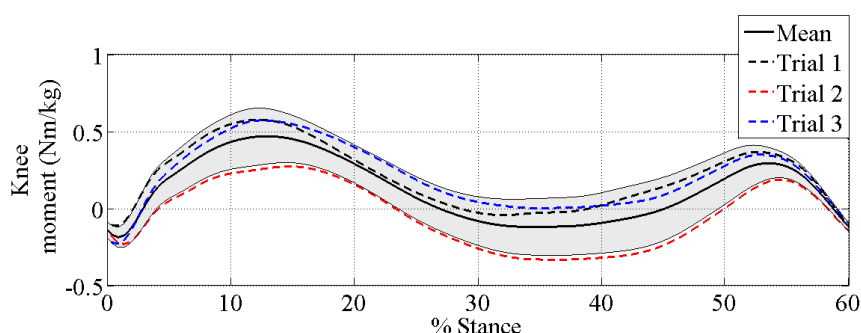
❖ Knee moment comparison

The Nexus software calculates the knee moment using inverse dynamics without the GRF data, therefore only the knee moment during swing phase is accurate. For this reason, the results obtained for each subject during stance phase in each session are compared to one another. Table 12 shows the intra-session comparison for each subject.

Table 12: Intra-session knee moment comparison

Subject	Session	Foot	Correlation coefficient, R [R ²]	Standard deviation (Nm/kg)	RMS error (Nm/kg)
1	1	Left	0.991 [0.982]	0.025 – 0.095	0.030 – 0.049
2	2		0.990 [0.980]	0.001 – 0.153	0.035 – 0.062
3	2		0.962 [0.925]	0.011 – 0.110	0.040 – 0.076
4	1	Right	0.989 [0.979]	0.007 – 0.069	0.028 – 0.033
5	1		0.975 [0.951]	0.026 – 0.209	0.090 – 0.174
6	2		0.996 [0.991]	0.001 – 0.058	0.018 – 0.028

There is a strong positive correlation between the PiG and OpenSim knee moments, as is evident by the correlation coefficients which are all over 0.96. The standard deviation indicates how far the trials within a session deviate from the mean knee moment for the session. The RMS error is calculated by comparing each trial to the mean of the three trials. For all the subjects, the maximum RMS error is always less than the maximum standard deviation for the session (Table 12). The subject with the largest standard deviation is subject five, and the three knee moments measured in subject five's session are shown in Figure 27 and are compared to the mean. The grey band represents a standard deviation band.

**Figure 27: Subject 5 intra-session knee moment comparison**

The knee moment measured in trial one and three are in the standard deviation band for the majority of stance phase (Figure 27). Although trial two correlates well with the other two trials, it produces a knee moment that is considerably less than the other two trials. When looking at the GRF comparison in Table B. 1, one can see that the standard deviation and RMS for subject five is greater than the other subjects. The same correlation is made between subject two and three's high standard deviation and RMS errors for the knee moment as well as the GRF.

❖ Residual reduction algorithm results comparison

The results of the RRA and CMC analyses will be compared within a session (intra-session) and between sessions (inter-session). Table 13 shows the mean RRA results achieved for each foot during session one and two.

Table 13: Mean RRA results for each foot in each session

Measurement	Threshold values			Session 1		Session 2	
	Good	Okay	Bad	Left	Right	Left	Right
Max residual Force (N)	0-10	10-25	>25	13.74	47.94	18.98	17.98
RMS residual Force (N)	0-5	5-10	>10	7.05	30.77	12.23	7.75
Max residual torque (Nm)	0-50	50-75	>75	39.13	53.22	34.26	25.87
RMS residual torque (Nm)	0-30	30-50	>25	20.61	38.72	14.93	15.09
Max positional error (cm)	0-2	2-5	>5	4.44	5.3	4.25	4.62
RMS positional error (cm)	0-2	2-4	>4	2.71	2.7	2.99	3.41
Max positional error (degrees)	0-2	2-5	>5	1.68	1.56	0.42	0.87
RMS positional error (degrees)	0-2	2-5	>5	1.03	1.04	0.23	0.55

In session one all of the left foot trial results are within acceptable ranges, except the maximum positional error of trial two which is 0.87 cm too big (Table B.2). The results obtained for the right foot trials in session one are not as positive, as is evident in the mean RRA results. Table B.2 in Appendix B shows that both trial one and trial three produce residual forces that are much too high (>25 N). Trial three also computes RMS residual moments that are too large (>75 Nm), as well as a maximum positional error that is outside the specified range (>5 cm).

The results obtained in session two are all within the acceptable limits, excluding the RMS residual force in trial two of the left foot and the positional errors of trial three of the right foot (Table B.3). The maximum and RMS positional errors of the right foot trial three are only 0.83 cm and 0.37 cm too large, respectively. The right foot trials of session one produce the largest mean residual forces and positional errors. Both the first and third right foot trials in session one produce large residual errors, but the second trial's results are all within the acceptable limits. To determine the cause of this difference, the knee moments for these trials are compared to one another as well as the GRF applied to the foot (Table 14). Figure 27 in the previous section compares the knee moments calculated for the right foot trials of session one.

Table 14: Session 1 left and right foot maximum knee moment and GRF data

Measure	Left			Right		
	Trial 1	Trial 2	Trial 3	Trial 1	Trial 2	Trial 3
Max knee moment (Nm)	30.81	29.80	27.47	41.21	19.53	40.97
Max ML force (N)	55.28	51.94	49.95	72.63	18.10	68.53
Max AP force (N)	131.50	146.86	136.62	146.99	79.48	132.52
Max vertical force (N)	791.78	786.56	796.99	735.01	721.51	770.30

The right knee moment for trial two is 47.4 % of trial one and 47.68 % of trial two. The same trend is seen in the GRF data as the mediolateral force of trial two is 24.92 % of trial one and 26.42 % of trial two. The anteroposterior force of trial two is 54.07 % and 59.98 % of trial one and three, respectively. The vertical forces measured in each trial are more similar to one another. The left foot trials have more consistent GRF data and more consistent RRA results.

❖ Computed muscle control results comparison

The resulting kinematics and model from the RRA analysis are used in the CMC analysis. The CMC results and threshold values are shown in Table 15.

Table 15: Mean CMC results for each foot in each session

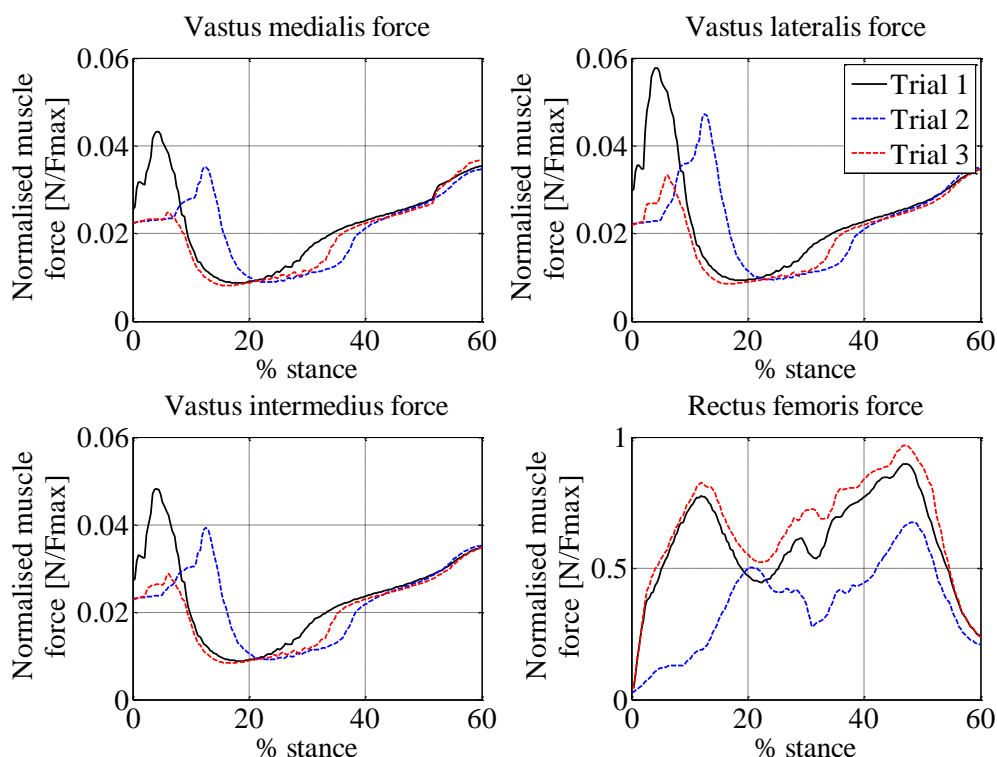
Measurement	Threshold values			Session 1		Session 2	
	Good	Okay	Bad	Left	Right	Left	Right
Max residual Force (N)	0-10	10-25	>25	13.75	47.66	19.12	18.04
RMS residual Force (N)	0-10	10-25	>25	7.27	29.91	12.44	7.57
Max residual Torque (Nm)	0-50	50-75	>75	37.68	52.1	32.17	25.85
RMS residual Torque (Nm)	0-30	30-50	>50	20.54	38.85	14.34	14.8
Max positional error (translation, cm)	0-1	1-2	>2	0.025	0.021	0.015	0.032
RMS positional error (translation, cm)	0-1	1-2	>2	0.015	0.009	0.009	0.011
Max positional error (rotation, degrees)	0-2	2-5	>5	1.4	2.81	0.62	1.58
RMS positional error (rotation, degrees)	0-2	2-5	>5	0.86	1.12	0.34	0.81
Max reserve torque (Nm)	0-25	25-50	>50	13.12	15.78	19.46	18.29
RMS reserve torque (Nm)	0-10	10-25	>25	2.91	4.19	3.23	2.64

The CMC results for the left foot trials of both sessions one and two and the right foot trials of session two are all within the acceptable limits specified by OpenSim. The individual trials in each session for the aforementioned feet are also all within the acceptable ranges (Table B. 5 and Table B.6). In contrast, the average residual forces measured for the right foot trials of session one are above the acceptable values. The right foot trials of session one are also the only trials to have mean residual moments outside the ‘good’ range. The same problem right foot trials from the RRA results in the previous section have high residual forces and moments (Table B. 5). Trial 2 of the right foot trials in session one produces CMC results that are within the specified range.

The main outcome of the CMC analysis is the muscle forces during stance phase. The muscle forces computed in each trial are first compared to the forces computed in the same session as shown in Table 16 and Figure 28.

Table 16: Intra-session comparison of muscle forces

Muscle	Session 1		Session 2	
	Left	Right	Left	Right
Vastus medialis	0.944 [0.890]	0.904 [0.817]	0.949 [0.900]	0.937 [0.879]
Vastus lateralis	0.944 [0.891]	0.850 [0.720]	0.951 [0.905]	0.947 [0.898]
Vastus intermedius	0.944 [0.892]	0.889 [0.790]	0.950 [0.902]	0.942 [0.888]
Semimembranosus	0.987 [0.974]	0.955 [0.913]	0.965 [0.931]	0.936 [0.876]
Semitendinosus	0.995 [0.991]	0.994 [0.988]	0.986 [0.972]	0.993 [0.987]
Bicep femoris long head	0.988 [0.976]	0.969 [0.940]	0.967 [0.936]	0.988 [0.976]
Bicep femoris short head	0.943 [0.889]	0.965 [0.931]	0.961 [0.924]	0.954 [0.909]
Rectus femoris	0.853 [0.728]	0.907 [0.822]	0.819 [0.670]	0.964 [0.929]
Medial gastrocnemius	0.940 [0.884]	0.993 [0.985]	0.968 [0.936]	0.980 [0.961]
Lateral gastrocnemius	0.944 [0.890]	0.904 [0.817]	0.949 [0.900]	0.937 [0.879]

**Figure 28: Normalised session 1 right leg extensor muscle forces**

The results in the table above show that the muscle forces computed using the data from the same session correlate well with one another ($R > 0.8$). The lowest correlation is 0.819 ($R^2 = 0.67$) for the rectus femoris of the left leg in session two. The three right foot trials from session one differed greatly in their GRF data, knee moment, RRA results and CMC results. Although these three trials achieved high

correlation coefficients when the muscle forces are compared to one another, Table 16 shows that the extensor muscle forces computed for these trials do not fit the same data points as well ($COD < 0.82$). Figure 28 compares the extensor muscle forces during stance phase for the three right foot trials of session one. The vasti muscle forces produced in trial one are greater than trial two and three. Trial three produces the smallest vasti forces, however its rectus femoris force is similar in magnitude to trial one. The mean muscle forces in each session are now compared to the muscle forces produced from the same leg using the data from the other session. Table 17 and Figure 29 show the inter-session comparison.

Table 17: Inter-session muscle force comparison

Muscle	Correlation coefficient, R [R ²]		RMS error (N)	
	Left	Right	Left	Right
Vastus medialis	0.898 [0.897]	0.663 [0.439]	18.64	10.83
Vastus lateralis	0.947 [0.896]	0.623 [0.388]	39.34	23.66
Vastus intermedius	0.930 [0.865]	0.662 [0.438]	26.24	12.54
Semimembranosus	0.984 [0.969]	0.927 [0.860]	21.33	16.69
Semitendinosus	0.986 [0.973]	0.979 [0.959]	5.18	3.38
Bicep femoris long head	0.981 [0.963]	0.958 [0.919]	14.02	11.64
Bicep femoris short head	0.936 [0.876]	0.952 [0.906]	107.96	65.07
Rectus femoris	0.621 [0.386]	0.531 [0.282]	71.73	243.88
Medial gastrocnemius	0.997 [0.993]	0.958 [0.917]	92.22	111.83
Lateral gastrocnemius	0.978 [0.957]	0.920 [0.846]	59.61	40.83

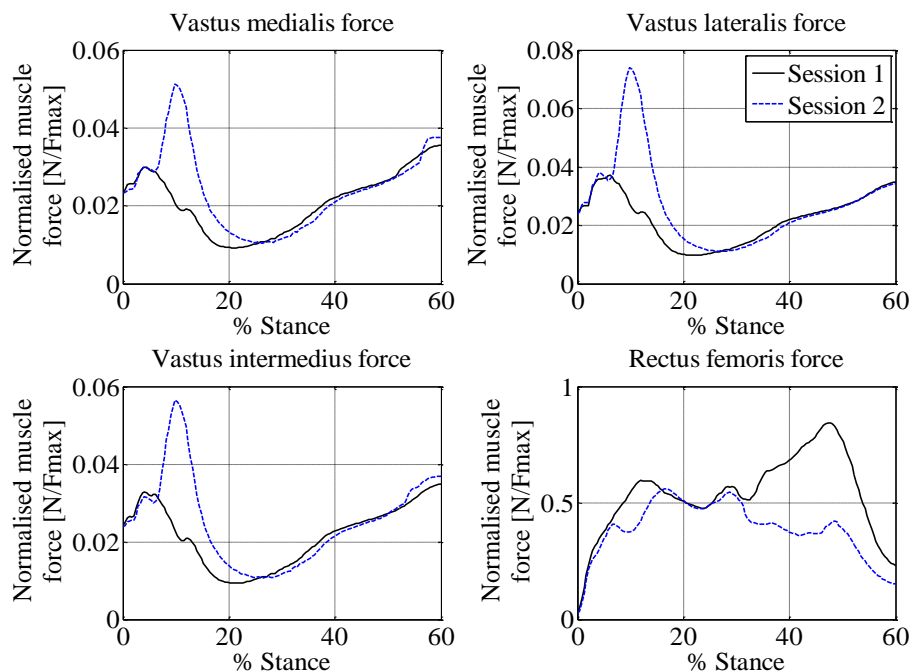


Figure 29: Right leg extensor muscle force comparison between sessions

Figure 29 shows the comparison between the session one and two right leg extensor muscle forces. The other muscle force comparisons are shown in Appendix B. From Figure 29 and Table 17 it is clear that the smallest correlation between the two session's muscle forces occurs between the extensor muscles. This is especially true for the right leg with the lowest correlation coefficient being 0.531 ($R^2 = 0.282$) for the rectus femoris muscle. The correlation coefficients for the left leg extensor muscles are not as low, although the rectus femoris has a correlation coefficient of 0.621 ($R^2 = 0.386$).

Table 18: Maximum residual forces and moments and extensor muscle forces

Measure	Direction	Maximum value	
		Session 1	Session 2
Residual force (N)	Mediolateral	-10.29	-2.39
	Anteroposterior	5.73	2.13
	Vertical	-40.25	-11.05
Residual moment (Nm)	Mediolateral	-36.31	16.60
	Anteroposterior	40.68	-11.74
	Vertical	16.83	7.14
Vastus medialis	-	46.1106	66.394
Vastus lateralis	-	69.5411	138.4996
Vastus intermedius	-	47.6785	77.1629
Rectus femoris	-	986.0709	654.4464

Besides the extensor muscles, all the other muscle forces calculated in session one and two correlate well with one another (>0.9). The right leg extensor muscle forces produced in each session differ greatly. To determine the reason behind the large difference, the residual forces from session one's right leg trials are compared to those of session two (Table 18). Session one produces higher residual forces and moments than session two, but this results in lower extensor muscle forces in the right leg during stance phase. Session one's maximum residual forces and moments are more than double those of session two. The extensor muscle forces in session two are much larger than those in session one, with an exception to the rectus femoris force that is larger in session one.

5.4 Discussion

As previously stated, a limitation of this project is that the majority of the capture data does not contain the kinematic information of the upper body. One cannot perform the RRA and CMC analyses without this data. Therefore, data only containing lower extremity kinematics is used in all the analyses up to and including the Inverse Dynamic analysis.

5.4.1 Comparison between torso and non-torso trials

To ensure that the results obtained using a model with no torso kinematics are accurate, the IK and ID analyses are performed using the same trial's data on a model with a torso and a model without a torso and the results are compared. The investigated joint angles and knee moment computed using a model with a torso match the same angles using a model without a torso very accurately as is evident by the COD and RMS errors. These results show that a model without a torso produces accurate results when performing an IK and ID analysis. The reason why the joint moments produced by both models are so similar is because the ID tool calculates the joint moment from the ground up. Therefore the torso kinematics has little effect on the knee moment.

5.4.2 Comparison between filtered and unfiltered trials

During renovations it became clear that the mounted force plate in the laboratory is not mounted correctly. The force plate is not attached to the foundations of the building using mounting plates; therefore the effective mass of the force plate is a lot less. The portable force plate used in session two is also not mounted to the foundations of the building.

The decision was taken to filter the GRF data as the artefact present could be due to rocking of the force plate when it is first contacted. This is not uncommon, however, as other studies also filter the GRF data [63]–[66], and a study by Revill *et al.* shows that the transient peaks witnessed during initial contact are not biologically relevant [65]. Filtering the GRF data removes the artefact from the first 10 % of the gait cycle. The artefact present in the knee moment computed from

unfiltered data (Figure 24) is not evident in knee moments published in literature [38], [67]–[69]. Furthermore, filtering the GRF data also improves the RRA results and ensures that the residual force measured for the left foot is within the suitable limit.

Due to the results discussed above and the fact that both the force plates used are not mounted correctly and there are artefacts in the force and COP data in all direction, the decision is taken to filter the GRF data before using it in the OpenSim modelling pipeline. The data is filtered using a fourth order low-pass Butterworth filter with a cut-off frequency of 10 Hz.

5.4.3 Repeatability study

❖ Joint angles comparison

When comparing the joint angles measured using the PiG model to those computed using the IK analysis in OpenSim, it is clear that OpenSim reproduces PiG knee flexion-extension angles and hip flexion-extension angles. The aim of this study is to achieve correlation coefficients of 0.9 or higher and maximum error percentages of less than 10 % when comparing the knee and hip flexion angles measured in OpenSim to those measured using a PiG model with Nexus software. This goal is successfully achieved for all trials.

The hip adduction and rotation angles do not compare as well to the angles produced using the PiG model. The hip adduction angles calculated using OpenSim correlate well with the angles produced using the PiG model, however the magnitude of the angles do not compare as well to one another as is suggested by the average maximum error percentage range. The same can be said for the hip rotation angles, where the maximum error percentage ranges indicate that the maximum hip rotation error is three to five times the maximum hip rotation angle measured using the PiG model. However, the hip rotation angles measured using OpenSim follows a similar linear pattern to the rotation angle measured using the PiG model as is evident in the strong positive correlation coefficient. It is important to note that the hip adduction and rotation angles in stance phase are lower than the hip flexion angles (Figure 26), therefore a small difference can still result in a large maximum error percentage. This is evident in Table 11.

The hip knee and ankle joint together make up a kinetic chain [70], which indicates that instead of working as isolated units, they work together to perform a specific function. The movement of one link of the chain will affect the movement of the other segments [71]. Therefore, the discrepancy between the OpenSim and PiG model hip adduction and rotation angles is explained by the simplified lower extremity model used in OpenSim. The knee joint in the OpenSim model is approximated as a one degree of freedom hinge joint, whereas the PiG model has a three degree of freedom knee joint that is capable of flexion, adduction and rotation. Furthermore, the subtalar and MTP joints of the ankle are locked in the OpenSim

model. OpenSim suggests that the subtalar and MTP joints must be locked for the RRA analysis, and since the kinematics from the IK analysis are used in the RRA, these joints should be locked prior to the IK analysis.

Due to the simplified knee joint and locked joints in the model's feet, all adduction and rotation of the lower limb will translate to the hip joint. In comparison, the PiG model has adduction and rotation in the ankle, knee and hip joint. The range of motion of the knee is 9.4° in rotation and 6.4° in adduction [72]. Although these values are low, the RMS errors shown in Table 11 are within the ranges of 2.335° to 2.7° for hip adduction and 7.78° to 9.73° for hip rotation, which are similar to the range of motion of the knee. The altered hip kinematics, however, can influence the biomechanics of the patellofemoral joint according to various sources [11], [73]–[76]. Lee *et al.* reported that femoral rotation (hip rotation) as well as tibial rotation (knee rotation) result in an increase in patellofemoral contact stress [74]. Powers reported that hip adduction results in valgus of the lower extremity, which then increases the lateral forces on the patella and effects the patella kinematics [77]. Besier *et al.* also proved that femoral rotation has a direct effect on patellofemoral contact stress and patella kinematics, this is due to the line of action of the quadriceps muscle changing during hip rotation and adduction [11].

Although the knee is being analysed during pure flexion-extension for this project, the hip adduction and rotation angles can affect the patellofemoral contact force and patella kinematics. Therefore, it is not enough to have knee and hip flexion angles that correlate well with those measured using the PiG model, but the hip adduction and rotation angles should too. To do this a more complex knee and ankle model must be utilized in the OpenSim modeling pipeline.

❖ **Knee moment comparison**

The high COD for the computed knee moments shows that the moments for each trial within each subject's session not only correlate well with one another, but also fit within the same data range. However, all of the subject's knee moments produced in each trial are not within the standard deviation band for the session as seen in Figure 27 and the figures in Appendix B. More specifically, subjects two, three and five produce larger RMS errors and standard deviations between trials. However, due to factors such as the GRF magnitude, COP position and walking speed all affecting the knee moment, one can expect a variation in knee moment as one does not reproduce the same gait speed and GRF during each stance.

When comparing the GRF of each trial (Table B. 1), the same subjects with the largest knee moment errors have the largest standard deviation and RMS errors between the GRF data of each trial. Therefore, a correlation can be drawn between the increased deviation in the resulting knee moment and the larger difference in the GRF data, more specifically the vertical GRF. The reason for the varying GRF could be due to a difference in walking speeds, or the subject contacts the force plate with a larger force due to adjusting his/her step. An example here of is shown

in Figure B.15, where the first peak of subject three's trial two moment occurs before the first peak of trial one and three. This indicates that the subject slowed down during his/her stance in trial two and this effects the knee moment.

The shape of the knee moment curve is affected by the knee angle and the magnitude of the moment is affected by the GRF applied to the model. Since the knee angle produced in each trial for each session is repeatable (as discussed in the previous section), the knee moments computed during the ID analysis have a strong intra-session linear correlation. The GRF data varies in magnitude due to the speed of walking and force with which the force plate is struck. This has a direct effect on the knee moment which will then differ accordingly.

When comparing the knee moments calculated to those in literature, both the shape and magnitude of the moment compares well [67], [78], [79]. Heino Brechter and Powers computed peak knee moments of 0.43 Nm/kg [79], Ward and Powers calculated peak knee moments of ± 0.5 Nm/kg [78], and Besier *et al.* computed peak knee moments of roughly 0.6 Nm/kg [67]. In this project the mean peak knee moment is 0.3792 Nm/kg (standard deviation = 0.1791 Nm/kg) for all six trials. Due to the fact that the knee moments compare well to one another and literature, this step of the OpenSim pipeline is validated for this project.

❖ Residual reduction algorithm results comparison

When analysing the RRA and CMC results it is important to note that the superimposition method has been applied to the foot not striking the force plate, therefore the RRA tool is trying to match the kinematics of this leg to approximated GRF data. According to James Dunne, who is an OpenSim Project Administrator at Stanford University, making such assumptions will result in limitations such as higher errors [80]. Since the model's kinematics are varied to compensate for the ground reaction forces, the superimposed forces on the foot not striking the force plate will cause larger positional errors during walking as well as larger residual forces that act on the pelvis.

Despite this, the mean RRA errors for both the left foot trials of session one and the right foot trials of session two are within the acceptable limits suggested by OpenSim. Looking specifically at the intra-session repeatability of the RRA results, within session one the results for left foot strikes compare well except for the maximum positional error in trial two that is 0.87 cm too large.

This can be explained by the fact that the mass of the individual bone segments of the OpenSim model are adjusted to better fit the magnitude of the vertical GRF force applied to the model. Since the vertical GRF measured in trial two of session one is less than those measured for the other trials (Table 14), the effective mass of the model will be less in trial two. However, the same force is applied to all three trials at heel strike and toe off when the force is superimposed onto the foot not striking the force plate and their knee moments are all similar to one another. Therefore, the lighter model is not equipped for the larger force during these stages

of stance phase, resulting in a positive displacement at heel strike. The same logic applies to trial three of session two's right foot trials.

The RRA results for the right foot strikes of session one do not compare as well as all the other trials. Trial one and three produce the largest residual forces and positional errors (trial three only) in both session one and two. The positional error in trial three is explained by the vertical force which is much higher than those of trial one and two (Table 14). It is interesting to note that trial two produces RRA results that are within the acceptable threshold values. The maximum GRF data and computed knee moment is compared between the three trials to determine the cause of the high residual forces in trial one and three

The knee moment calculated during trial two is approximately half of trial one and three's maximum knee moments (Table 14 and Figure 27). The large difference in knee moment is explained by the large difference in the measured GRF for each trial. The mediolateral force measured during trial two is 24.92 % and 26.42 % of trial one and three, respectively. Similar to the knee moment, the anteroposterior force of trial two is 54.07 % of trial one's force and 59.98 % of trial three. Therefore, a direct correlation can be drawn between the difference in GRF magnitude and the difference in knee moment.

Furthermore, when comparing the vertical GRF of the left foot strikes to the right foot strikes, the left foot vertical GRF is much larger than those measured on the right foot. Thus, when this left foot data is superimposed onto the model during the right foot strike on the force plate it results in larger errors. This is because the body mass is adjusted according to the right foot strike (since it is the majority of stance phase) and then the model is exposed to vertical forces up to ± 50 N bigger. This is, unfortunately, a downfall of applying the superimposition method. The large residual force computed in trial two of session two's left foot trial could be due to this reason. As the average maximum vertical force of the right foot trials is 792.2 N and the maximum vertical force of trial two is much less (755.34 N).

The difference in the computed knee moment, together with the impact of the superimposed forces on the foot not striking the force plate, leads to larger residual forces in the model. Although the superimposition method is used, the RRA results are predominantly within the specific ranges, except for the five isolated cases that can be explained. Therefore the RRA step is validated and the CMC analysis can now be performed.

❖ **Computed muscle control results comparison**

Except for trial one and three of session one's right foot trials, all the CMC results fall within the acceptable range provided by OpenSim (Table B. 5 and B6). These two trials are the same trials that produced high residual forces with the RRA tool. Since the adjusted model and kinematics that result from the RRA analysis are used as inputs for the CMC tool, the high residual forces produced using CMC are directly linked to the high residual forces obtained using the RRA tool.

Within the RRA analysis, the aim is to minimize the residuals by as much as possible so that the motion of the model is generated purely by internal joint moments [39]. When using the CMC tool, these moments are generated by the forces exerted by the muscles surrounding the joints. During the RRA and CMC if a joint moment large enough cannot be produced to propel the model, the residual forces increase. Therefore, if the muscles need to exceed their maximum isometric force to produce a motion, the residual forces will increase so that the maximum isometric force of the muscles is not exceeded. According to OpenSim's user guide, the residual forces should be low to prevent the optimizer from "wanting" to use the residual actuators. This is because an actuator with a large optimal force and low excitation is "cheap" in the optimizer cost [39], i.e. if the residual force is high the model will make use of the residual actuator instead of the muscles.

The aforementioned scenario is evident in the muscle force results shown in Figure 28. Trial three calculates exceptionally high residual forces, and in Figure 28 one can see that the vasti muscles produce much lower forces than both the other trials. This is because the residual forces are being used with the other muscles to propel the model. For trial one of session one's right foot trials, the residual forces are not too high to take over the muscle's functions, therefore the extensor muscles are producing larger forces in order to match the model kinematics and GRF data.

The subject whose data is used to compute the knee muscle forces in this project experienced patellofemoral pain in session one, but after the physiotherapeutic intervention, no longer experienced the pain in session two. Powers *et al.* determined that subjects with anterior knee pain produced lower vasti muscle forces compared to subjects without patellofemoral pain [81].

When comparing the mean resultant muscle forces from each session to one another, there is a strong correlation between all the muscles surrounding the knee except for the extensor muscles. This is especially true for the right leg (Table 17). Figure 29 shows that the vasti muscle forces computed in session two are much larger than those computed in session one, which agrees with the findings of Powers *et al.* [81]. However, it could also be due to computational errors as the RRA and CMC results for the right leg in session one were outside the threshold values. Therefore, the average residual forces and moments are compared between sessions, as well as the maximum muscle forces during stance phase (Table 18).

The mean residual forces and moments computed during session two's trials are more than half those of session one. On the other hand, except for the rectus femoris, session two produces larger muscle forces. Therefore, once again there is a link between large residual forces and smaller muscle forces. Furthermore, the GRF measured during session two is also larger than the GRF measured in session one (Table 14 and Table B.4). Both of these factors contribute to the larger muscle forces measured during session two. The left leg muscles forces produced during session one and two have a stronger correlation coefficient and COD when compared to one another (Table 17). As can be seen in Figure B.19, session two

produces larger vasti muscle forces. Although the vertical GRF measured for the left foot in each session is within the same range, the right foot trials mean GRF data is applied to the foot not striking the force plate and in session one the right foot vertical GRF is much lower than the trials from session two.

It is clear from the RRA and CMC results that the GRF applied to the model has a large influence on the results of the analyses, as James Dunne suggested [80]. Consequently, the superimposition method results in increased residual forces and errors. This is especially true when the GRF applied to each foot differs greatly (session 1). However, ten of the twelve trials used in the RRA and CMC analyses produce CMC results that are within acceptable ranges.

To ensure that the shape and magnitude of the muscle forces produced are accurate, the results are compared to literature. Arnold *et al.* [82], Besier *et al.* [67], and Castermans *et al.* [83] all report on muscle forces during walking. Arnold *et al.* and Castermans *et al.* both plot processed EMG signals, whereas Besier *et al.* plots computed muscle forces normalized by the maximum isometric force (F_{OM}) of each muscle (like this project).

When comparing the shape of the muscle force curves to those in literature, all the muscle forces computed in this project exhibit a similar shape to the muscle forces reported by the aforementioned sources. All the vasti forces exhibit a peak in the first 25 % of the gait cycle and the rectus femoris force has two distinct peaks at roughly 20 % and 50 % of the gait cycle. However, the rectus femoris peaks are more distinct in the studies by Castermans *et al.* [83] and Arnold *et al.* [82] compared to the results in this project. In the aforementioned studies the rectus femoris force decreases by more than 60 % after the first peak between 20 to 50 % of the gait cycle. However, Besier *et al.* reports on a rectus femoris force that does not experience a dramatic decrease in force in the same period [35].

When comparing the magnitude of the forces to those in literature, Besier *et al.* and Arnold *et al.* report on normalised rectus femoris forces that are roughly 20 % of those computed in this project. However, the forces produced by the vasti muscles in these source's studies are roughly 20 % more than those computed in this project. Thus, the quadriceps force produced in this project is roughly the same in magnitude as those in literature. The reason for the difference in vasti and rectus femoris forces could be due to the simplified knee model used in this project. Arnold *et al.* makes use of a model that has five degrees of freedom for the hip, knee and ankle joint. Castermans *et al.* plots EMG activity patterns and is therefore not constrained by a simplified knee model. Besier *et al.* makes use of the same generic musculoskeletal model with a one degree of freedom knee joint. However, they use raw EMG data and joint kinematics as inputs to determine the muscle forces and their model has a patella.

These differences could result in larger vasti muscle forces. Firstly, the more complex knee joint allows for adduction and rotation of the knee which results in

lateral displacement of the patella. This could affect the vasti muscle forces due to the fact that along with aiding in knee extension, the vasti muscles contribute to patella stability during stance phase [17], [84]. According to Palastanga, the vastus medialis resists lateral displacement of the patella caused by the angle of the femur and resulting angle due to rotation and adduction of the knee. Therefore, if there is no adduction and rotation, and the model does not contain a patella, the vasti muscles will essentially have less work to do. And since the rectus femoris is in line with the quadriceps tendon, it is 'easier' for the static optimizer to apply a larger force with the rectus femoris to produce the knee flexion-extension during stance phase.

Secondly, if raw EMG data is used, the resulting muscle forces will be proportionally consistent to one another. Therefore the relationship between the rectus femoris and vasti forces will not change and the quadriceps force will be broken up between the muscles as was measured by the EMG.

The other muscles forces produced in this project are more similar in magnitude to those in literature. The semimembranosus, semitendinosus, and bicep femoris all decrease gradually during stance phase, while the medial and lateral gastrocnemius muscles increase from 20 % to 60 % of the gait cycle [35], [82].

Chapter 6

Subject specific musculoskeletal patellofemoral joint model

6.1 Introduction

The aim of this project as a whole is to develop a modelling pipeline that can be used to detect changes within the patellofemoral joint, more specifically looking at the patellofemoral contact force and kinematics of the patella. This modelling pipeline is used within a broader study where the effect of anterior knee pain is being study. The study attempts to link the underlying biomechanical mechanisms of the patellofemoral joint to the pain and discomfort experienced by the subjects.

This chapter will discuss the method used for the final steps of this projects modelling pipeline, where after the results will be discussed and compared intra- and inter-session. The data used throughout the full modelling pipeline was obtained from one subject within two sessions. Three left foot force plate strikes and three right foot strikes were captured in each session, respectively. The data captured in these trials are used in the full modelling pipeline shown in Figure 30.

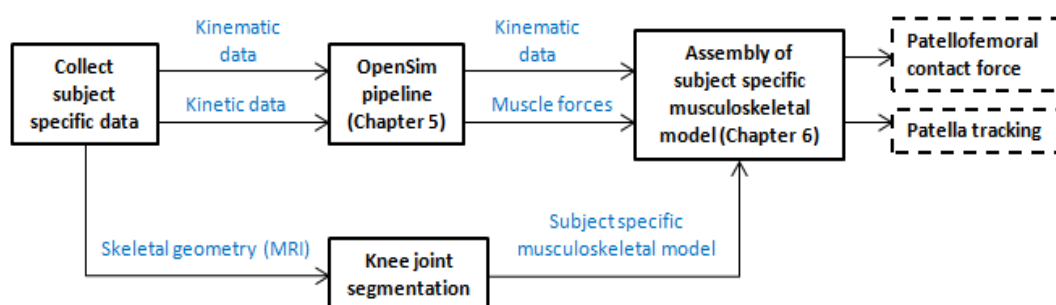


Figure 30: Computational modelling pipeline flowchart

6.2 Methods

After processing the subject's data in the OpenSim modelling pipeline, the muscle forces and knee kinematics computed are used in the next step of the modelling pipeline discussed in this section. The full modelling pipeline is applied using data from one subject who complains of anterior knee pain in the right leg during squatting, lunging, prolonged sitting and running on uneven surfaces. Therefore the right leg is investigated. Table 19 shows the subject's physical measurements.

Table 19: Physical measurements of subject

	Gender	Age	Mass	height	Injured leg
Subject one	Male	35	71	1.73	Right

6.2.1 Segmentation procedure

During segmentation, data from an MRI scan is extracted and processed on Mimics software (Mimics 16.0, Materialise, Leuven, Belgium) to produce a three-dimensional subject specific computational model. The stack of two-dimensional MRI images of the knee joint, which are in the sagittal plane, are loaded into Mimics. Mimics then computes and creates images in the coronal and sagittal direction.

During segmentation, the structures of interest are selected within each cross-sectional slice of data and are fused together to form the full three-dimensional structure. To select the structures one must be able to identify each separate structure within the MRI. MRIs consist of greyscale information. The models in Mimics are constructed based on greyvalues within the images, which are numbers associated with an image pixel that defines the shade of the pixel (black, white, or grey). The greyvalue assigned to a material is directly related to its density; therefore it is easy to differentiate between muscle, bone and cartilage.

One can either manually segment a structure by “colouring in” the bone or cartilage of interest (Figure 31), or one can use thresholding, which is when similar greyvalues are grouped together automatically to segment the data. Within this project manual segmentation was predominantly used. To create a three-dimensional musculoskeletal knee joint, the femur, femur cartilage, tibia, fibula, patella and patella cartilage are segmented. Since the subject experienced pain in the right knee, an MRI of only the right knee was taken.

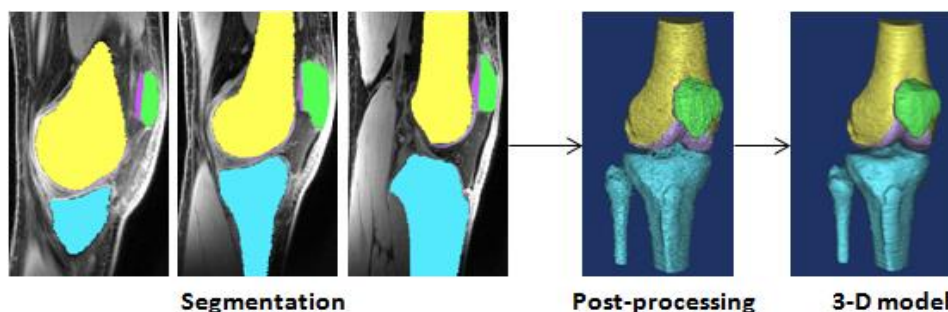


Figure 31: Segmentation procedure

After segmenting the aforementioned structures, the three-dimensional model must be post-processed to remove any artefacts that results from the segmentation procedure (Figure 31). This post-processing is also performed in Mimics through smoothing the surfaces of the model. Once the patient specific musculoskeletal knee-joint model (from here on referred to as model) has been post-processed, it is exported as a .stl* file to be used in the next step of the pipeline.

6.2.2 Define bone axes

Before applying the muscle forces and knee joint kinematics to the model, the local axes of the femur and tibia must be identified and created in software called 3-Matic

(3-Matic, Materialise, Leuven, Belgium). The axes are defined in a similar manner to methods applied by Jan Victor [85].

❖ Femur

To define the distal femur head local axes, both the proximal and distal femur heads are imported into 3-Matic (Figure 32)

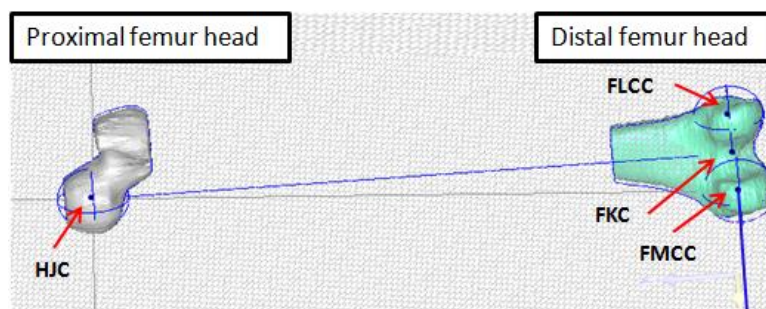


Figure 32: Femur local axes definition

With reference to Figure 32 the method below is followed:

1. The hip joint centre (HJC) is defined by fitting a sphere to the proximal femoral head, of which the HJC is the centre of the sphere.
2. To locate the femoral knee centre (FKC), two separate spheres are fitted to the medial and lateral condyles of the distal femur head. The centre of these spheres are the femoral medial condylar centre (FMCC) and femoral lateral condylar centre (FLCC), respectively. The midpoint of the line connecting the FMCC and FLCC is the femoral knee centre (FKC)
3. Finally, the femoral co-ordinate axes are identified with the FKC as the origin. The vertical (mechanical) axis is the line connecting the FKC and HJC, and the mediolateral axis is normal to the vertical axis, in the same plane as the mechanical axis and epicondylar axis.

❖ Tibia

To define the tibia local axes, the tibia and fibula proximal and distal heads are imported into 3-Matic (Figure 33).



Figure 33: Tibia local axes definition

The local axes of the tibia are defined with reference to Figure 33 as follows:

1. To identify the ankle centre (AC) select the most medial point on the lateral malleolus of the fibula and the most lateral point on the medial malleolus of the tibia. These are the ankle lateral malleolus (ALM) and ankle medial malleolus (AMM), respectively. The AC is the midpoint of the line connecting the ALM and AMM.
2. The tibial knee centre (TKC) is a point selected on the top of the proximal tibia head between the two prominences, as shown in Figure 34.

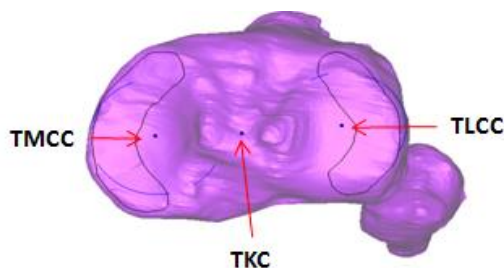


Figure 34: Define the tibia knee centre

3. To define the tibial medial and lateral condylar centres (TMCC and TLCC), mark the medial and lateral condyle borders as shown in Figure 34, and fit an arc to the marked areas. The centres of these arcs are the TMCC and TLCC, respectively.
4. To create the tibia local axes connect the AC and TKC using a cylinder (Figure 33). Next, fit a sketch plane that is coincident on the TLCC and TMCC and normal to the top of the cylinder. Use this sketch plane to define the local axis system with the TKC as the origin. The line between the AC and TKC is the vertical/mechanical axis and a line normal to this is the mediolateral axis.

6.2.3 Computational technique

The final step of the computational modelling pipeline is to apply the muscle forces and knee joint kinematics to the patient specific musculoskeletal model developed through segmentation. This step of the pipeline is performed with Adams VIEW (Adams 2015, MSC Software, Santa Ana, California). The aim is to determine the patellofemoral joint reaction force and track the patella kinematics. This section explains how the computational technique is applied.

❖ Define bone axes

The geometries of the distal femur head, proximal tibia and fibula heads, patella, femur cartilage and patella cartilage are imported into Adams. The local femur and tibia axes defined in the previous subsection must be created in Adams. To do this the FKC and TKC origins are defined using the same co-ordinates as the 3-Matic

software. To determine the direction of the tibia and femur local axes, the method as explained for the femur below is applied for both bones.

1. Define the FKC in Adams.
2. In 3-Matic, move the FKC 1 cm in the vertical direction using the defined femur local axis and record the co-ordinate position.
3. Define this co-ordinate position in Adams.
4. Create a polyline between the FKC in Adams and the new point created. This is the direction of the vertical local axis of the femur.
5. Repeat steps two to four in the mediolateral and anteroposterior direction to define the complete local axes.
6. Steps one to five are repeated using the TKC and tibia local axes in 3-Matic to define the axes in Adams.

❖ Define joints

Once the local axes have been defined, the following joints are created in Adams:

1. A fixed joint is created between the femur and ground to stop the femur from translating or rotating.
2. A fixed joint is created between the patella and patella cartilage to ensure these structures move together, and the same is done between the femur and femur cartilage.
3. A revolute joint is created between the tibia and femur. The revolute joint is defined at the FKC and it enables the tibia to rotate about the mediolateral axis of the femur.

❖ Define motion and muscle forces

Next the knee angle computed using the IK analysis in Chapter 5 is imported into Adams. The motion of the knee joint is defined as follows:

1. Create a point motion in Adams where the moving point is the TKC of the tibia and the reference point is the FKC of the femur.
2. Select that the direction of the motion is around the mediolateral axis of the femur local axis.
3. Define the motion using a function:
 - a. Use the Akima spline fitting method in Adams to apply the joint angles measured in OpenSim to the model. The Akima spline fitting method creates an interpolated curve from the input points with a specified number of values.

Next the muscles must be defined. The extensor muscles (quadriceps muscle) of the knee are used in the model. To define the insertion points of the muscles both literature and OpenSim are used. The insertion point of each muscle on the patella is approximated using the positions shown in literature [50], [86]. A marker is created for each muscle at their insertion points on the patella (Figure 35).

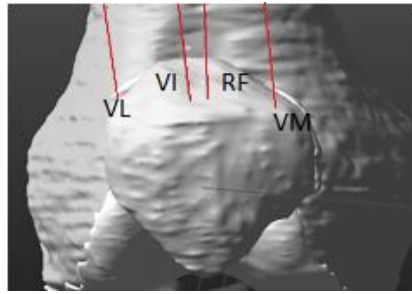


Figure 35: Insertion points of the extensor muscles on the patella.

Since the distal head of the femur is the only part of the femur imported into Adams, the superior insertion point of each muscle cannot be defined using its position relative to the skeletal structure. Therefore, the direction of the muscle force must be defined using the direction of the muscle force in the OpenSim software. In OpenSim, the co-ordinates of the insertion points of each muscle on the patella and where ever else it is attached are recorded. The difference in the vertical, mediolateral and anteroposterior direction between both insertion points is then computed. Using the femur local axes in Adams and the insertion points of the muscles on the patella, the same difference is used to define a new point that represents the superior insertion point of the muscle.

A polyline is created in Adams between the insertion point on the patella and the insertion point that has been defined using the difference from OpenSim. A force is then created for each muscle at its respective insertion point on the patella, in the direction of the polyline. Similarly to the application followed to incorporate the knee angle, the force of each muscle is defined using the Akima spline fitting function in Adams. The muscle forces computed using the CMC tool in OpenSim are imported into Adams and applied to the model.

❖ Define soft tissues

The medial patellofemoral ligament (MPFL) and patella tendon (PT) must be defined in the model. This is accomplished by modeling the soft tissues as idealised tension-only parallel spring damper elements according to a method introduced by Blankevoort *et al.* [46], which is explained in Chapter 2. The values for the cross-sectional area and elastic modulus of the PT and MPFL are found in literature and used to compute the stiffness coefficient for each element of the MPFL and PT (Table 20). The area and elastic modulus of the aforementioned structures differ in literature; therefore an average values are taken from two sources for the MPFL [50], [87] and three sources for the PT [88]–[90].

Table 20: Stiffness properties of the model ligaments and tendons

Structure	A (mm ²)	E (MPa)	k (N)	No. of elements, n	k/n (N)
PT	119.95	1029.13	123444.50	5	24688.91
MPFL	42.70	19.10	815.57	5	544.35

The insertion points of the MPFL and PT are determined from literature as shown in Figure 35 for the MPFL [50], [91], [92].

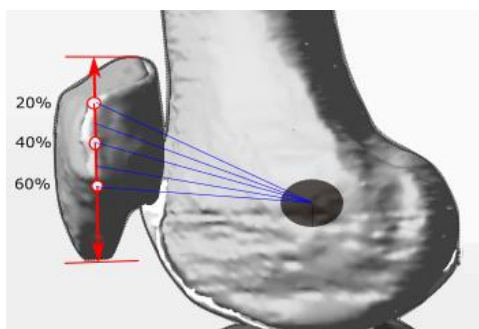


Figure 36: MPFL insertion points

❖ **Measurements**

After developing the knee joint in Adams, three measurements are made during stance phase using the model with the applied kinematics and muscle forces. These are the contact force between the patella and femur cartilages, the lateral displacement of the patella and the patella tilt angle.

The contact force is measured using the Adams built in contact function which is based on the Hertz’s contact model [47]. According to Guess *et al*, the contact friction in the patellofemoral joint is not statistically significant to contact pressures, therefore friction is ignored [93]. The mechanical properties used for the patella and femur cartilage are attained from literature and shown in Table 21.

Table 21: Mechanical properties of patella and femur cartilage

Structure	k_c (N/mm) [47]	exp_c [47]	B_c [47]	Density (kg/mm ³) [94]
Cartilage	500	1.5	5	1.3×10^{-6}

The lateral displacement of the patella is measured using the bisect offset index as demonstrated by Ward [95]. The bisect offset method and measurement of the patella tilt angle are discussed below with the aid of Figure 37.

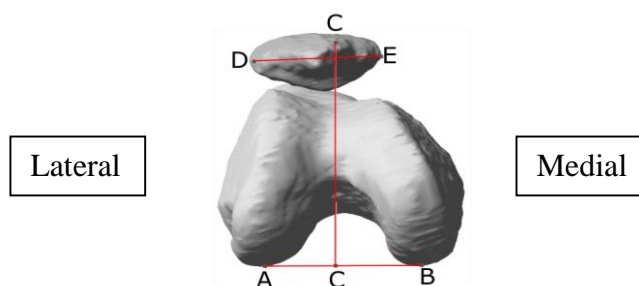


Figure 37: Lines used for the bisect offset and patella tilt measurement

A line AB is drawn between the most posterior points of the medial and lateral condyles of the distal femur. Line CC is projected perpendicular to line AB through the deepest point of the trochlear groove. Line CC intersects line DE, that spans across the full width of the patella. The bisect offset is a measure of the lateral displacement of the patella as a percentage of the patella width [95], as shown in equation 6.48.

$$BO = \frac{D \rightarrow CC}{DE} \times 100 \quad (6.48)$$

D→CC = length from D to CC (mm), measured perpendicular to CC

DE = Width of the patella (mm)

The lateral patella tilt angle is measured as the angle between the posterior condylar line (AB) and the patella width line (DE).

6.3 Results

The results obtained in this chapter are compared within sessions (intra-session), between sessions (inter-session) and to literature were applicable.

6.3.1 Patellofemoral contact force

The contact forces measured during each trial of each session are compared in Figure 38 and Table 22. Each trial is compared to the mean of the session.

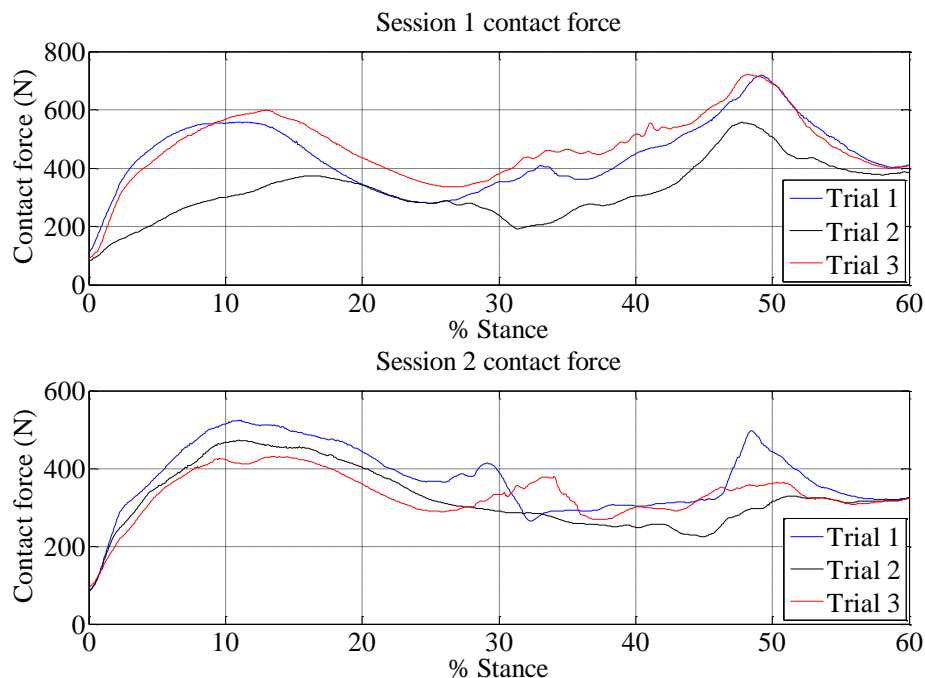


Figure 38: Intra-session comparison of computed contact force

Table 22: Intra-session contact force comparison

Trial	Session	Correlation coefficient, R [R ²]	RMS error (N)
1	1	0.951 [0.905]	48.17
2		0.874 [0.765]	104.93
3		0.968 [0.937]	68.14
1	2	0.967 [0.935]	39.97
2		0.960 [0.922]	29.59
3		0.926 [0.857]	30.09

The contact forces computed in session one and two correlate well with one another ($R > 0.85$). From Figure 38 and Table 22 one can see that during session one, trial two ($R = 0.874$) produces a contact force that is less than that of trial one ($R = 0.951$) and three ($R = 0.968$). This is also evident in the RMS error as the RMS error between trial two and the session mean is much larger for trial two (104.93 N) than for trial one (48.17 N) and three (68.14 N).

The data from session two produces contact forces that are more similar to one another ($R^2 > 0.85$). The RMS errors between each trial and the session mean are more similar to one another in session two, with trial one, two and three producing RMS errors of 39.97 N, 29.59, and 30.09 N, respectively.

The only difference between the models used in each trial's simulation is the muscle forces and knee kinematics applied to the model. Table 23 shows that all the knee angles used in the model correlate well with one another.

Table 23: Intra- and inter-session comparison of knee flexion angles

Session	Correlation coefficient, R [R ²]	RMS error (degrees)	%Max error
1	0.997 [0.995]	0.71 – 1.27	3.65 – 6.03
2	0.999 [0.997]	0.53 – 1.2	2.26 – 4.77
Session 1 vs. 2	0.999 [0.998]	0.71	2.76

The knee angles produced are repeatable as both sessions achieve correlation coefficients and COD of over 0.99 in all trials (Table C.1). Furthermore, when comparing session one and two's knee angles the correlation coefficient and COD are over 0.99 too. This indicates that similar knee angles are used in all the trials.

The average contact force in session one and two are compared in Figure 39. The correlation coefficient between the two session of 0.416 ($R^2 = 0.173$) indicates that the contact forces produced in the two sessions are dissimilar. However, when comparing the contact forces by eye, one can see that they follow similar trends from 0 to 30 % of the gait cycle and at 50 % of gait cycle they differ in magnitude.

Session one's data computes a larger contact force as is evident by the RMS error of 119.1 N between session one and two's contact force.

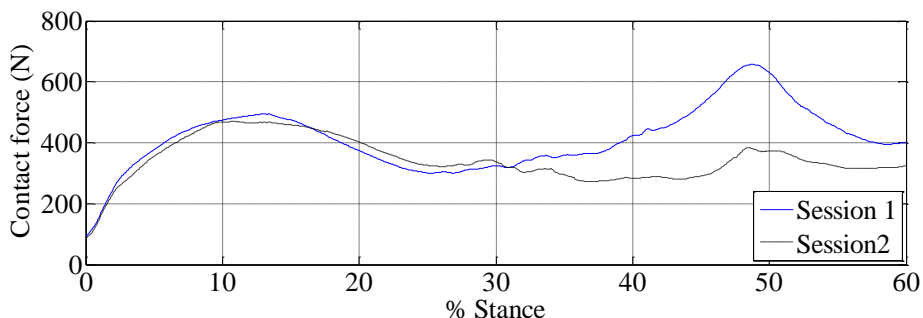


Figure 39: Inter-session contact force comparison

The mediolateral contact force is shown in Figure 40.

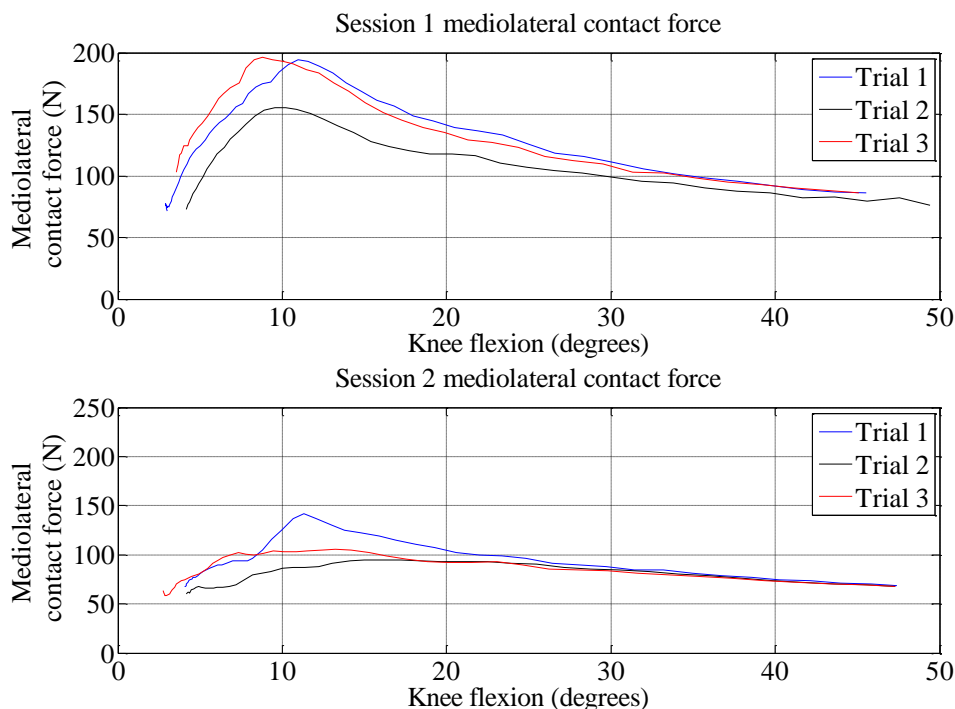


Figure 40: Mediolateral patellofemoral contact force

For all the trials the mediolateral contact force initially occurs on the lateral facet until engagement where it occurs on both the medial and lateral facet. The force on the lateral facet is greater, resulting in a force in the medial direction. As can be seen in Figure 40, the mediolateral force increases from 3° to 12° flexion and then decreases until 50° flexion. The peak mediolateral force in session one is 196.9 N (0.28 BW) compared to session two where it is 141.6 N (0.202 BW) for trial two.

Table 24: Average contact force to muscle force ratios

Muscle ratio	Ratio range [mean]		Standard deviation	
	Session 1	Session 2	Session 1	Session 2
CF/RF	0.47 – 2.12 [0.72]	0.52 – 2.54 [0.84]	0.271	0.349
CF/VL	2.04 - 20.22 [11.33]	1.94 – 16.07 [8.44]	4.276	4.032
CF/VM	3.1 – 32.58 [17.45]	2.89 – 24.26 [13.27]	6.845	6.250
CF/VI	2.83 – 29.77 [15.99]	2.67 – 22.57 [12.14]	6.235	5.830
CF/QF	0.39 – 0.93 [0.6]	0.43 – 0.95 [0.62]	0.129	0.106

To determine which muscle of the quadriceps has the greatest effect on the contact force, the average ratio of the contact force to each muscle is shown in Table 24. The contact force is on average 10 to 15 times larger than the vasti forces, but is roughly the same size as the rectus femoris force in both sessions. When the contact force is compared to the quadriceps force (QF) as a whole, it is 60 % and 62 % of the muscle force in session one and two, respectively. Figure 41 shows that the contact force to quadriceps force ratio increases from for both sessions throughout stance phase.

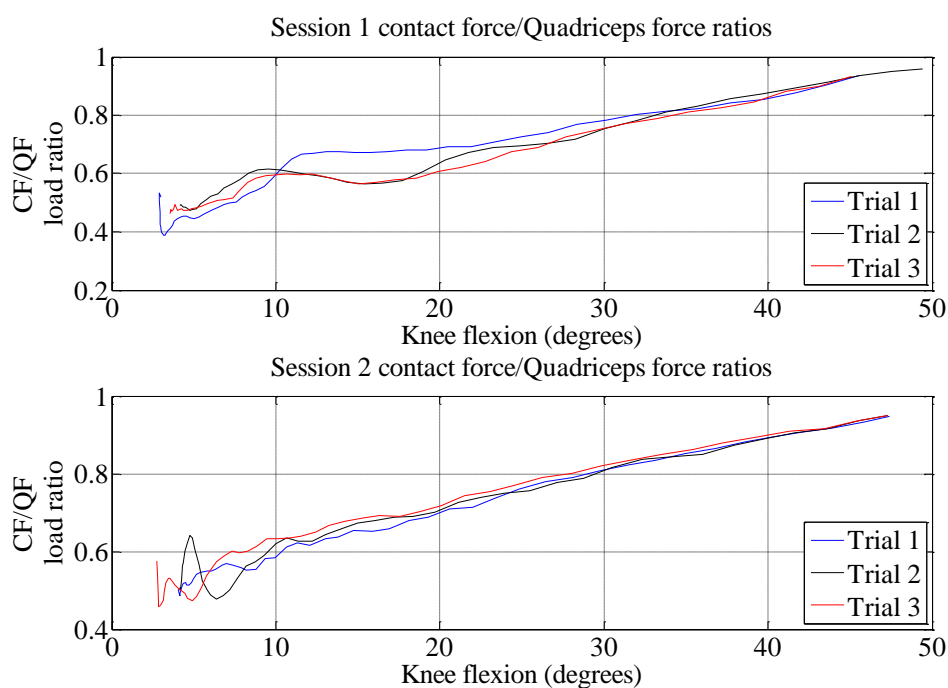
**Figure 41: Patellofemoral contact force and quadriceps force ratios in flexion**

Figure 42 shows that the tension in the MPFL decreases until trochlear engagement, where after it remains relatively constant until 50° flexion. In session one the MPFL tension is a maximum of 45.11 N (0.064 BW) and after trochlear engagement remains in the range of 1.74 N to 5.69 N (0.002-0.008 BW). In session two the MPFL maximum tension is 38.57 N (0.055 BW) and after trochlear engagement remains in the range of 1.94 N to 5.65 N (0.002-0.008 BW).

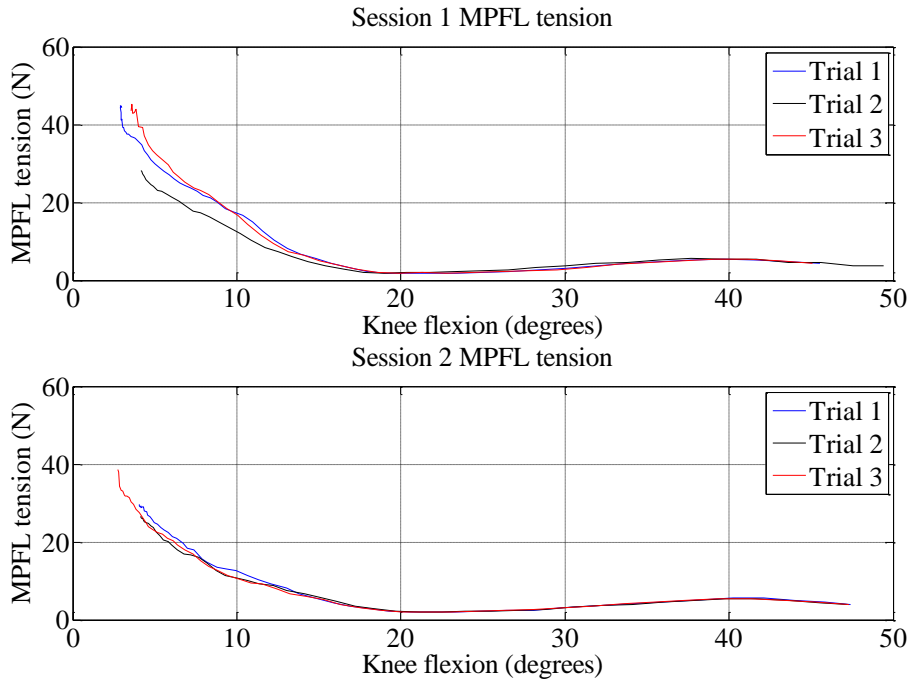


Figure 42: Medial patellofemoral ligament (MPFL) tension during flexion

6.3.2 Lateral patella displacement

The bisect offset values computed for each trial of each session are compared within the sessions in Figure 43 and Table 25.

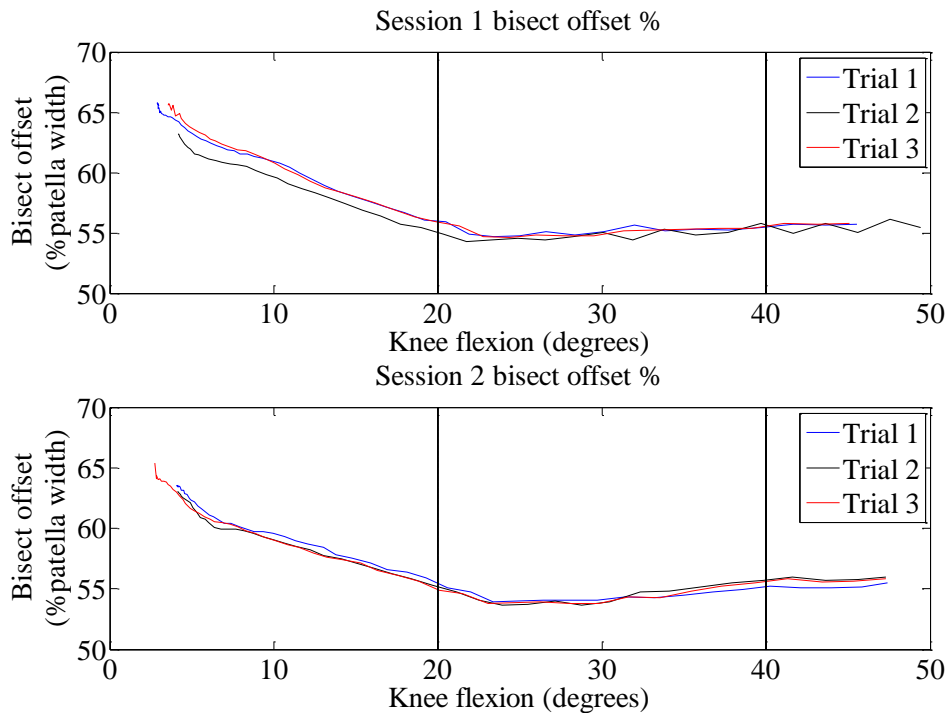
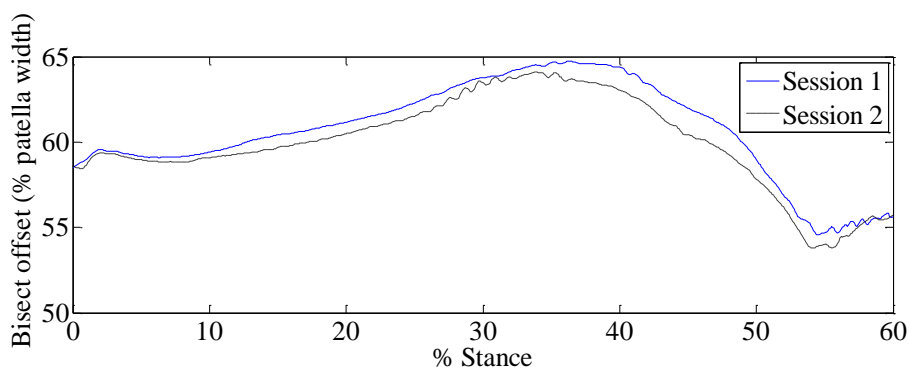


Figure 43: Bisect offset measured in each trial

Table 25: Intra-session bisect offset comparison

Trial	Session	Correlation coefficient, R [R ²]	RMS error (%)	% Max error
1	1	0.985 [0.97]	0.009	0.91
2		0.987 [0.974]	0.013	3.87
3		0.992 [0.983]	0.007	0.50
1	2	0.995 [0.991]	0.004	1.27
2		0.987 [0.973]	0.007	3.2
3		0.990 [0.98]	0.009	0.63

Each trial is compared to the mean bisect offset of the session it is in. In session one and two each trial predicts the mean bisect offset for its session with an accuracy of 98.5 % or higher ($R^2 > 0.97$). The largest RMS error between a trial and mean bisect offset is 0.013 % for trial two of session one, this further proves the intra-session repeatability of the lateral displacement of the patella. The final column in Table 25 shows the maximum error in each session as a percentage of the mean bisect offset for that session. These percentages are all below 4 % in both session one and two.

**Figure 44: Inter-session bisect offset comparison**

The average bisect offset computed in session one and two are compared in Figure 44. By looking at the figure above, a correlation coefficient of 0.97 ($R^2 = 0.944$) further proves that the linear relationship between the average bisect offset of each session is strong. The RMS error between session is 0.007 % and the maximum error between the sessions is 3.14 % of the bisect offset measured in session one.

6.3.3 Patella tilt angle

The patella tilt angles during stance phase are shown in Figure 45, where after an intra-session comparison of the angles is shown in Table 26.

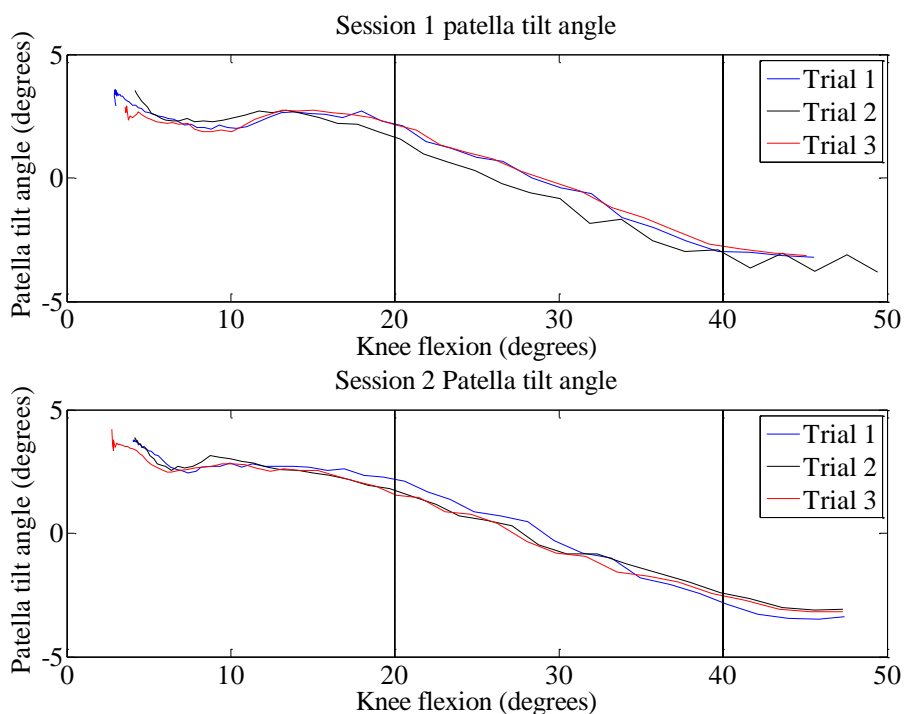


Figure 45: Intra-session patella tilt angle comparison

Table 26: Intra-session comparison between patella tilt angles

Trial	Session	Correlation coefficient, R [R ²]	RMS error (degrees)	% Max error
1	1	0.981 [0.962]	0.29	23.59
2		0.977 [0.955]	0.44	37.45
3		0.980 [0.96]	0.33	25.26
1	2	0.985 [0.970]	0.30	24.63
2		0.974 [0.949]	0.36	23.01
3		0.981 [0.962]	0.34	22.09

Similarly to the bisect offset, for both session one and two the patella tilt angle (referred to as tilt angle) computed in each trial correlates well with the tilt angles calculated in the other trials in the same session ($R > 0.97$). All trials in session one and two produce RMS errors less than 0.5° when compared to the mean tilt angle of the session they are in. However, the maximum errors in each trial are greater than 24 % of the maximum mean tilt angle in each session, with trial two of session one producing a maximum error that is 37.45 % of the maximum mean tilt angle of session one. The tilt angles are compared between sessions in Figure 46.

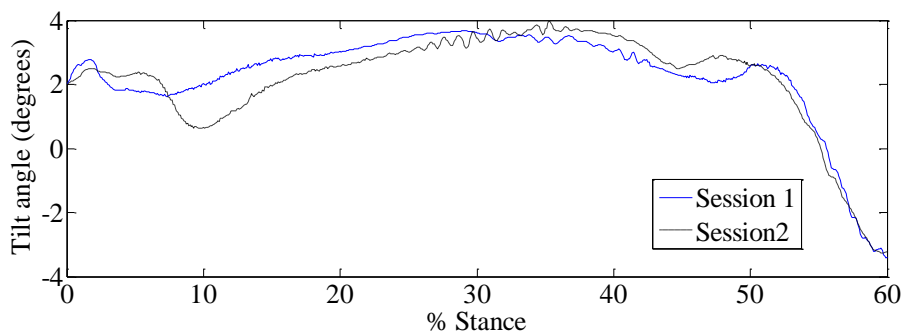


Figure 46: Inter-session comparison of patella tilt angle

The correlation coefficient achieved when comparing session one and two's tilt angles is 0.96 ($R^2 = 0.9216$). Although there is a small RMS error of 0.54° ; the maximum error between the calculated tilt angles is 38.8 % of the overall maximum tilt angle measured in both sessions.

6.4 Discussion

6.4.1 Patellofemoral contact force

Although the linear relationship between the contact forces measured in session one is strong ($R > 0.87$), trial two produces a smaller contact force throughout stance phase when compared to trial one and three. The only difference between the simulations run for each trial on Adams, is the knee joint kinematics and extensor muscle forces applied to the model. Since the knee angle throughout stance phase is repeatable, not only between trials within the same session, but also between trials in session one and two, the muscle force would lead to differences in the outputs of the Adams simulations.

In Chapter 5 the extensor muscle forces computed in session one and two were compared within each session and between the sessions. It was shown that the muscle forces produced in session one correlated strongly with one another; however Figure 29 shows that the rectus femoris force in trial two is considerably smaller than trial one and three. The forces produced by the vasti muscles in each trial are more similar, and those produced in trial two are between the forces produced in trial one and three.

Since the force produced by the rectus femoris is higher than those produced by the vasti muscles and the force is applied in the middle of the most superior point of the patella, this will have a greater influence on the contact force between the patella and femur. This is proven by Figure 41 and Table 24 where it is shown that the rectus femoris force is on average 78 % of the contact force for both sessions. In comparison, the contact force is on average 10.6 times larger than the vastus lateralis force, 16.4 times larger than the vastus medialis force and 15 times larger than the vastus intermedius force.

The contact force-quadriciceps force ratio increases gradually from 5° to 50° for both session one and two. This trend is also evident in studies performed by D'Lima *et al.* [31] and Fernandez *et al.* [44]. D'Lima *et al.* reported a load ratio of approximately 0.6 at 0° flexion and Fernandez *et al.* computed a ratio of 0.7 to 1 over 60° of knee flexion. The contact force-quadriciceps force ratio computed in session one and two of this project, agree with these results published in literature.

The contact forces computed in the trials of session two produce more repeatable results with smaller RMS errors compared to session one. This is expected as the extensor muscle forces have a stronger linear relationship with one another compared to those in session one (Figure B. 18). Trial one of session two has a peak at 50 % of stance that is not present in trial two and three. However, this can be explained by the peak in the rectus femoris force at the same point in time in trial one, which is not present in trial two and three.

Although the correlation coefficient between the contact forces measured in session one and two is very low, one can see in Figure 39 that the mean contact forces of each session have similar trends. Due to the fact that the rectus femoris muscle forces in session one are predominantly larger than those in session two (discussed in Chapter 5), the resultant mean patellofemoral contact force in session one is larger than session two.

The contact force during walking shown in literature has two distinct peaks throughout the gait cycle that occur at 0 to 25 % of the gait cycle and 50 to 75 % of the gait cycle [37], [49], [78], [79]. Within this project, there are two less distinct peaks in the measured contact force that occur at 0 to 25 % of the gait cycle and 40 to 60 % of the gait cycle (Figure 39).

The difference in the timing can be explained by comparing the knee moment computed in these sources to those computed in this paper. The moment at the end of stance phase in this project, occurs at ± 75 % of the gait cycle in both Ward *et al.* [78] and Heino Brechter *et al.*'s papers [79]. As has been mentioned, the peaks in the contact force are more distinct in these sources. This is similar to the comparison made in Chapter 5 between the rectus femoris force and those reported in literature. Both the rectus femoris and contact forces computed in this project do not decrease as much between peaks when compared to literature. Since the rectus femoris is predominantly responsible for the contact force in this project, as previously proven, the slight decrease in contact force is not unlikely.

The magnitude of the contact force compares well to those in literature. The first peak of the mean contact force computed in each session of this subject is 494.5 N (6.89 N/kg) in session one and 470.3 N (6.55 N/kg) in session two. In comparison, Ward and Powers calculated a maximum contact force of ± 550 N [78], Lin *et al.* computed a maximum contact force of approximately 250 N [49], and Heino Brechter and Powers reported a maximum contact force of 7.46 N/kg for patients with patellofemoral pain and 9.51 N/kg for normal patients [79].

The mediolateral contact force for all trials in session one first increases gradually from 5° to 10° of flexion and then gradually decreases until 50° flexion. In session two this trend is evident in trial one, but not in the other two trials. These trends are not consistent with literature. D’Lima *et al.* [31] and Elias and Cosgarea [45] compute a mediolateral contact force that increases with an increase in knee flexion. The resultant shear contact force calculated in this project is in the medial direction during stance phase, whereas the aforementioned sources computed a shear contact force that acts in the medial direction from 0° to 20° flexion and then acts laterally. Mesfar and Shirazi-Adl found that the mediolateral contact force decreased slightly from 0° to 90° flexion [50], which is more similar to the results in this project.

The resultant shear contact force on the patella calculated in this project acts in the medial direction during stance phase. The difference in shear contact force could be due to the inaccurate hip kinematics discussed in the previous chapter. Powers states that altered hip kinematics may influence the lateral forces acting on the patella [73]. Specifically, hip adduction results in the patella shifting medially and thus results in an increased lateral contact force. Furthermore, the difference between the shear contact force computed in this project and literature could also be due to model differences. D’Lima *et al.* developed a finite element model of the knee consisting of the femur, tibia, patella, patella tendon and quadriceps tendon [31], and applied a single force to the quadriceps tendon. Elias and Cosgarea modelled the knee using the femur, tibia, patella, patella tendon, MPFL, lateral retinaculum and medial patellomeniscal ligament (MPML) [45], and applied the same muscle forces as this project. Mesfar and Shirazi-Adl developed a model consisting of the femur, tibia, patella, patella tendon, MPFL and lateral patellofemoral ligament (LPFL) [50], and applied the same muscle forces as this project.

The added lateral and medial ligaments in these sources models further stabilise the patella in the mediolateral direction. Within this project the patella is stabilised in the mediolateral direction by the MPFL. Figure 42 shows that the tension in the MPFL decreases from 0° to 20° flexion and then remains constant at a low force. This trend agrees with results published by Mesfar and Shirzai-Adl [50] and Elias and Cosgarea [45]. Therefore, the MPFL only applies a considerable force to the patella before trochlear engagement.

It is clear that the contact force is dependent on the muscle forces applied to the model, as the knee angles computed in this project are very similar. Within this project the rectus femoris muscle is mainly responsible for the contact force, since the vasti muscle forces are much less. Therefore, any trend seen in the rectus femoris force is evident in the contact force. Although the contact force measured in this project does not correlate perfectly with literature (due to rectus femoris force), it still has two peaks and is similar in magnitude.

6.4.2 Lateral patella displacement

The lateral displacement of the patella in each trial is correlated well with one another as is evident by the repeatability of the bisect offset measured in each trial. In session one and two the correlation coefficients between trials and the mean of each respective session are all over 0.98 which implies that the trials have a strong linear relationship. However, this is also true between sessions as the correlation coefficient between session one and two's mean bisect offset percentage is 0.99.

For this subject the patella is situated more laterally when the knee is in a relaxed position, but when the knee begins to flex the patella moves medially until it engages with the trochlear groove where after the bisect offset percentage is more constant. This is evident in Figure 43, where bisect offset decreases with initial flexion from 5° to 25°, but then becomes more constant for the rest of stance phase. These results coincide with the MPFL tension during flexion as the patella is initially displaced laterally by the MPFL until trochlear engagement.

The patella displacement computed in this project compares well to values reported by Ward [95]. The bisect offset decreases from $\pm 70\%$ to $\pm 55\%$ during 0° to 25° of knee flexion, but then becomes more constant until 60° flexion. Within this project the bisect offset is on average $\pm 65\%$ to $\pm 55\%$ from 5° to 25° of flexion and then becomes more constant for the remainder of stance phase.

6.4.3 Patella tilt angle

Within each session the computed patella tilt angle produces repeatable results in terms of the correlation coefficient, COD and RMS errors achieved between trials and the mean tilt angle in their respective sessions. On the other hand, the maximum tilt angle error as a percentage of the maximum tilt angle in stance phase is well over 10% in all the trials. This could be due to the large amount of fluctuation in the tilt angles (seen as the wave-like form). It is important to remember that the patella is being pulled by four different muscles in different directions superiorly, the MPFL laterally, and the PT inferiorly. Therefore any difference in the muscle force applied to the model will result in a slight change in the patella tilt, even if for an instant.

Although the correlation coefficient achieved when comparing session one and two's tilt angles is high, Figure 46 suggests that the tilt angles produced in each session differs slightly. A larger minimum peak is evident in session two's mean tilt angle at roughly 10% of the gait cycle, where after the tilt angles of the two sessions have a stronger linear relationship

The large difference in tilt angles occurs in the first 15% of the gait cycle in both sessions (Figure 44), which is also when the largest difference occurs between the extensor muscle forces in both sessions (Figure 29 and Figure B. 18). Therefore, once again the muscle forces greatly influence the outputs of the musculoskeletal model.

As can be seen in Figure 37, the patella initially tilts laterally when the knee is in a resting position. However, due to prominence of the lateral facet of the femur lateral condyle and the fact that the model only has a MPFL and no lateral retinaculum, the patella begins to tilt medially and continues to do so until 50° of knee flexion when the patella tilt angle is completely medial.

Ward also showed that the patella tilts medially from 0° to 60° of knee flexion, however the patella tilt angle at 60° flexion is still positive and therefore the patella is laterally tilted [95]. Ward applied a similar approach as this project to measure the patella tilt angle. Amis *et al.* performed an *in vitro* study where the patella kinematics were tracked using an electromagnetic receiver which was mounted onto the anterior surface of the patella [23]. They found that from 0° to 60° of flexion the patella tilts laterally. Fernandez *et al.* measured the patella tilt about a longitudinal axis through the superior-inferior poles of the patella, and found that the patella first has a medial tilt, but tilted laterally with increased flexion [96].

Brunet *et al.* performed an *in vitro* study where the patella tilt angle is also tracked using an electromagnetic receiver [97]. Similar to this project, they found that the patella initially tilted laterally and then tilted medially from 10° to 90° tibiofemoral flexion. It is evident that the literature varies on the reported patella tilt angles during flexion. Katchburian *et al.* explains that patella tracking is affected by how the co-ordinate frames and reference points for measurements are defined [98]. They further explain that most literature agree that the patella translates medially in early knee flexion (like in this project) and then translates laterally. However, the results are less consistent with regards to the patella tilt angle according to Katchburian *et al.*

From the results and discussion in this chapter, one can see that the subject specific musculoskeletal models in both session one and two produce repeatable results within the sessions and between sessions. Throughout this modelling pipeline certain approximations and simplifications result in errors that compound and sometimes produce variable results when compared to literature. This is only evident in the vasti muscle force magnitudes and rectus femoris force which does not have a large decrease between the two peaks. This then affects the patellofemoral contact force, which differs from literature in the same way the rectus femoris does. However due to the repeatability of the results produced in this pipeline and the agreement between certain results and literature, with fewer approximations it could be possible to produce more accurate patellofemoral contact forces.

Chapter 7

Conclusion

This project forms part of a prospective study on anterior knee pain for which the aim is to assess the effect of physiotherapeutic intervention on patellofemoral risk factors and clinical outcomes in subjects with anterior knee pain during functional movement. Specifically, the aim of this project was to develop and apply a computational modelling pipeline using experimental data obtained from a motion analysis clinic to predict the knee joint kinematics and muscle forces, patellofemoral reaction forces and patella kinematics during stance phase of over ground level walking. This was achieved by applying three consecutive modelling approaches which together make up the full computational modelling pipeline:

- A method to incorporate the GRF data of the foot not striking the force plate is applied using kinematic and kinetic data obtained in the motion analysis clinic.
- Experimental kinematic and kinetic data is used in a modelling pipeline applied using OpenSim software to obtain the knee joint kinematics and muscle forces during stance phase.
- A three-dimensional subject specific musculoskeletal model of the patellofemoral joint is generated from MRI scans. The medial patellofemoral ligament (MPFL) and patella tendon were included and modelled as idealised spring elements. The muscle forces and knee joint kinematics computed using the OpenSim pipeline were applied to the musculoskeletal model to replicate the motion of the subjects knee as measured in the motion analysis clinic. The patellofemoral contact force and patella kinematics were then computed during stance phase.

7.1 Aims

The aims identified to successfully complete this project are discussed below:

Aim 1: Measure joint geometry, kinematic and kinetic drivers for the musculoskeletal model during over ground level walking and stair descent.

Eleven subjects with anterior knee pain were used to obtain experimental data. Each subject underwent an MRI scan of the affected knee which is later used in a segmentation procedure to develop computational model of the patellofemoral joint. All subjects performed various functional movements in the Central Analytical Facility (CAF) Motion Analysis Clinic where their body kinematics and kinetics were recorded. The movement of the subjects was recorded using motion capture equipment where markers are tracked on relative body segments. The trajectories of these markers are used to reproduce the same motion using a musculoskeletal model with markers placed in the same anatomical positions. The ground reaction force between the subject and laboratory floor is measured using a force plate and FScan pressure measurement insoles.

This project was the first project being done at the CAF Motion Analysis Clinic where all the measuring equipment being used was combined. Therefore over the course of the project it evolved and certain challenges and limitations were identified. Initially the kinematics of the upper extremity were not tracked with the motion capture system, but later it was determined that these kinematics must be tracked to perform a successful RRA and CMC analysis in OpenSim. Hence, not all trials have motion capture data for the upper extremity and are modelled using only the lower extremity. However, one can still compute the knee joint kinematics and moment using a model that only contains the lower extremity. Chapter 5 proves that a model with and without a torso produce knee flexion-extension angles and knee flexion-extension moments that are 99.9 % similar to one another. The knee moment and kinematics computed using a model with no upper extremity is used in an in-house muscle model developed by a member of the Biomedical Engineering Research Group (BERG).

Another limitation is the fact that the laboratory only has one force plate installed. It is necessary to measure the GRF applied to both feet individually to perform a successful biomechanical analysis. This is because even though one leg is being analysed, the force applied to the other leg generates a moment on the body and is needed to determine the muscle forces during walking. To overcome this challenge two methods are investigated that are discussed under the second and third aims.

During this study the CAF Motion Analysis Clinic underwent renovations and it was found that the force plate was not correctly mounted to the floor. This resulted in an artefact in the GRF and COP measured by the force plate at 8 % of the gait cycle. The decision was taken to filter the GRF data. Due to the fact that the CAF Motion Analysis Clinic was undergoing renovations, I advised them to obtain two more force plates and properly mount the force plates, to produce more accurate results in the future. They agreed and have now acquired two more force plates and mounted the existing force plate correctly.

Aim 2: Estimate the position of the centre of pressure (COP) of the foot not striking the force plate during stance phase.

Two methods were introduced to estimate the COP of the foot not striking the force plate. Namely, a method to incorporate a FScan insole pressure measurement system that records the GRF normal to the insole and the COP thereof is used and compared to a method where an average GRF and COP measured in trials where the investigated foot strikes the force plate is superimposed onto the same foot when it is not striking the force plate.

The F-Scan system begins recording the normal GRF and COP just after the other measuring equipment has begun recording. This time delay is not consistent; therefore a method is applied that successfully synchronises the F-Scan experimental data and the data obtained from the other measuring equipment. The FScan COP is recorded in a local co-ordinate reference frame and is converted into the global capture volume co-ordinate frame. This produces a COP that is on

average 98.6 % and 63.2 % similar to the COP measured by the force plate in the anteroposterior and mediolateral directions, respectively. The superimposition method estimates a COP that is on average 98.8 % and 60.7 % similar to the COP measured by the force plate in the anteroposterior and mediolateral directions, respectively, but produces smaller RMS errors compared to the FScan method. These results are within the same range as values reported in literature [54], [61].

Due to the rigid foot model approximation used in both methods, the estimated COP differs most from the measured COP in the first and last 10 % of stance phase. During these periods of time the foot is not flat on the ground, therefore by not assuming a rigid foot model and taking the deformation of the foot during stance phase into account, one could achieve more accurate results.

Aim 3: Estimate the complete ground reaction force (GRF) of the foot not striking the force plate during stance phase.

Two methods were discussed that estimate the complete GRF acting on the foot not striking the force plate. Firstly, the normal force measured by the FScan insole is converted to a three-dimensional ground reaction force using numerical optimization and the foot marker kinematics. Secondly, an average is taken of the GRF measured by the force plate and is superimposed onto the same foot when it is not striking the force plate.

The FScan method reproduces the GRF measured by the force plate with an average accuracy of 48 %, 96.9 % and 92.6 % in the mediolateral, anteroposterior and vertical directions, respectively. The superimposition method computes a GRF that is 88.8 %, 99.3 % and 98.1 % similar in the mediolateral, anteroposterior and vertical direction, respectively. Furthermore the superimposition method is able to estimate the free moment acting on the foot with an accuracy of 61.6 %. The weaker correlation between the estimated free moment and experimental free moment is due to the fact that the COP and force computed using the superimposition method is used to calculate the free moment. Therefore, the inaccuracy of each measure will result in a larger error in the free moment.

The FScan method is not able to estimate the complete GRF using an insole as accurately as studies in literature [54], [62], however the superimposition method is able to produce comparable results and compute the free moment acting on the foot (this is something that is not accomplished in literature using a pressure measurement insole). The superimposition method results in a knee moment that correlates more strongly with the knee moment computed using experimental data. It is of utmost importance that the generated knee moment is accurate as the muscle forces are computed using this moment.

Both methods present the user with drawbacks. Within the FScan method, the insole can slip which results in an altered GRF and COP reading, and the damping caused by the sole of the shoe is not accounted for. The superimposition method assumes that the GRF measured during each trial is repeatable. This is not always the case

as the subject can adjust their velocity during walking or strike the ground with a larger force. This will result in a different COP and GRF.

Although both methods produce accurate results when estimating the COP, the superimposition method more accurately computes the GRF. The superimposition method is therefore applied in the computational modelling pipeline and the GRF and COP on the foot not striking the force plate is successfully estimated.

Aim 4: Apply a modelling pipeline in OpenSim to determine the knee joint kinematics and muscle forces during stance phase.

The subjects kinematic and kinetic data, along with the GRF data computed using the superimposition method were used an OpenSim modelling pipeline. A generic musculoskeletal model was scaled according to experimental marker positions to match the anthropometric properties of the subject being tested.

Within scaling and the inverse kinematic (IK) analysis, all models achieved maximum and RMS errors within the values put forward by OpenSim. The knee and hip flexion-extension angles computed using OpenSim have a strong positive correlation with the same angles computed using the PiG model in Nexus. The scaled model consisted of a knee joint with one degree of freedom and the subtalar and MTP joints were locked. This resulted in hip adduction and rotation angles that correlated well with the PiG model angles, but differed in magnitude. This is due to the fact that the joint of the lower extremity work together in a kinetic-chain to achieve motion. Therefore, if the knee and ankle joint are not able to adduct and rotate, this results in an altered adduction and rotation at the hip.

The residual reduction algorithm (RRA) analysis resulted in large residual forces in three out of the twelve trials and large positional errors in three out of the twelve trials. The RRA tool applies residual forces to the models pelvis, alters the mass of individual bone segments and alters the kinematics of the model, all to better match the model kinematics to the GRF applied to the model. Therefore, if the GRF data applied to the foot not striking the force plate is inaccurate, it can result in larger errors. This is evident in the results of this project. For example, if the GRF applied in one out of the three trials is much smaller, it results in positional and/or residual force errors. This is because the same force is applied to the non-striking foot of all three trials, but the force on the striking foot differs in magnitude. Since the models adjusted mass is computed using the vertical force on the model and the majority of the vertical force is experienced by the foot striking the force plate, the lower force results in a lighter model that is not capable of withstanding the larger forces off the force plate. This results in positional and/or residual forces errors during the first and last 10 % of stance.

The adjusted kinematics and musculoskeletal model from the RRA analysis are used in the computed muscle control (CMC) analysis to calculate the muscle force on the knee joint. Therefore, the trials which experienced very large residual forces and positional errors in the RRA analysis are the same trials that have large errors

in the CMC analysis. However, only two out of the twelve trials have errors that are too large.

The muscle forces computed in this project follow the same linear pattern as the muscle forces shown in literature [43], [82], [83], with the only difference being that the rectus femoris force in this project does not have as distinct peaks as those in two of the three sources compared to. The magnitude of the quadriceps femoris force computed in this study compares well to values reported in literature, but the separate muscle force components which make it up differ. The rectus femoris force is larger than values in literature, but the vasti forces are lower. This could be due to the simplified knee joint and altered hip kinematics of the OpenSim model as knee and hip adduction and rotation result in mediolateral displacement of the patella. Since the vasti muscles contribute to patella stability, the lack of a patella and mediolateral displacement thereof could result in inaccurate vasti forces. Furthermore, since the rectus femoris is in line with the quadriceps tendon, it is 'easier' for the static optimizer to apply a larger force with the rectus femoris to produce the knee flexion-extension during stance phase.

From the OpenSim modelling pipeline it is clear that the GRF data applied to each foot greatly influences the knee moment and muscle forces computed by the musculoskeletal model. Therefore, the superimposition method results in large errors in trials where the superimposed force and force measured by the force plate differ greatly. However, although the rectus femoris and vasti muscles forces differ in magnitude, all muscle forces agree with the shape of the muscle forces published in literature and the force of the quadriceps muscle agrees in magnitude with that shown in literature.

Aim 5: Develop a subject specific musculoskeletal model to measure the patellofemoral contact force and track the patella kinematics.

MRI scans were used to successfully generate a three-dimensional subject specific musculoskeletal model of the patellofemoral joint. The MPFL and patella tendon were modelled as idealised tension only spring elements for which the material properties and insertion points were found in literature. The individual muscle forces of the quadriceps muscle were applied to the patella at insertion points determined using the scaled generic musculoskeletal model from OpenSim and literature. The muscle forces and knee flexion-extension angle computed in the OpenSim modelling pipeline were applied to the subject specific musculoskeletal model in order to compute the patella kinematics and patellofemoral contact force.

It was found that the rectus femoris force had the largest influence on the contact force as it was the largest force produced by the extensor muscles. This had a direct effect on the contact force, as the shape of the contact force during stance phase agrees with the shape seen in literature. However, as is with the rectus femoris force, the two peaks seen in the contact force during stance phase are not as distinct as those shown in literature [37], [49], [78], [79]. The magnitude of the contact force compares well to the patellofemoral contact forces published in literature, and so

does the ratio between the contact force and quadriceps tendon force. The mediolateral (shear) contact force computed in this study does not compare as well to literature. The reaction force acts predominantly in the medial direction, whereas the opposite is true for values published in literature [31], [45], [50]. This difference could be due to the difference in vasti muscles forces which result from the altered hip kinematics and simplified knee model used in OpenSim. Furthermore these sources use models with more soft tissue stabilizers which results in greater patella stability.

The tension experienced in the MPFL is consistent with trends shown in literature [45], [50]. The values computed during flexion show that the MPFL only applies considerable tension to the patella during trochlear engagement, where after the tension force remains low and constant. This tension has an effect on the lateral displacement of the patella in the first 20° of flexion. The lateral displacement of the patella is shown as a percentage of the patella width known as the bisect offset. The bisect offset values computed in this study agree with values published in literature by Ward [95]. The patella was situated more laterally when the knee was relaxed and when the knee begins to flex it moves medially until trochlear engagement, where after the bisect offset percentage becomes more constant..

The patella tilt angle computed in this project compared well to values shown in one out of three literature sources. The patella initially tilts laterally when the knee is in a resting position. However, due to prominence of the lateral facet of the femur lateral condyle and the fact that the model only has a MPFL, the patella begins to tilt medially and continues to do so until 50° of knee flexion when the patella tilt angle is completely medial. Rotation and adduction of the knee also has an effect on the patella kinematics, therefore the simplified knee model could affect the tilt angle during flexion.

Katchburian *et al.* explains that patella tracking is affected by how the co-ordinate frames and reference points for measurements are defined [98]. They further explain that most literature agree that the patella translates medially in early knee flexion (like in this project) and then translates laterally. However, the results are less consistent with regards to the patella tilt angle according to Katchburian *et al.*

Aim 6: Validate each step in the modelling pipeline by testing the intra-subject variability and repeatability.

To validate the modelling pipeline proposed in this project, the results are compared inter- and intra-session, when applicable, for each subject. It is important to note that the validity of the modelling pipeline is not affected by the input data, but the resulting patellofemoral loads and muscle forces are.

- The IK analysis produced knee flexion-extension angles that were on average 98.7 % similar to the angles computed using the PiG model.
- The hip flexion, adduction and rotation angles produced were on average 99.9 %, 81 % and 74.2 % similar to angles measured with the PiG model.

- The intra-session repeatability of the knee moment computed in the ID analysis was strong as indicated by the average correlation coefficient of 98.4 % ($R^2 = 96.8$). The difference in magnitude is explained by the difference in magnitude between the GRF forces applied to the model.
- The correlation coefficients between muscle forces computed within the same session are all over 0.9 except for the extensor muscle forces which have a minimum correlation coefficient of 0.819 for the rectus femoris. The difference in extensor muscle force magnitudes can be explained by the difference between the GRF applied to the foot striking the force plate and the foot on which a force is superimposed.
- When comparing muscle forces between sessions, all the muscles have a correlation coefficient of over 0.9 except for the extensor muscle forces which have a minimum correlation coefficient of 0.531 for the rectus femoris. This could be due to the difference in magnitude of the GRF between the two sessions and the large optimization errors achieved in session one.
- The contact force within each session has an average intra-session correlation coefficient of 94.1 %. An inter-session correlation coefficient of 0.416 indicates that they differ greatly, but when inspecting the contact force for each session by eye they follow similar trends for 50 % of stance phase where after session one's contact force increases more than session two. Once again this difference in contact force can be explained by the difference in muscle force as a result of the varying GRF between sessions.
- The lateral displacement of the patella is on average 97.9 % similar between trials within a session and is 94.4 % similar between sessions.
- The patella tilt angle during flexion is 96 % similar between trials within a session is 92.2 % similar between the two sessions.

The strong correlations achieved for most of the results of the modelling pipeline, show that the pipeline produces repeatable results, with the exception of the hip adduction and rotation angles that differ greatly in magnitude. In the two cases where the inter-session comparison produces less repeatable results, the difference can be explained by the difference in GRF data applied to the respective models as well as the errors that resulted from the RRA and CMC analyses.

7.2 Limitations

Due to constraints in the study, such as a shortage of force plates and renovations being done on the laboratory where testing is done, the results produced pre- and post-intervention could not be compared to one another to determine if there is a correlation between the patellofemoral biomechanics and the pain experienced by a subject. The reason for this is that the data obtained in session one was captured in the CAF Motion Analysis Clinic, while the data in session two was captured in a different laboratory with a different force plate. Secondly, the GRF data applied to the foot not striking the force plate is not the actual force experienced by the subject. Therefore, the results cannot be accurately compared to one another in terms of detecting differences within the knee joint; however the results can be used

to determine the repeatability of the results obtained using the modelling pipeline put forward in this project.

The difference between the superimposed GRF and measured GRF proved to influence the RRA and CMC results and therefore affected the muscle forces computed. However, this was only true for three of the twelve trials that were used. The simplified knee model and locked subtalar and MTP joints resulted in inaccurate hip adduction and rotation angles throughout stance phase. This then affects the muscle forces, patellofemoral contact force and patella kinematics.

7.3 Future work

The computational pipeline should be improved in the following ways:

- Three force plates should be used to apply accurate GRF data on both feet throughout stance phase.
- A finite element model should be used to determine the mechanical properties of the cartilage in the musculoskeletal model.
- A more complex knee joint should be used in the OpenSim modelling pipeline to better approximate the subjects movement.
- The lateral retinaculum should be added to the patient specific musculoskeletal model to better stabilise the patella.
- After applying these changes the same procedure applied in this study should be applied using data from subjects tested in a motion laboratory pre- and post-intervention. The effect of the intervention on the underlying biomechanical mechanism can then be determined.

7.4 Contribution to the field

This project puts forward a computational modelling pipeline to determine the muscle forces, patellofemoral contact loads and patella kinematics during stance phase. Within the pipeline two methods are introduced to incorporate the COP of the foot not striking a force plate, which differ to those shown in literature and produce comparable results. Although the modelling pipeline is not novel, it computes results that can be compared to similar studies in literature and shows the effect of applying inaccurate GRF data to the model.

The assumptions made in this project resulted in inaccuracies in some of the results. However, the rest of the results are repeatable within sessions and between sessions, as well as when they are compared to literature. The repeatability of the results computed in this project validates the modelling pipeline applied. Any discrepancies between results achieved in different sessions are explained by the difference in the GRF force applied in these sessions.

References

- [1] R. M. Biedert and V. Sanchis-Alfonso, "Sources of anterior knee pain.," *Clin. Sports Med.*, vol. 21, no. 3, pp. 335–47, vii, Jul. 2002.
- [2] R. Parker and J. Jelsma, "The prevalence and functional impact of musculoskeletal conditions amongst clients of a primary health care facility in an under-resourced area of Cape Town.," *BMC Musculoskelet. Disord.*, vol. 11, no. 1, p. 2, Jan. 2010.
- [3] J. C. Fairbank, P. B. Pynsent, J. A. van Poortvliet, and H. Phillips, "Mechanical factors in the incidence of knee pain in adolescents and young adults.," *J. Bone Joint Surg. Br.*, vol. 66, no. 5, pp. 685–93, Nov. 1984.
- [4] "JOSPT perspectives for patients. Anterior knee pain: a holistic approach to treatment.," *J. Orthop. Sports Phys. Ther.*, vol. 42, no. 6, p. 573, Jun. 2012.
- [5] N. J. Collins, L. M. Bisset, K. M. Crossley, and B. Vicenzino, "Efficacy of nonsurgical interventions for anterior knee pain: systematic review and meta-analysis of randomized trials.," *Sports Med.*, vol. 42, no. 1, pp. 31–49, Jan. 2012.
- [6] K. Crossley, K. Bennell, S. Green, and J. McConnell, "A systematic review of physical interventions for patellofemoral pain syndrome.," *Clin. J. Sport Med.*, vol. 11, no. 2, pp. 103–10, Apr. 2001.
- [7] J. Näslund, "Patellofemoral pain syndrome : Clinical and pathophysiological considerations." Institutionen för fysiologi och farmakologi / Department of Physiology and Pharmacology, 24-Feb-2006.
- [8] C. M. Powers, L. Bolgla, M. Callaghan, N. Collins, and F. Sheehan, "Patellofemoral Pain Syndrome: Proximal, Distal, and Local Factors—International Research Retreat, April 30–May 2, 2009, Baltimore, Maryland." *Journal of Orthopaedic & Sports Physical Therapy*. JOSPT, Inc. JOSPT, 1033 North Fairfax Street, Suite 304, Alexandria, VA 22134-1540, 01-Mar-2011.
- [9] T. F. Besier, G. E. Gold, G. S. Beaupre, and S. L. Delp, "A Modeling Framework to Estimate Patellofemoral Joint Cartilage Stress In Vivo," *Med. Sci. Sport. Exerc.*, vol. 37, no. 11, pp. 1924–1930, Nov. 2005.
- [10] S. Farrokhi, J. H. Keyak, and C. M. Powers, "Individuals with patellofemoral pain exhibit greater patellofemoral joint stress: a finite element analysis study.," *Osteoarthritis Cartilage*, vol. 19, no. 3, pp. 287–94, Mar. 2011.
- [11] T. F. Besier, G. E. Gold, S. L. Delp, M. Fredericson, and G. S. Beaupré, "The influence of femoral internal and external rotation on cartilage stresses within the patellofemoral joint.," *J. Orthop. Res.*, vol. 26, no. 12, pp. 1627–35, Dec. 2008.
- [12] T. Besier, C. Draper, S. Pal, M. Fredericson, G. Gold, S. Delp, and G.

- Beaupré, “Imaging and Musculoskeletal Modeling to Investigate the Mechanical Etiology of Patellofemoral Pain,” in *Atlas of the Patellofemoral Joint SE - 18*, V. Sanchis-Alfonso, Ed. Springer London, 2013, pp. 125–133.
- [13] C. K. Fitzpatrick, M. A. Baldwin, P. J. Laz, D. P. FitzPatrick, A. L. Lerner, and P. J. Rullkoetter, “Development of a statistical shape model of the patellofemoral joint for investigating relationships between shape and function,” *J. Biomech.*, vol. 44, no. 13, pp. 2446–52, Sep. 2011.
- [14] J. J. Elias, D. R. Wilson, R. Adamson, and A. J. Cosgarea, “Evaluation of a computational model used to predict the patellofemoral contact pressure distribution,” *J. Biomech.*, vol. 37, no. 3, pp. 295–302, Mar. 2004.
- [15] C. M. Powers, Y.-J. Chen, I. Scher, and T. Q. Lee, “The influence of patellofemoral joint contact geometry on the modeling of three dimensional patellofemoral joint forces,” *J. Biomech.*, vol. 39, no. 15, pp. 2783–91, Jan. 2006.
- [16] J. J. Elias, D. R. Wilson, R. Adamson, and A. J. Cosgarea, “Evaluation of a computational model used to predict the patellofemoral contact pressure distribution,” *J. Biomech.*, vol. 37, no. 3, pp. 295–302, Mar. 2004.
- [17] N. Palastanga, D. Field, and R. Soames, “Anatomy and human movement: structure and function,” 2006.
- [18] J. P. Goldblatt and J. C. Richmond, “Anatomy and Biomechanics of the Knee,” vol. 11, no. 3, pp. 172–186, 2003.
- [19] D. S. Hungerford and M. Barry, “Biomechanics of the patellofemoral joint,” *Clin. Orthop. Relat. Res.*, no. 144, pp. 9–15, Oct. 1979.
- [20] P. Aglietti and P. P. M. Menchetti, “Biomechanics of the patellofemoral joint,” in *The Patella*, Springer, 1995, pp. 25–48.
- [21] J. T. Andrish, “Biomechanics of the Patellofemoral Joint,” *Oper. Tech. Sports Med.*, vol. 23, no. 2, pp. 62–67, Jun. 2015.
- [22] A. A. Amis, “Current concepts on anatomy and biomechanics of patellar stability,” *Sports Med. Arthrosc.*, vol. 15, no. 2, pp. 48–56, Jun. 2007.
- [23] A. A. Amis, W. Senavongse, and A. M. J. Bull, “Patellofemoral kinematics during knee flexion-extension: an in vitro study,” *J. Orthop. Res.*, vol. 24, no. 12, pp. 2201–11, Dec. 2006.
- [24] S. M. Desio, R. T. Burks, and K. N. Bachus, “Soft tissue restraints to lateral patellar translation in the human knee,” *Am. J. Sports Med.*, vol. 26, no. 1, pp. 59–65, Jan. .
- [25] “The human skeletal foot,” 28/03/2015. [Online]. Available: <http://www.turbosquid.com/3d-models/max-human-skeleton-foot/910603>. [Accessed: 30-Jul-2015].

- [26] M. Whittle, *Gait Analysis: An Introduction*, Fourth Edi. Butterworth-Heinemann, 2007.
- [27] C. L. Vaughan, B. L. Davis, and J. C. O'Connor, *Dynamics of human gait, Volume 2*. Human Kinetics Publishers, 1992.
- [28] F. Verdini, M. Marcucci, M. G. Benedetti, and T. Leo, "Identification and characterisation of heel strike transient," *Gait Posture*, vol. 24, no. 1, pp. 77–84, Aug. 2006.
- [29] W. Herzog, D. Longino, and A. Clark, "The role of muscles in joint adaptation and degeneration.," *Langenbecks. Arch. Surg.*, vol. 388, no. 5, pp. 305–15, Oct. 2003.
- [30] D. D. D'Lima, S. Patil, N. Steklov, J. E. Slamin, and C. W. Colwell, "Tibial forces measured in vivo after total knee arthroplasty.," *J. Arthroplasty*, vol. 21, no. 2, pp. 255–62, Feb. 2006.
- [31] D. D. D'Lima, P. C. Chen, M. A. Kester, and C. W. Colwell, "Impact of patellofemoral design on patellofemoral forces and polyethylene stresses.," *J. Bone Joint Surg. Am.*, vol. 85-A Suppl, pp. 85–93, Jan. 2003.
- [32] T. J. Withrow, L. J. Huston, E. M. Wojtys, and J. A. Ashton-Miller, "The relationship between quadriceps muscle force, knee flexion, and anterior cruciate ligament strain in an in vitro simulated jump landing.," *Am. J. Sports Med.*, vol. 34, no. 2, pp. 269–74, Mar. 2006.
- [33] H.-J. Wilke, A. Rohlmann, S. Neller, F. Graichen, L. Claes, and G. Bergmann, "ISSLS prize winner: A novel approach to determine trunk muscle forces during flexion and extension: a comparison of data from an in vitro experiment and in vivo measurements.," *Spine (Phila. Pa. 1976)*, vol. 28, no. 23, pp. 2585–93, Dec. 2003.
- [34] C. M. Powers, Y.-J. Chen, I. Scher, and T. Q. Lee, "The influence of patellofemoral joint contact geometry on the modeling of three dimensional patellofemoral joint forces.," *J. Biomech.*, vol. 39, no. 15, pp. 2783–91, Jan. 2006.
- [35] T. F. Besier, M. Fredericson, G. E. Gold, G. S. Beaupré, and S. L. Delp, "Knee muscle forces during walking and running in patellofemoral pain patients and pain-free controls.," *J. Biomech.*, vol. 42, no. 7, pp. 898–905, May 2009.
- [36] D. Kumar, K. T. Manal, and K. S. Rudolph, "Knee joint loading during gait in healthy controls and individuals with knee osteoarthritis.," *Osteoarthritis Cartilage*, vol. 21, no. 2, pp. 298–305, Mar. 2013.
- [37] K. B. Shelburne, M. R. Torry, and M. G. Pandy, "Muscle, ligament, and joint-contact forces at the knee during walking.," *Med. Sci. Sports Exerc.*, vol. 37, no. 11, pp. 1948–56, Nov. 2005.
- [38] S. J. Olney and D. A. Winter, "Predictions of knee and ankle moments of

- force in walking from EMG and kinematic data,” *J. Biomech.*, vol. 18, no. 1, pp. 9–20, Jan. 1985.
- [39] J. Hicks, “OpenSim User’s Guide.” [Online]. Available: [http://simtk-confluence.stanford.edu:8080/display/OpenSim/User’s Guide](http://simtk-confluence.stanford.edu:8080/display/OpenSim/User's+Guide). [Accessed: 30-Jul-2015].
- [40] S. L. Delp, J. P. Loan, M. G. Hoy, F. E. Zajac, E. L. Topp, and J. M. Rosen, “An interactive graphics-based model of the lower extremity to study orthopaedic surgical procedures,” *IEEE Trans. Biomed. Eng.*, vol. 37, no. 8, pp. 757–67, Aug. 1990.
- [41] S. L. Delp, F. C. Anderson, A. S. Arnold, P. Loan, A. Habib, C. T. John, E. Guendelman, and D. G. Thelen, “OpenSim: open-source software to create and analyze dynamic simulations of movement,” *IEEE Trans. Biomed. Eng.*, vol. 54, no. 11, pp. 1940–50, Nov. 2007.
- [42] D. G. Thelen, F. C. Anderson, and S. L. Delp, “Generating dynamic simulations of movement using computed muscle control,” *J. Biomech.*, vol. 36, no. 3, pp. 321–328, Mar. 2003.
- [43] T. S. Buchanan, D. G. Lloyd, K. Manal, and T. F. Besier, “Estimation of Muscle Forces and Joint Moments Using a Forward-Inverse Dynamics Model,” *Med. Sci. Sport. Exerc.*, vol. 37, no. 11, pp. 1911–1916, Nov. 2005.
- [44] J. W. Fernandez and M. G. Pandy, “Integrating modelling and experiments to assess dynamic musculoskeletal function in humans,” *Exp. Physiol.*, vol. 91, no. 2, pp. 371–82, Mar. 2006.
- [45] J. J. Elias and A. J. Cosgarea, “Technical errors during medial patellofemoral ligament reconstruction could overload medial patellofemoral cartilage: a computational analysis,” *Am. J. Sports Med.*, vol. 34, no. 9, pp. 1478–85, Sep. 2006.
- [46] L. Blankevoort, J. H. Kuiper, R. Huiskes, and H. J. Grootenboer, “Articular contact in a three-dimensional model of the knee,” *J. Biomech.*, vol. 24, no. 11, pp. 1019–1031, Jan. 1991.
- [47] T. M. Guess, G. Thiagarajan, M. Kia, and M. Mishra, “A subject specific multibody model of the knee with menisci,” *Med. Eng. Phys.*, vol. 32, no. 5, pp. 505–515, Jun. 2010.
- [48] D. G. Lloyd and T. F. Besier, “An EMG-driven musculoskeletal model to estimate muscle forces and knee joint moments in vivo,” *J. Biomech.*, vol. 36, no. 6, pp. 765–776, Jun. 2003.
- [49] Y.-C. Lin, J. P. Walter, S. A. Banks, M. G. Pandy, and B. J. Fregly, “Simultaneous prediction of muscle and contact forces in the knee during gait,” *J. Biomech.*, vol. 43, no. 5, pp. 945–52, Mar. 2010.
- [50] W. Mesfar and A. Shirazi-Adl, “Biomechanics of the knee joint in flexion under various quadriceps forces,” *Knee*, vol. 12, no. 6, pp. 424–34, Dec.

2005.

- [51] “Female human body outline clipart.” [Online]. Available: <http://tursweet.com/f/female-human-body-outline-clipart.html>. [Accessed: 13-Aug-2015].
- [52] G. Paolini, “Plug in Gait WebEx Training.” [Online]. Available: http://www.analisedemarcha.com/papers/manutencao/manuais/Vicon_Plug_in_Gait_WebEx_Training_-_Session3.pdf. [Accessed: 20-Jan-2016].
- [53] A. Forner Cordero, H. J. F. M. Koopman, and F. C. T. van der Helm, “Use of pressure insoles to calculate the complete ground reaction forces.,” *J. Biomech.*, vol. 37, no. 9, pp. 1427–32, Sep. 2004.
- [54] A. Forner-Cordero, H. J. F. M. Koopman, and F. C. T. van der Helm, “Inverse dynamics calculations during gait with restricted ground reaction force information from pressure insoles.,” *Gait Posture*, vol. 23, no. 2, pp. 189–99, Feb. 2006.
- [55] L. Fradet, J. Siegel, M. Dahl, M. Alimusaj, and S. I. Wolf, “Spatial synchronization of an insole pressure distribution system with a 3D motion analysis system for center of pressure measurements.,” *Med. Biol. Eng. Comput.*, vol. 47, no. 1, pp. 85–92, Jan. 2009.
- [56] S. Kim and M. A. Nussbaum, “Evaluation of two approaches for aligning data obtained from a motion capture system and an in-shoe pressure measurement system.,” *Sensors (Basel)*, vol. 14, no. 9, pp. 16994–7007, Jan. 2014.
- [57] H. Rouhani, J. Favre, X. Crevoisier, and K. Aminian, “Ambulatory assessment of 3D ground reaction force using plantar pressure distribution.,” *Gait Posture*, vol. 32, no. 3, pp. 311–6, Jul. 2010.
- [58] D. J. Rumsey, *Statistics For Dummies*. John Wiley & Sons, 2011.
- [59] J. A. Rice, “Mathematical statistics and data analysis third edition,” *Thomson Brooks/Cole 2007Duxbury*, vol. 138, 2011.
- [60] D. M. Roberts and F. H. Roberts, “Correlation coefficient,” 2015. [Online]. Available: <http://mathbits.com/MathBits/TISection/Statistics2/correlation.htm>. [Accessed: 12-Aug-2015].
- [61] E. S. Chumanov, C. D. Remy, and D. G. Thelen, “Computational techniques for using insole pressure sensors to analyse three-dimensional joint kinetics.,” *Comput. Methods Biomech. Biomed. Engin.*, vol. 13, no. 5, pp. 505–14, Oct. 2010.
- [62] D. T.-P. Fong, Y.-Y. Chan, Y. Hong, P. S.-H. Yung, K.-Y. Fung, and K.-M. Chan, “Estimating the complete ground reaction forces with pressure insoles in walking.,” *J. Biomech.*, vol. 41, no. 11, pp. 2597–601, Aug. 2008.
- [63] C. M. Kim and J. J. Eng, “Symmetry in vertical ground reaction force is

- accompanied by symmetry in temporal but not distance variables of gait in persons with stroke,” *Gait Posture*, vol. 18, no. 1, pp. 23–28, Aug. 2003.
- [64] K. Masani, M. Kouzaki, and T. Fukunaga, “Variability of ground reaction forces during treadmill walking,” *J. Appl. Physiol.*, vol. 92, no. 5, pp. 1885–90, May 2002.
- [65] A. L. Reville, S. D. Perry, A. Michelle Edwards, and J. P. Dickey, “Variability of the impact transient during repeated barefoot walking trials,” *J. Biomech.*, vol. 41, no. 4, pp. 926–930, Jan. 2008.
- [66] J. W. Wannop, J. T. Worobets, and D. J. Stefanyshyn, “Normalization of ground reaction forces, joint moments, and free moments in human locomotion,” *J. Appl. Biomech.*, vol. 28, no. 6, pp. 665–76, Dec. 2012.
- [67] T. F. Besier, M. Fredericson, G. E. Gold, G. S. Beaupré, and S. L. Delp, “Knee muscle forces during walking and running in patellofemoral pain patients and pain-free controls,” *J. Biomech.*, vol. 42, no. 7, pp. 898–905, May 2009.
- [68] J. J. Eng and D. A. Winter, “Kinetic analysis of the lower limbs during walking: What information can be gained from a three-dimensional model?,” *J. Biomech.*, vol. 28, no. 6, pp. 753–758, Jun. 1995.
- [69] O. D. Schipplein and T. P. Andriacchi, “Interaction between active and passive knee stabilizers during level walking,” *J. Orthop. Res.*, vol. 9, no. 1, pp. 113–119, Jan. 1991.
- [70] R. A. Palmitier, K.-N. An, S. G. Scott, and E. Y. S. Chao, “Kinetic Chain Exercise in Knee Rehabilitation,” *Sport. Med.*, vol. 11, no. 6, pp. 402–413, Jun. 1991.
- [71] E. E. Bunton, W. A. Pitney, T. A. Cappaert, and A. W. Kane, “The role of limb torque, muscle action and proprioception during closed kinetic chain rehabilitation of the lower extremity,” *J. Athl. Train.*, vol. 28, no. 1, pp. 10–20, Jan. 1993.
- [72] M. A. Lafortune, P. R. Cavanagh, H. J. Sommer, and A. Kalenak, “Three-dimensional kinematics of the human knee during walking,” *J. Biomech.*, vol. 25, no. 4, pp. 347–357, Apr. 1992.
- [73] C. M. Powers, “The influence of abnormal hip mechanics on knee injury: a biomechanical perspective,” *J. Orthop. Sports Phys. Ther.*, vol. 40, no. 2, pp. 42–51, Feb. 2010.
- [74] T. Q. Lee, G. Morris, and R. P. Csintalan, “The influence of tibial and femoral rotation on patellofemoral contact area and pressure,” *J. Orthop. Sports Phys. Ther.*, vol. 33, no. 11, pp. 686–93, Nov. 2003.
- [75] B. Noehren, J. Scholz, and I. Davis, “The effect of real-time gait retraining on hip kinematics, pain and function in subjects with patellofemoral pain syndrome,” *Br. J. Sports Med.*, vol. 45, no. 9, pp. 691–6, Jul. 2011.

- [76] R. B. Souza and C. M. Powers, "Differences in hip kinematics, muscle strength, and muscle activation between subjects with and without patellofemoral pain.," *J. Orthop. Sports Phys. Ther.*, vol. 39, no. 1, pp. 12–9, Jan. 2009.
- [77] C. M. Powers, "The influence of altered lower-extremity kinematics on patellofemoral joint dysfunction: a theoretical perspective.," *J. Orthop. Sports Phys. Ther.*, vol. 33, no. 11, pp. 639–46, Nov. 2003.
- [78] S. R. Ward and C. M. Powers, "The influence of patella alta on patellofemoral joint stress during normal and fast walking.," *Clin. Biomech. (Bristol, Avon)*, vol. 19, no. 10, pp. 1040–7, Dec. 2004.
- [79] J. Heino Brechter and C. M. Powers, "Patellofemoral stress during walking in persons with and without patellofemoral pain.," *Med. Sci. Sports Exerc.*, vol. 34, no. 10, pp. 1582–93, Oct. 2002.
- [80] J. Dunne, "Email conversation with James Dunne," 2015. .
- [81] C. M. Powers, R. Landel, and J. Perry, "Timing and intensity of vastus muscle activity during functional activities in subjects with and without patellofemoral pain.," *Phys. Ther.*, vol. 76, no. 9, pp. 946–55; discussion 956–67, Sep. 1996.
- [82] E. M. Arnold, S. R. Hamner, A. Seth, M. Millard, and S. L. Delp, "How muscle fiber lengths and velocities affect muscle force generation as humans walk and run at different speeds.," *J. Exp. Biol.*, vol. 216, no. Pt 11, pp. 2150–60, Jun. 2013.
- [83] T. Castermans, M. Duvinage, G. Cheron, and T. Dutoit, "Towards effective non-invasive brain-computer interfaces dedicated to gait rehabilitation systems.," *Brain Sci.*, vol. 4, no. 1, pp. 1–48, Jan. 2013.
- [84] M. N. Doral, *Sports Injuries: Prevention, Diagnosis, Treatment and Rehabilitation*, vol. 7. Springer Science & Business Media, 2011.
- [85] J. Victor, "A Comparative Study on the Biomechanics of the Native Human Knee Joint and Total Knee Arthroplasty," Sep. 2009.
- [86] W. Mesfar and A. Shirazi-Adl, "Biomechanics of changes in ACL and PCL material properties or prestrains in flexion under muscle force-implications in ligament reconstruction.," *Comput. Methods Biomech. Biomed. Engin.*, vol. 9, no. 4, pp. 201–9, Aug. 2006.
- [87] P. Atkinson, T. Atkinson, C. Huang, and R. Doane, "A comparison of the mechanical and dimensional properties of the human medial and lateral patellofemoral ligaments," in *Proceedings of the 46th Annual Meeting of the Orthopaedic Research Society, Orlando, FL*, 2000.
- [88] P. Hansen, J. Bojsen-Moller, P. Aagaard, M. Kjaer, and S. P. Magnusson, "Mechanical properties of the human patellar tendon, in vivo.," *Clin. Biomech. (Bristol, Avon)*, vol. 21, no. 1, pp. 54–8, Jan. 2006.

- [89] T. D. O'Brien, N. D. Reeves, V. Baltzopoulos, D. A. Jones, and C. N. Maganaris, "Mechanical properties of the patellar tendon in adults and children.," *J. Biomech.*, vol. 43, no. 6, pp. 1190–5, Apr. 2010.
- [90] C. Couppé, P. Hansen, M. Kongsgaard, V. Kovanen, C. Suetta, P. Aagaard, M. Kjaer, and S. P. Magnusson, "Mechanical properties and collagen cross-linking of the patellar tendon in old and young men.," *J. Appl. Physiol.*, vol. 107, no. 3, pp. 880–6, Sep. 2009.
- [91] J. Victor, P. Wong, E. Witvrouw, J. Vander Sloten, and J. Bellemans, "How isometric are the medial patellofemoral, superficial medial collateral, and lateral collateral ligaments of the knee?," *Am. J. Sports Med.*, vol. 37, no. 10, pp. 2028–36, Oct. 2009.
- [92] R. F. LaPrade, A. H. Engebretsen, T. V Ly, S. Johansen, F. A. Wentorf, and L. Engebretsen, "The anatomy of the medial part of the knee.," *J. Bone Joint Surg. Am.*, vol. 89, no. 9, pp. 2000–10, Sep. 2007.
- [93] T. M. Guess, H. Liu, S. Bhashyam, and G. Thiagarajan, "A multibody knee model with discrete cartilage prediction of tibio-femoral contact mechanics.," *Comput. Methods Biomech. Biomed. Engin.*, vol. 16, no. 3, pp. 256–70, Jan. 2013.
- [94] Y.-H. Wen, L.-P. Hsu, P.-R. Chen, and C.-F. Lee, "Design optimization of cartilage myringoplasty using finite element analysis," *Tzu Chi Med J*, vol. 18, no. 5, pp. 370–377, 2006.
- [95] S. R. Ward, "Patella Alta: Association with Patellofemoral Alignment and Changes in Contact Area During Weight-Bearing," *J. Bone Jt. Surg.*, vol. 89, no. 8, p. 1749, Aug. 2007.
- [96] J. W. Fernandez, M. Akbarshahi, H. J. Kim, and M. G. Pandey, "Integrating modelling, motion capture and x-ray fluoroscopy to investigate patellofemoral function during dynamic activity," *Comput. Methods Biomech. Biomed. Engin.*, vol. 11, no. 1, pp. 41–53, Feb. 2008.
- [97] M. E. Brunet, M. R. Brinker, S. D. Cook, P. Christakis, B. Fong, L. Patron, and D. P. O'Connor, "Patellar tracking during simulated quadriceps contraction.," *Clin. Orthop. Relat. Res.*, vol. 414, no. 414, pp. 266–75, Sep. 2003.
- [98] M. V Katchburian, A. M. J. Bull, Y.-F. Shih, F. W. Heatley, and A. A. Amis, "Measurement of patellar tracking: assessment and analysis of the literature.," *Clin. Orthop. Relat. Res.*, no. 412, pp. 241–59, Jul. 2003.
- [99] C. Krames, "Knee anatomy - patella reflected to show knee anatomy [Image online]," 2001. [Online]. Available: www.kramesstudio.com. [Accessed: 21-Jul-2015].

Appendices

Appendix A: FScan and superimposition method results

A.1 Centre of pressure comparison

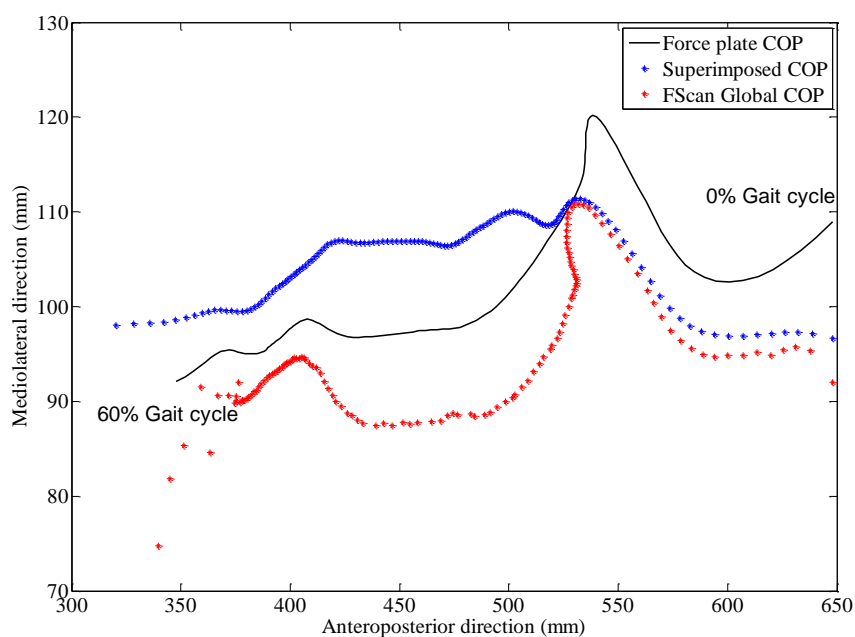


Figure A.1: Subject 1 trial 2 COP position comparison for superimposed and FScan methods

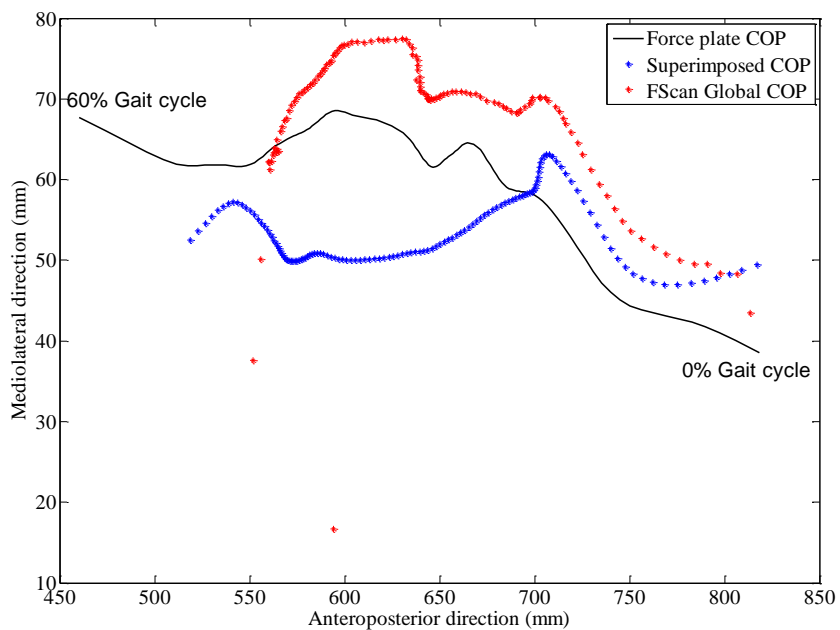


Figure A.2: Subject 1 trial 3 COP position comparison for superimposed and FScan methods

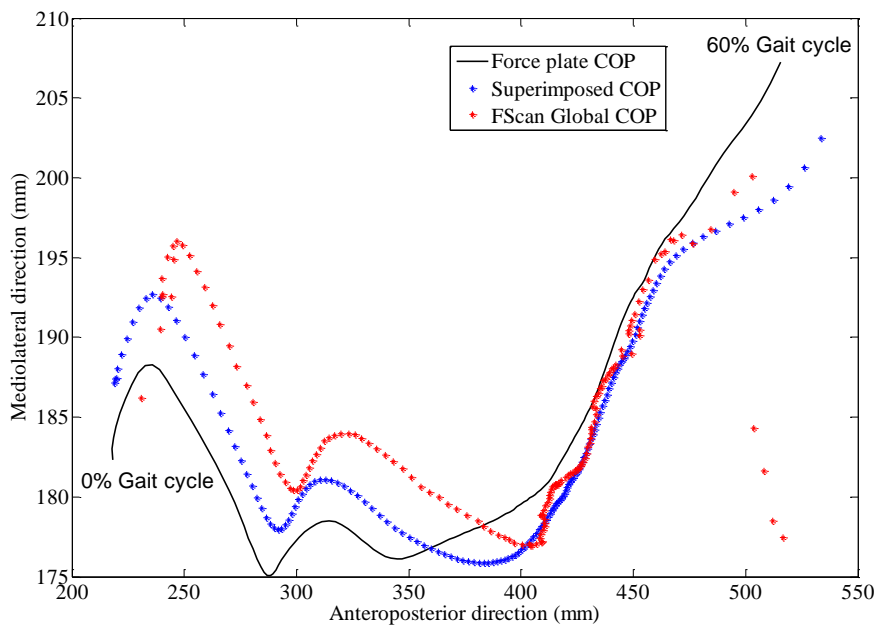


Figure A.3: Subject 2 trial 2 COP position comparison for superimposed and FScan methods

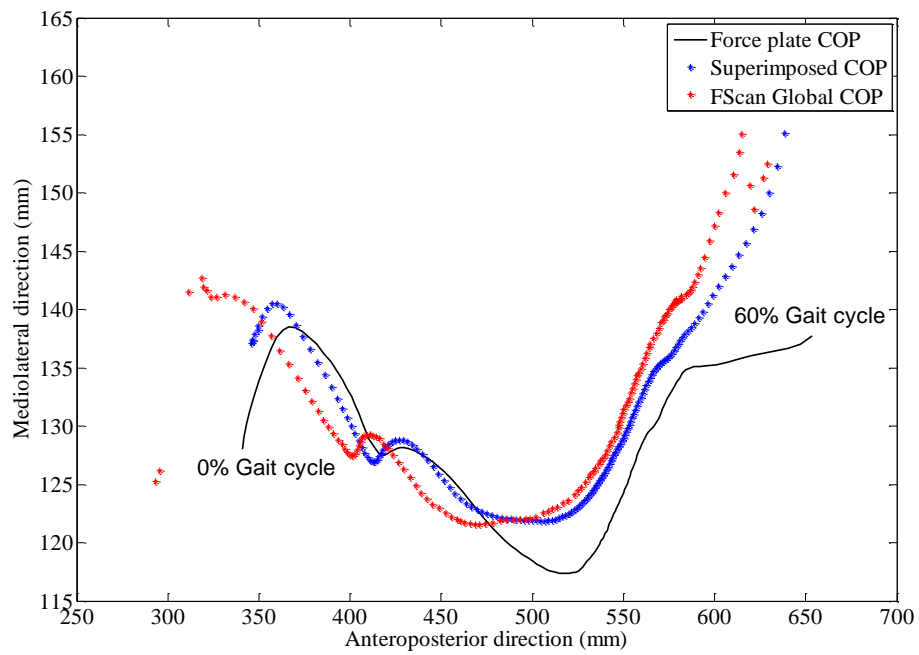


Figure A.4: Subject 2 trial 3 COP position comparison for superimposed and FScan methods

A. 2 Estimated ground reaction force comparison

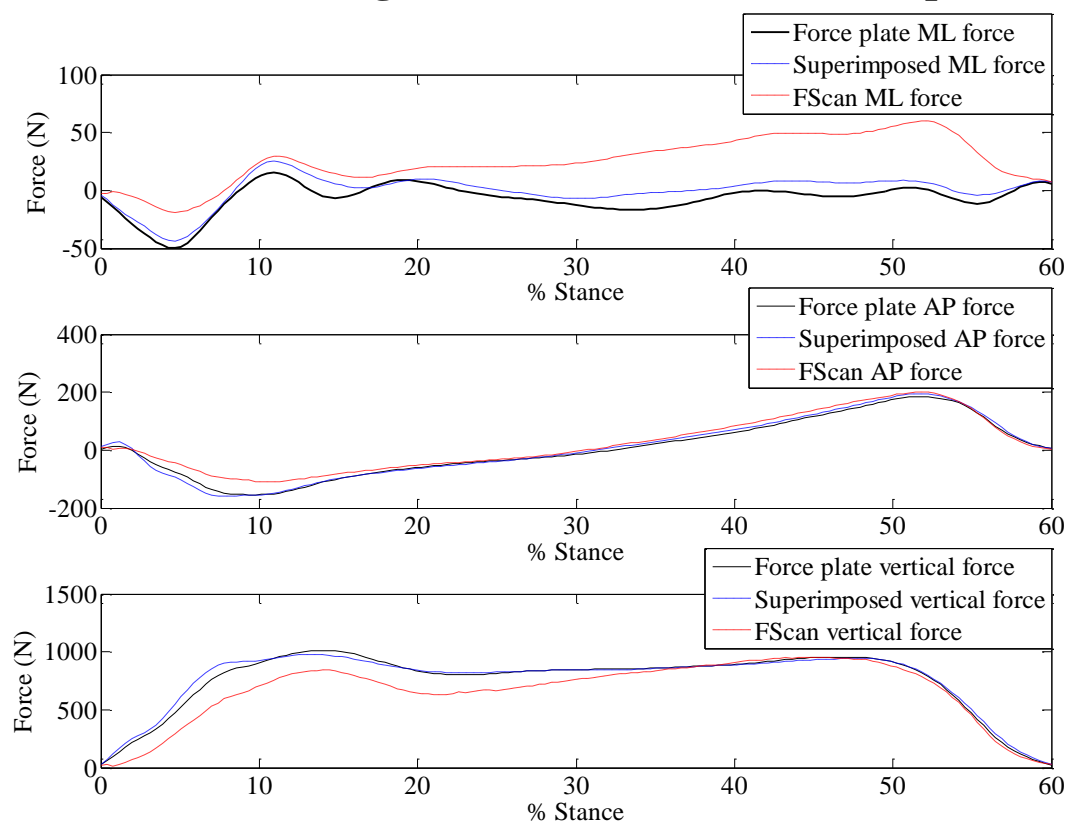


Figure A.5 : Subject 2 trial 1 comparison of GRF estimation for superimposed and FScan methods

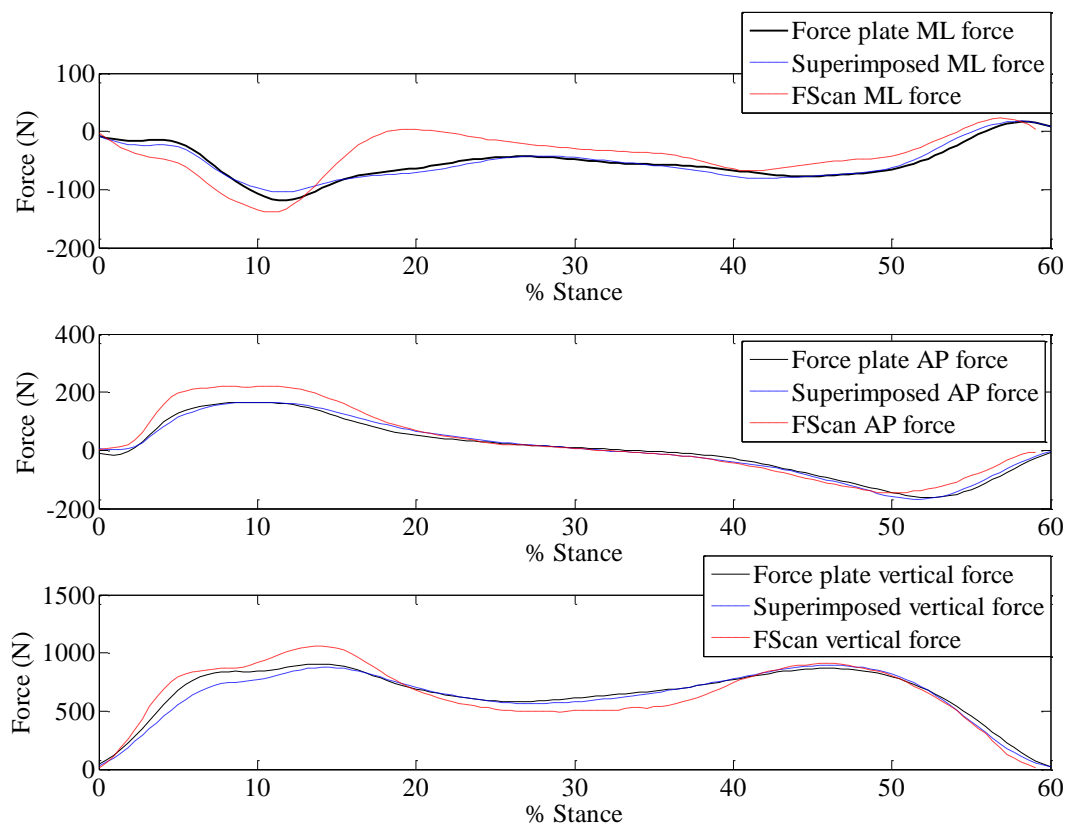


Figure A.6: Subject 1 trial 2 comparison of GRF estimation for superimposed and FScan methods

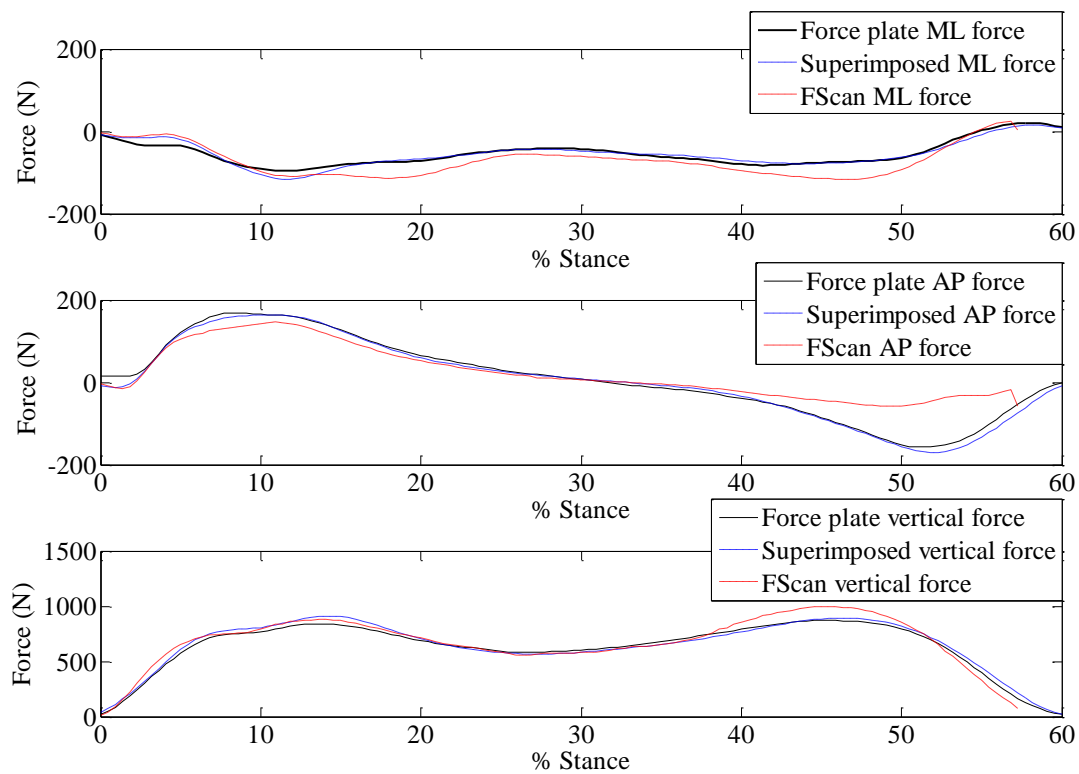


Figure A.7: Subject 1 trial 3 comparison of GRF estimation for superimposed and FScan methods

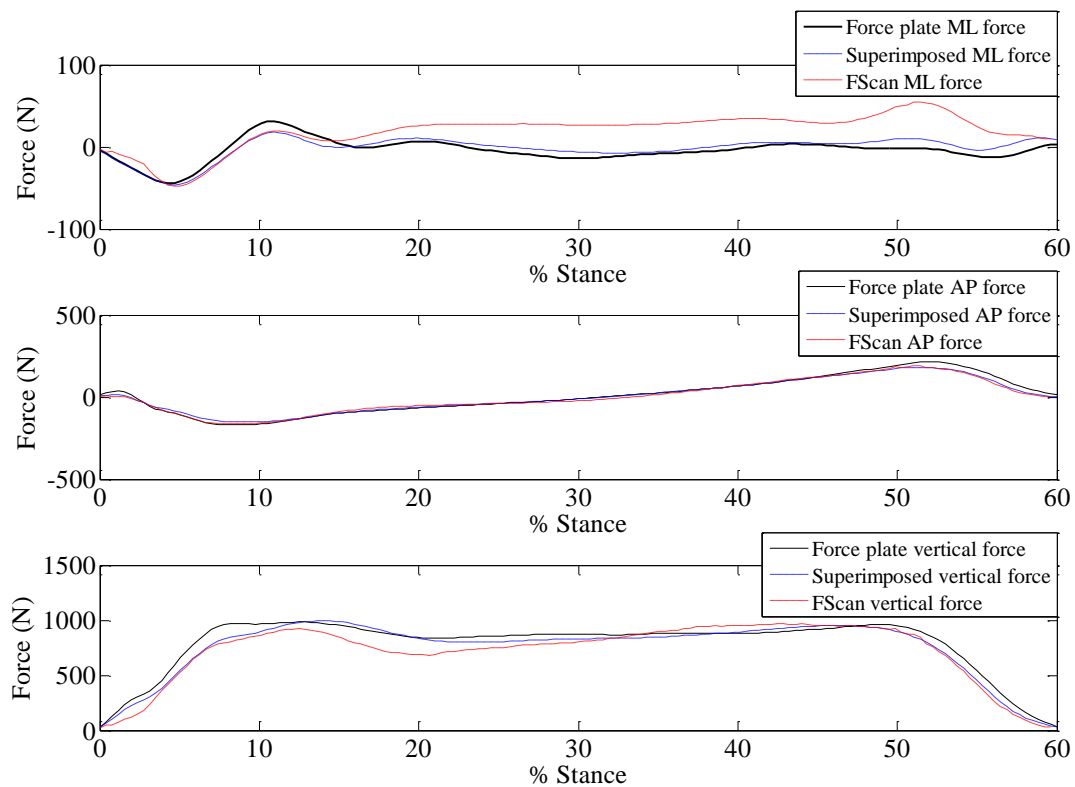


Figure A.8: Subject 2 trial 2 comparison of GRF estimation for superimposed and FScan methods

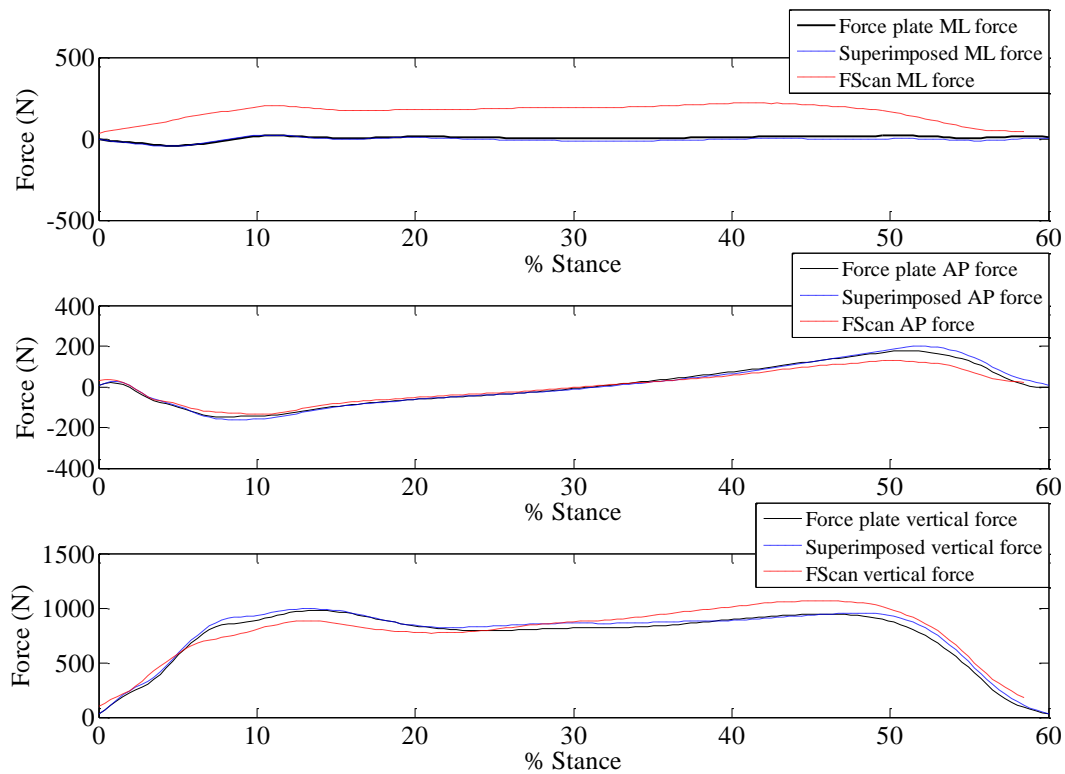


Figure A.9: Subject 2 trial 3 comparison of GRF estimation for superimposed and FScan methods

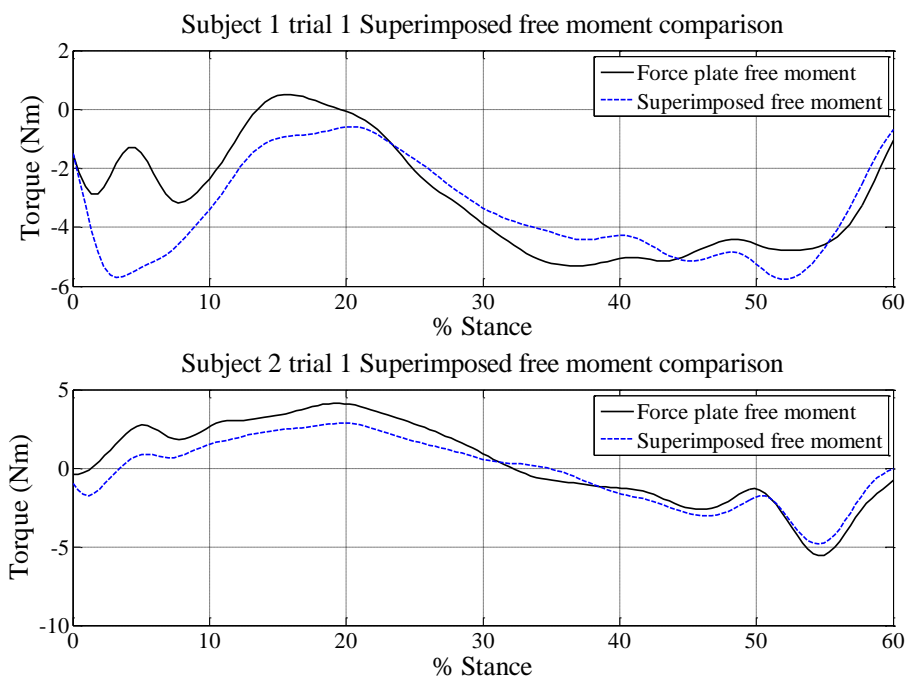


Figure A.10: Comparison of superimposed free moment to actual free moment

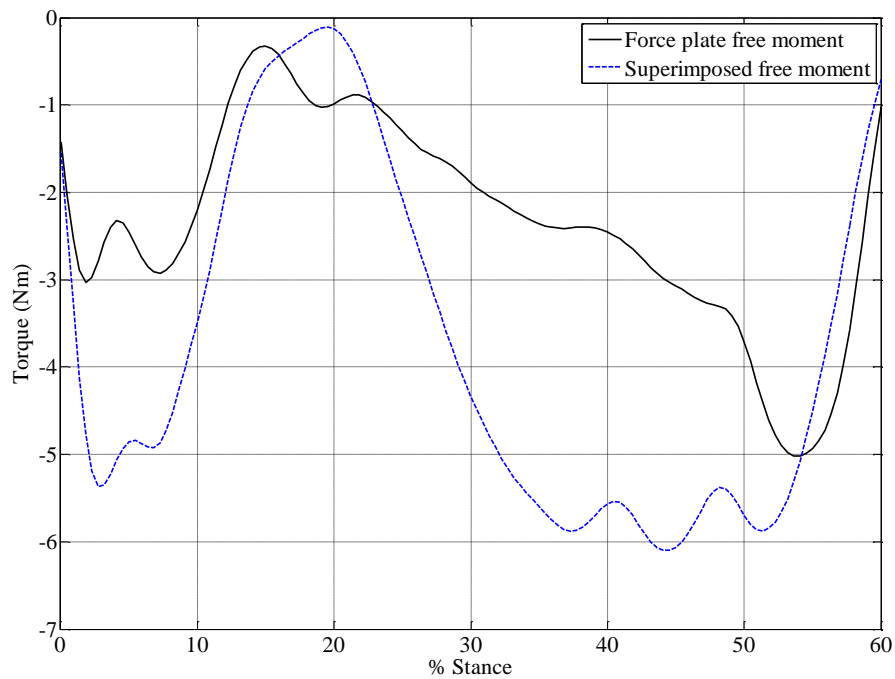


Figure A.11: Subject 1 trial 2 comparison of superimposed free moment to actual free moment

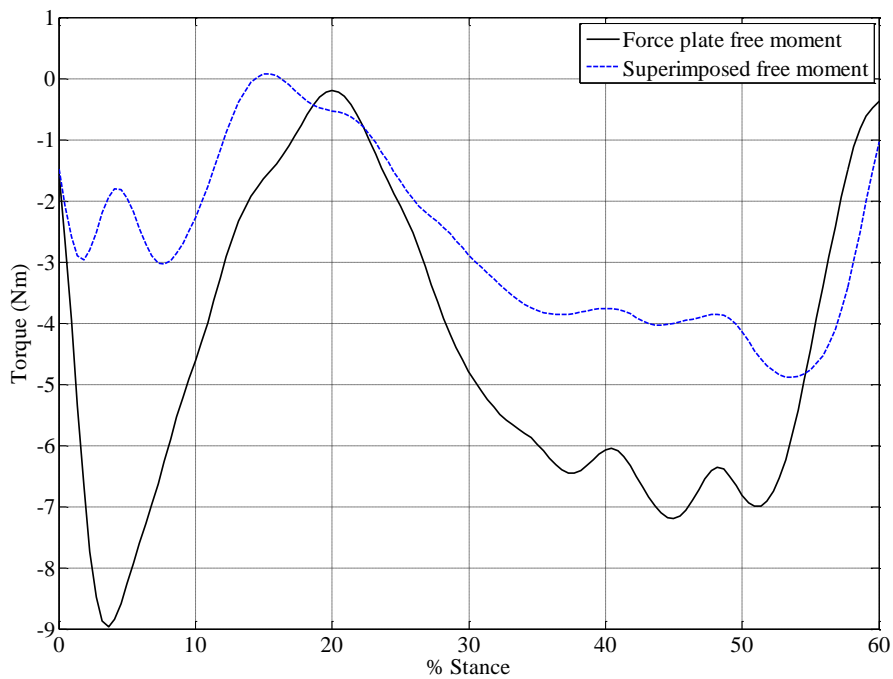


Figure A.12: Subject 1 trial 3 comparison of superimposed free moment to actual free moment

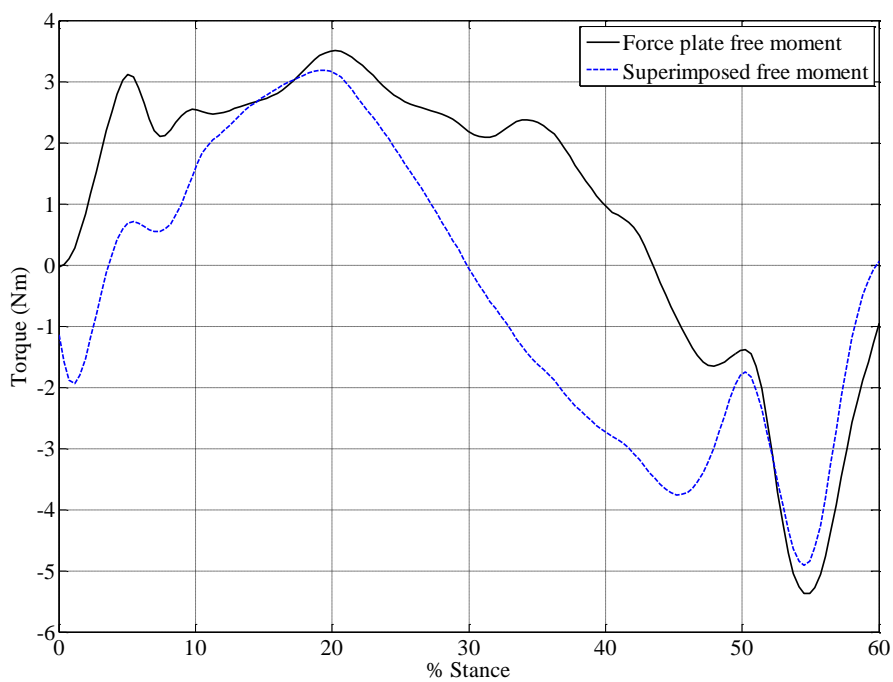


Figure A.13: Subject 2 trial 2 comparison of superimposed free moment to actual free moment

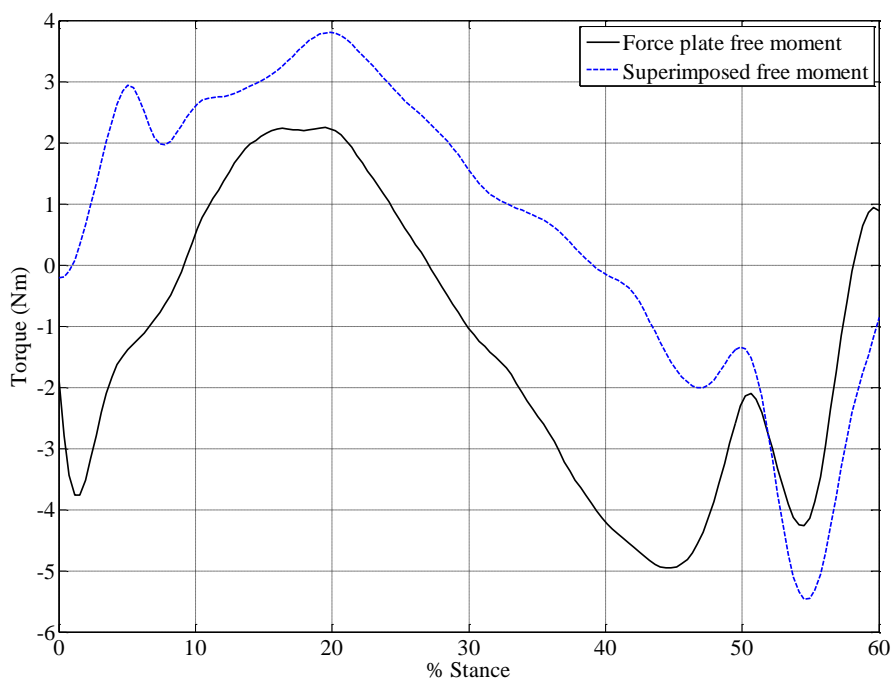


Figure A.14: Subject 2 trial 3 comparison of superimposed free moment to actual free moment

A .3 Knee moment comparison

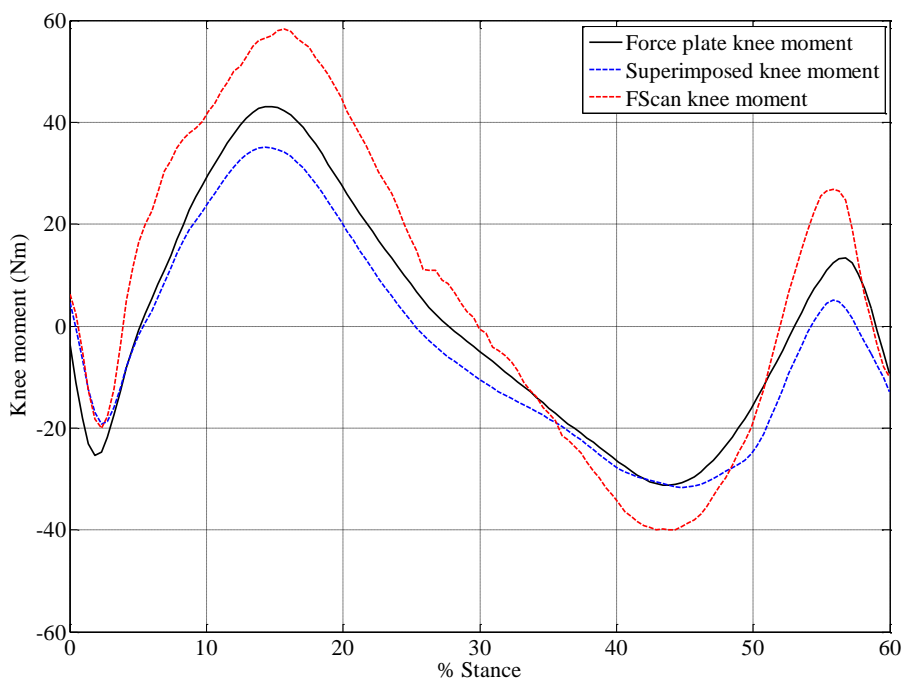


Figure A.15: Subject 1 trial 2 knee moment comparisons for superimposed and FScan methods

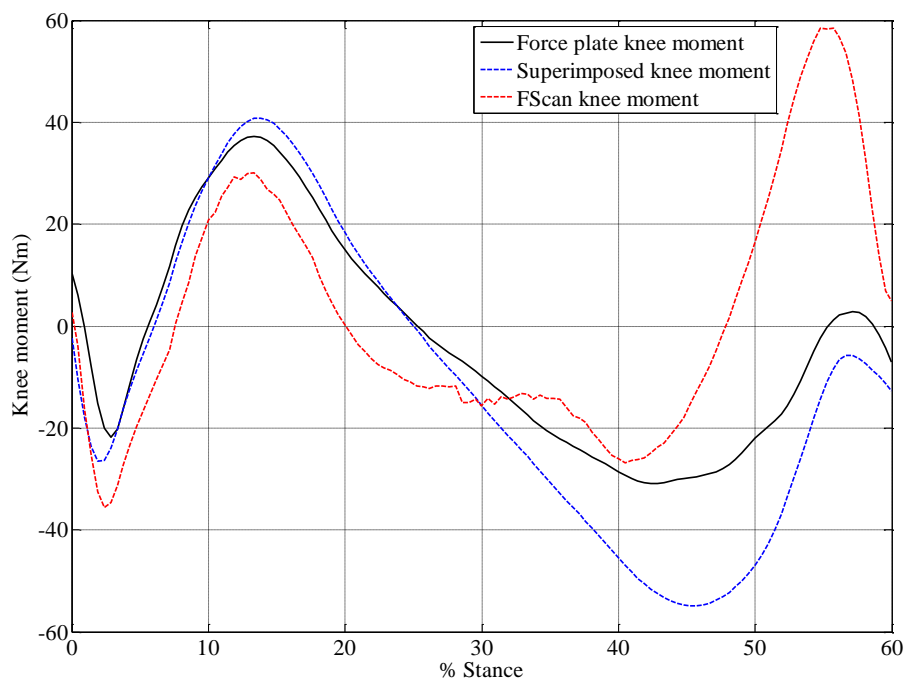


Figure A.16: Subject 1 trial 3 knee moment comparisons for superimposed and FScan methods

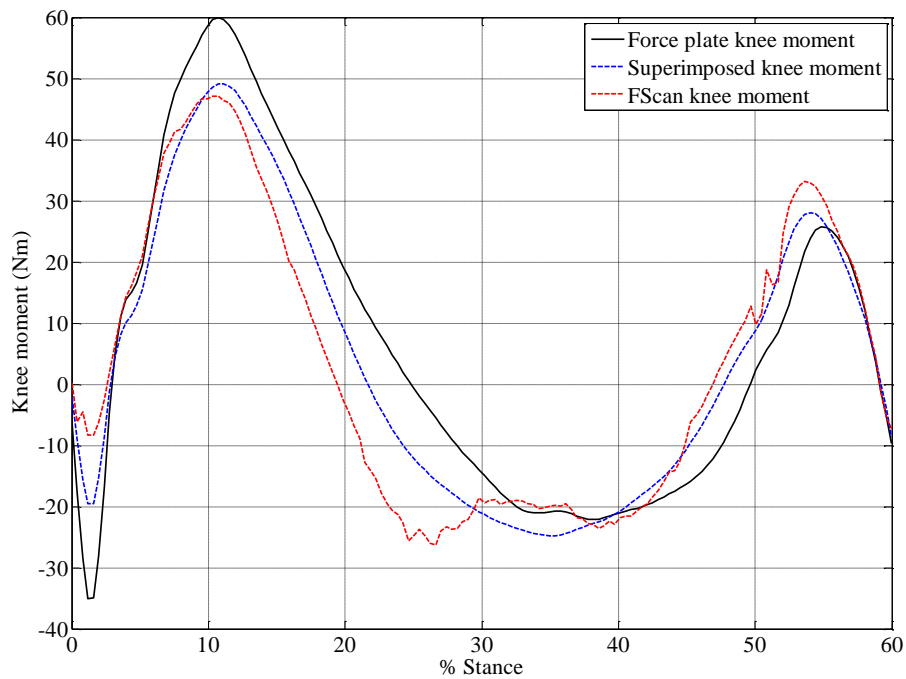


Figure A.17: Subject 2 trial 2 knee moment comparisons for superimposed and FScan methods

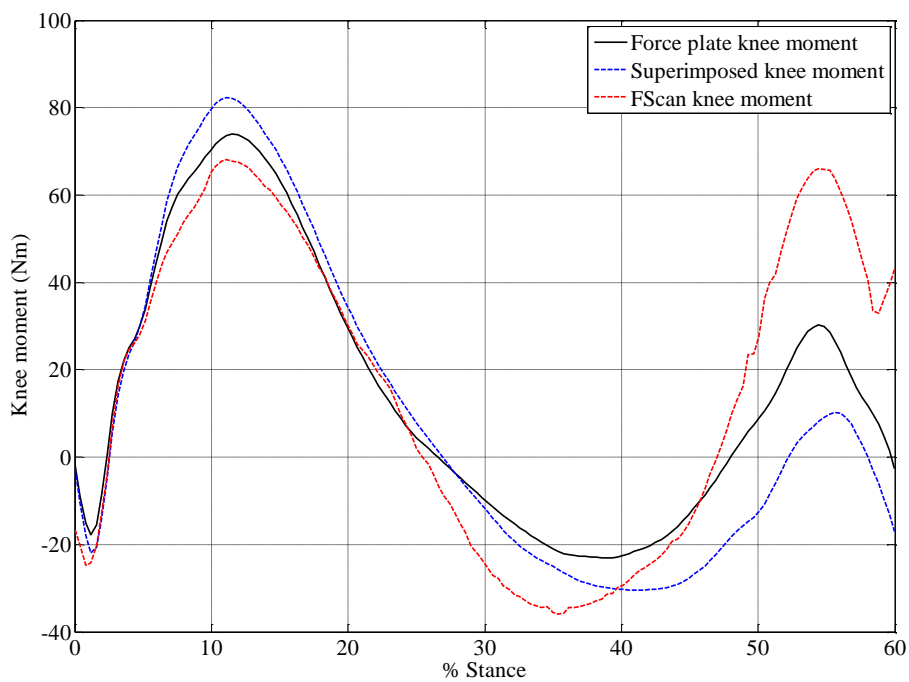


Figure A.18: Subject 2 trial 3 knee moment comparisons for superimposed and FScan methods

Appendix B: OpenSim results

B.1 Comparison of torso and non-torso trials

B.1.1 Joint angle comparison

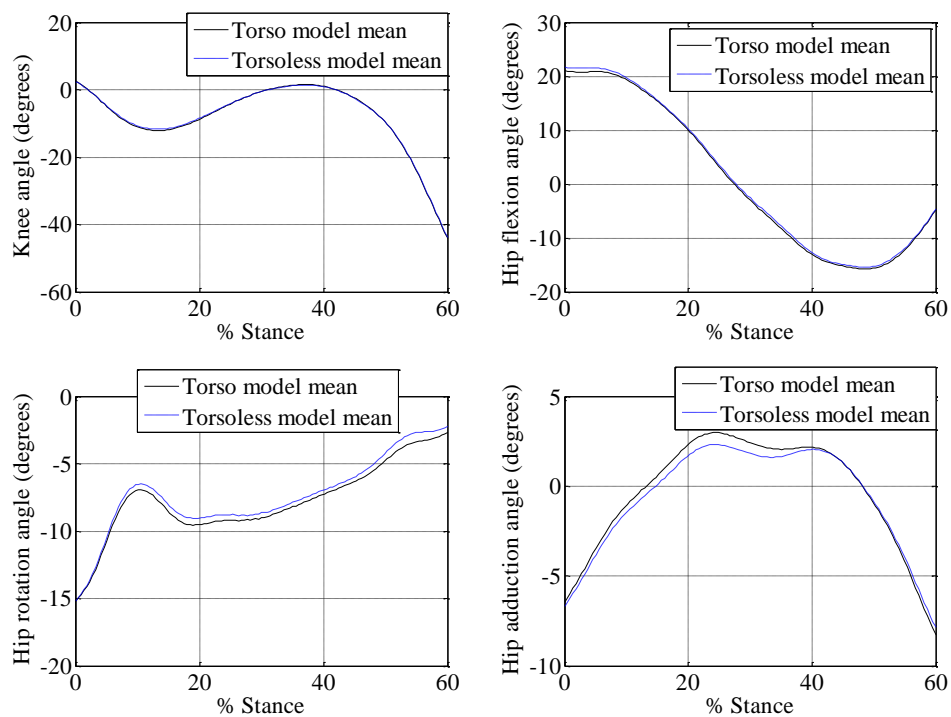


Figure B.1: Mean left knee, hip flexion, hip adduction, and hip rotation angle for a model with and without a torso

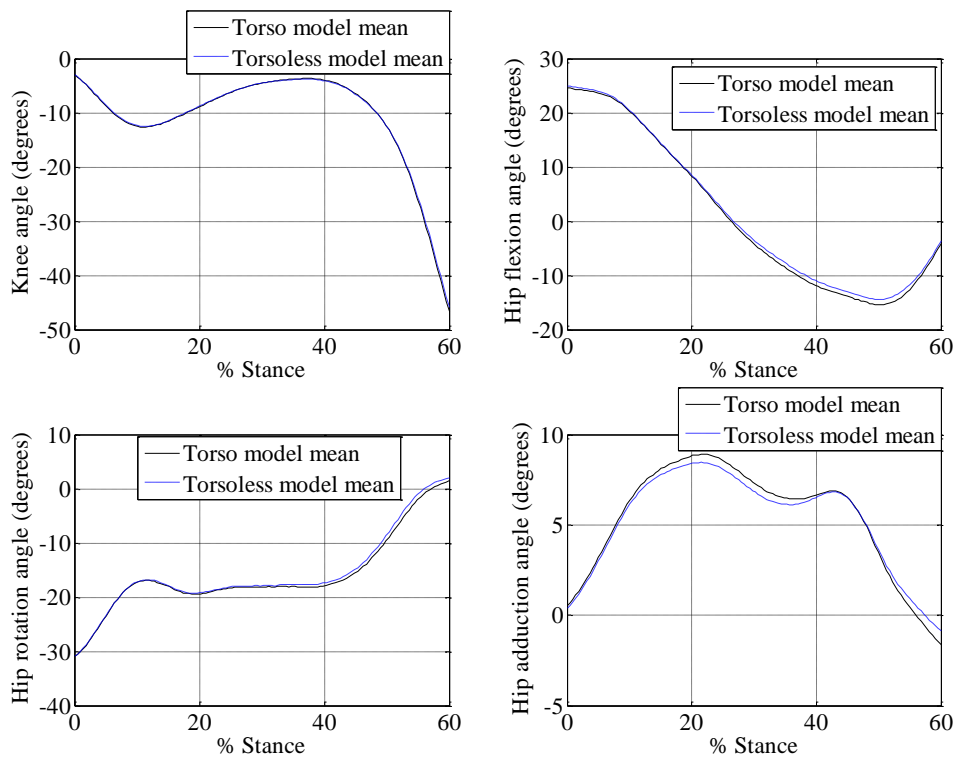


Figure B.2: Mean right knee, hip flexion, hip adduction, and hip rotation angle for a model with and without a torso

B.2 Repeatability analysis

B.2.1 Joint angle comparison

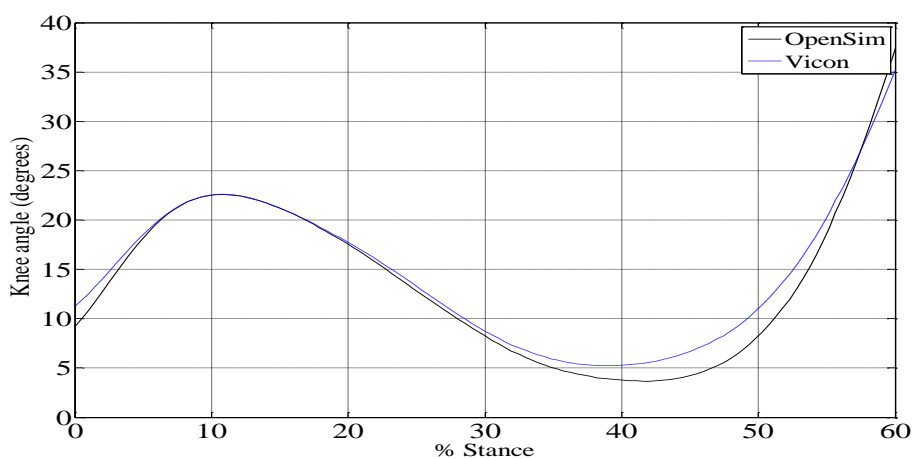


Figure B.3: Subject 2 knee angle comparison during stance phase

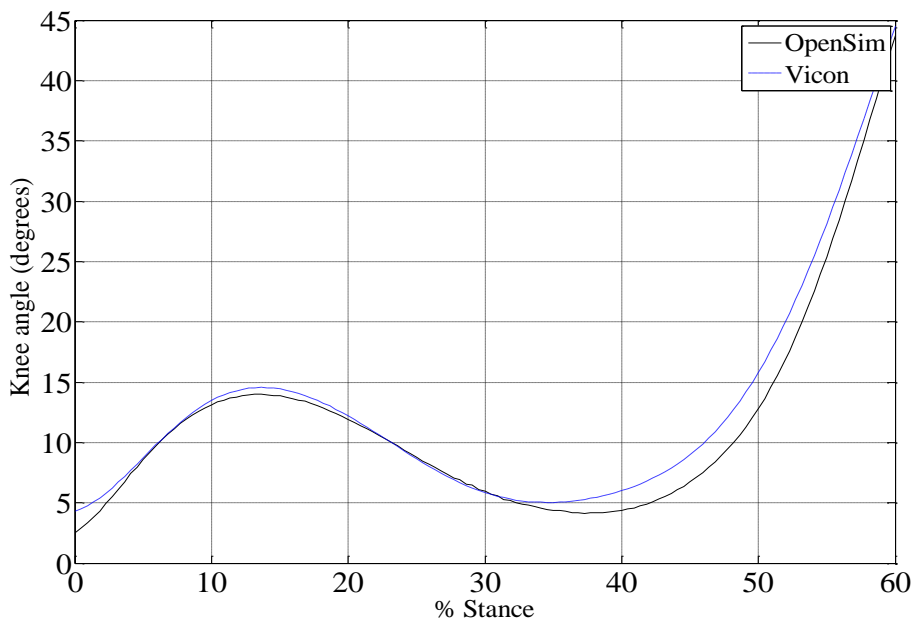


Figure B.4: Subject 3 knee angle comparison during stance phase

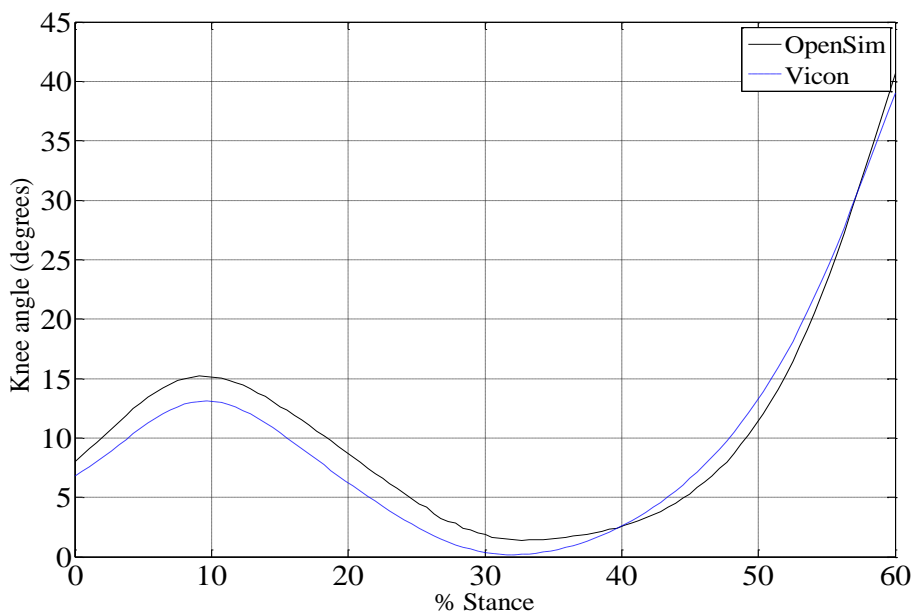


Figure B.5: Subject 4 knee angle comparison during stance phase

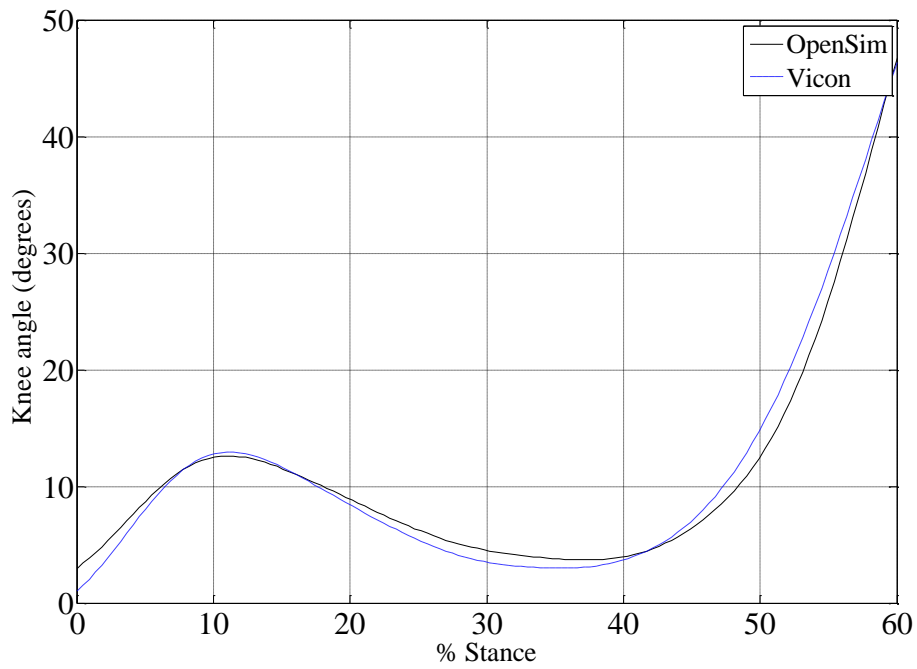


Figure B.6: Subject 5 knee angle comparison during stance phase

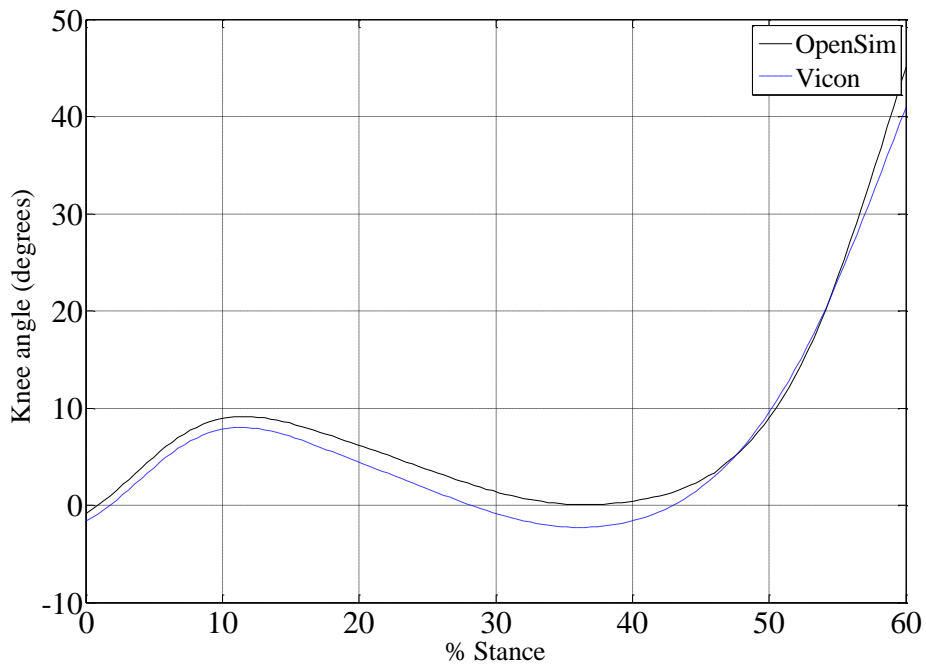


Figure B.7: Subject 6 knee angle comparison during stance phase

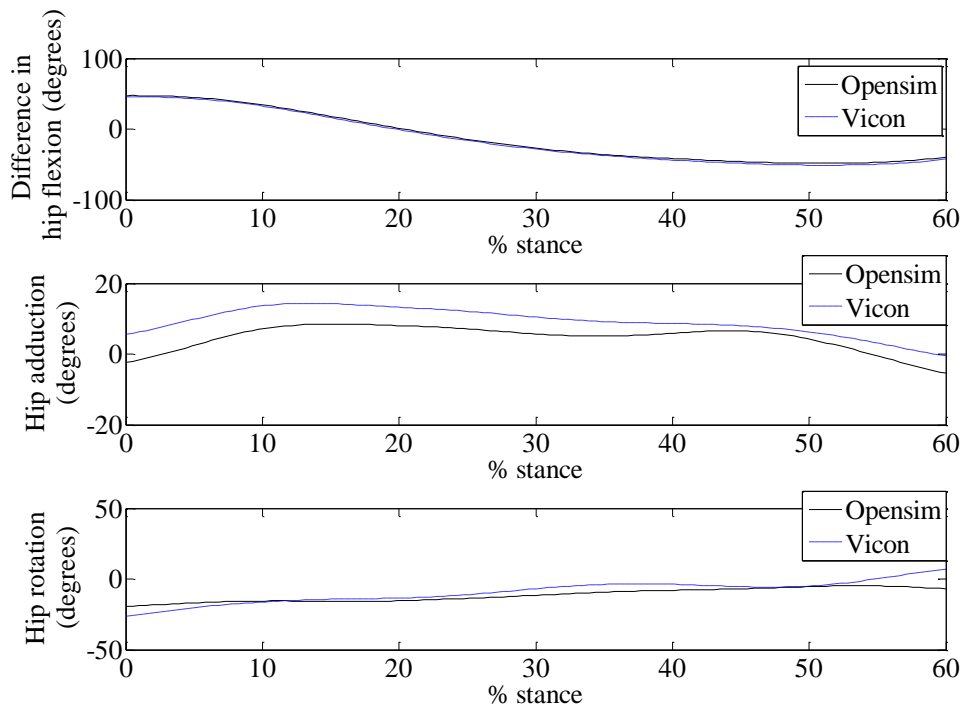


Figure B.8: Subject 2 left hip angles comparison

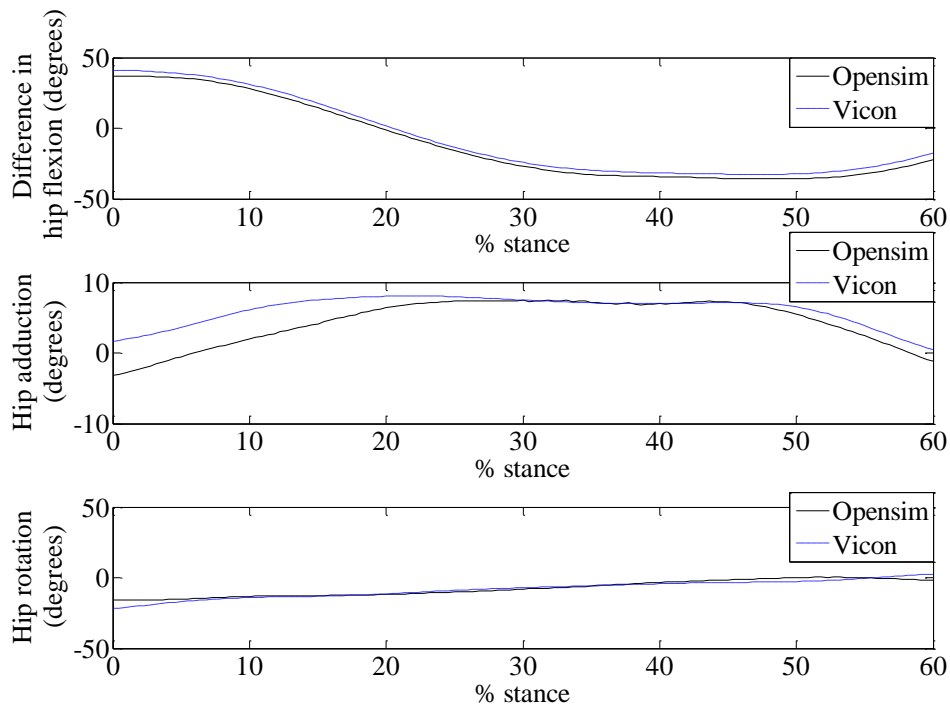


Figure B.9: Subject 3 left hip angles comparison

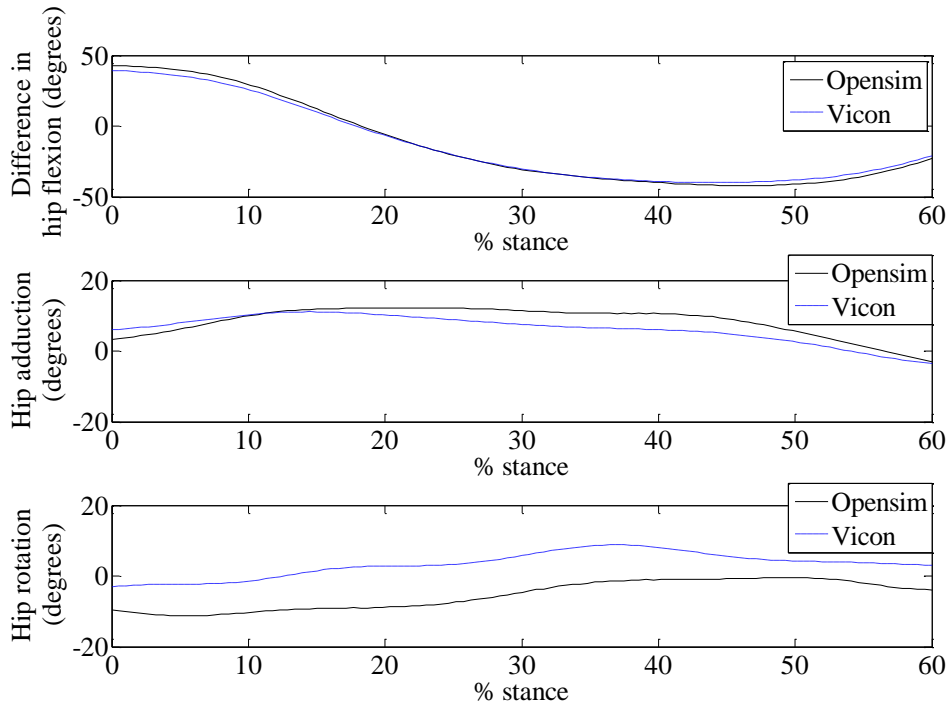


Figure B.10: Subject 4 right hip angles comparison

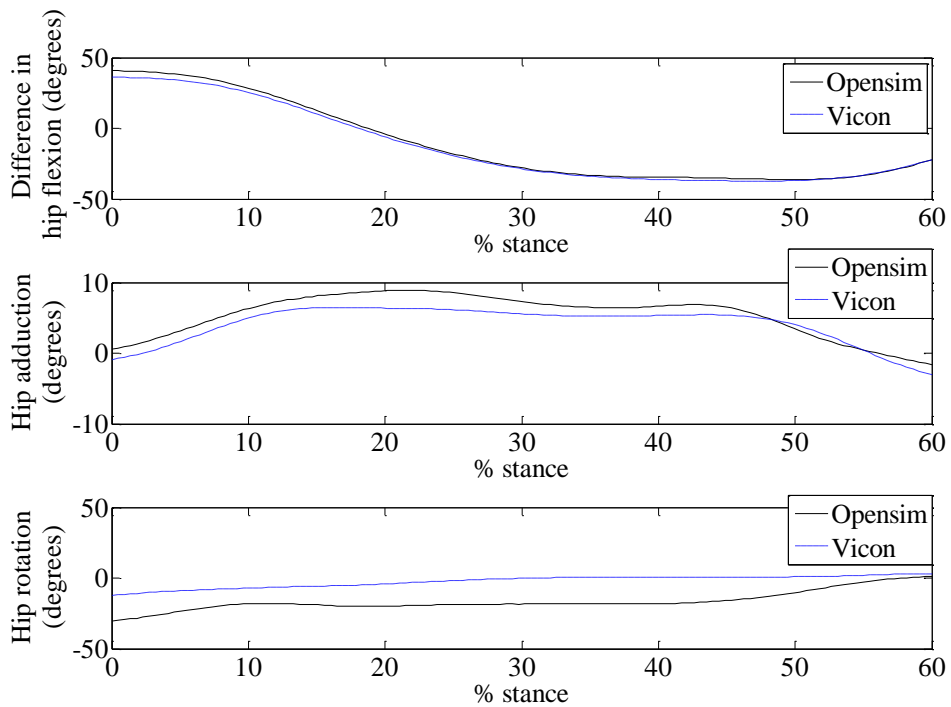


Figure B.11: Subject 5 right hip angles comparison

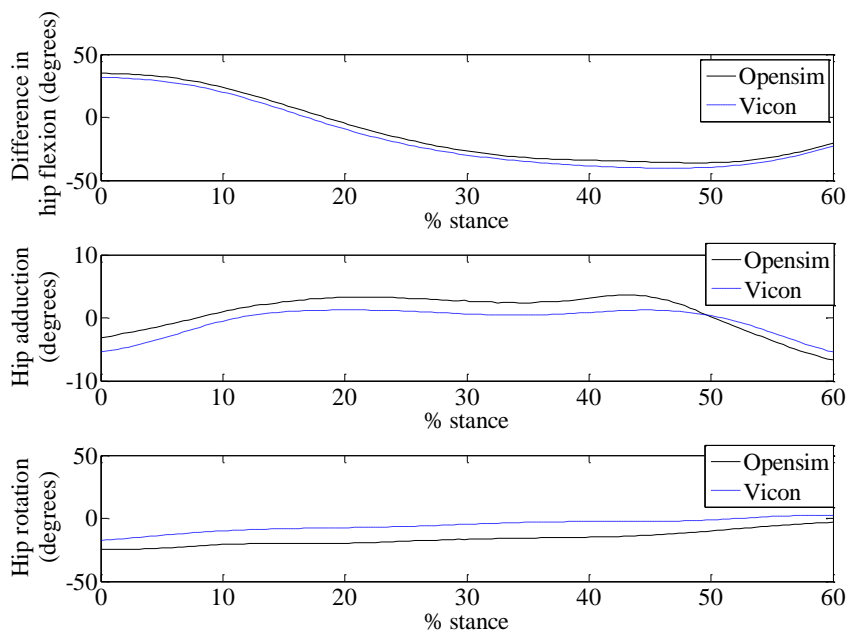


Figure B.12: Subject 6 right hip angles comparison

B.2.2 Knee moment comparison

Table B. 1: Repeatability study ground reaction force comparison

Subject	Session	Foot	Direction	Correlation coefficient, R [R ²]	Standard deviation (N)	RMS error (N)
1	1	Left	ML	0.994 [0.989]	0.20 - 8.11	2.31 - 4.07
			AP	0.997 [0.995]	2.90 - 11.70	5.47 - 8.71
			Vertical	0.998 [0.995]	0.43 - 31.82	8.6 - 13.75
2	2	Left	ML	0.986 [0.972]	1.71 - 13.22	4.64 - 10.29
			AP	0.999 [0.998]	0.62 - 29.89	4.67 - 12.53
			Vertical	0.989 [0.979]	1.08 - 103.14	9.97 - 33.32
3	2	Left	ML	0.955 [0.913]	1.04 - 10.90	3.94 - 4.85
			AP	0.993 [0.985]	1.87 - 25.55	6.66 - 10.41
			Vertical	0.991 [0.983]	2.95 - 70.66	13.69 - 31.27
4	1	Right	ML	0.993 [0.987]	1.11 - 12.30	2.29 - 5.56
			AP	0.988 [0.976]	1.70 - 25.40	8.85 - 15.62
			Vertical	0.995 [0.989]	1.67 - 58.84	15.23 - 22.76
5	1	Right	ML	0.993 [0.986]	1.01 - 10.79	3.83-6.85
			AP	0.998 [0.996]	2.26 - 14.58	4.23- 8.20
			Vertical	0.992 [0.984]	5.95 - 83.80	19.99 - 38.09
6	2	Right	ML	0.985 [0.970]	0.33 - 14.80	2.35 - 6.75
			AP	0.998 [0.997]	0.10 - 11.25	2.71 - 5.46
			Vertical	0.994 [0.988]	1.28 - 74.61	11.15 - 28.69

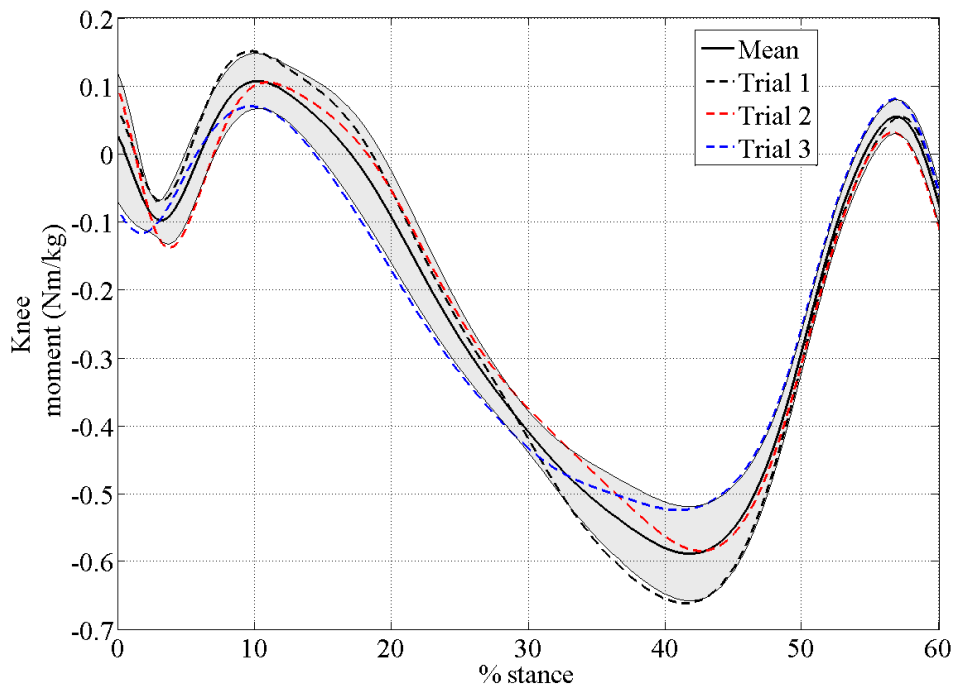


Figure B.13: Subject 1 intra-session knee moment comparison

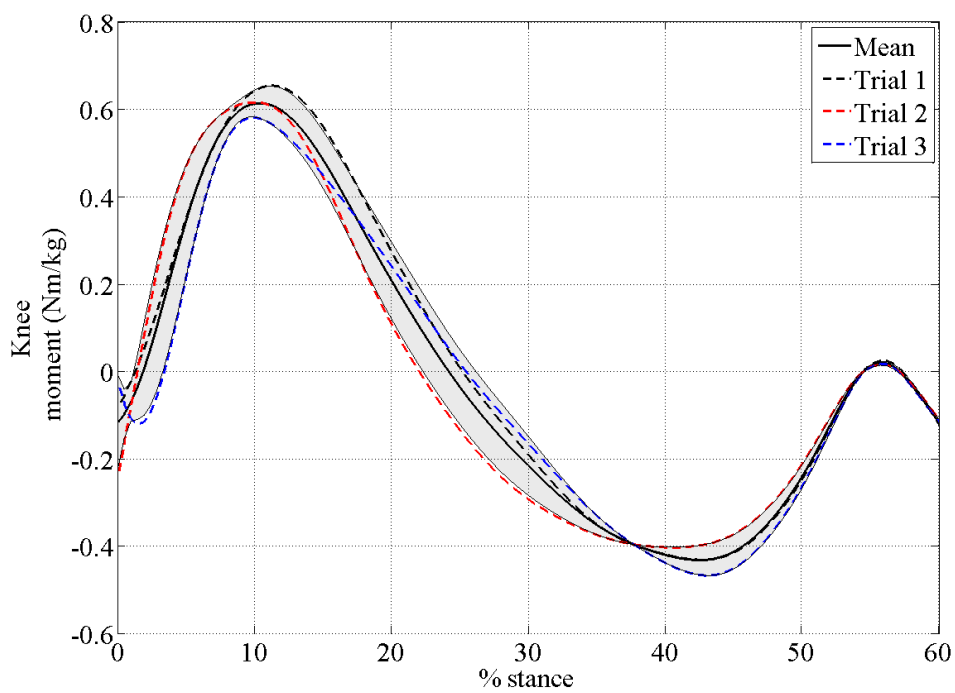


Figure B.14: Subject 2 intra-session knee moment comparison

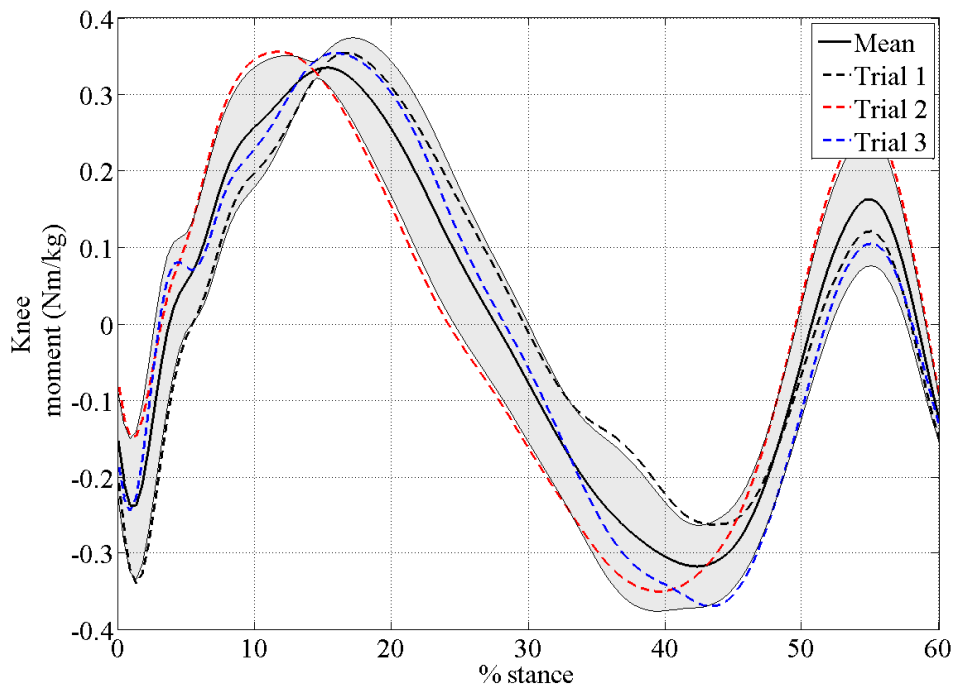


Figure B.15: Subject 3 intra-session knee moment comparison

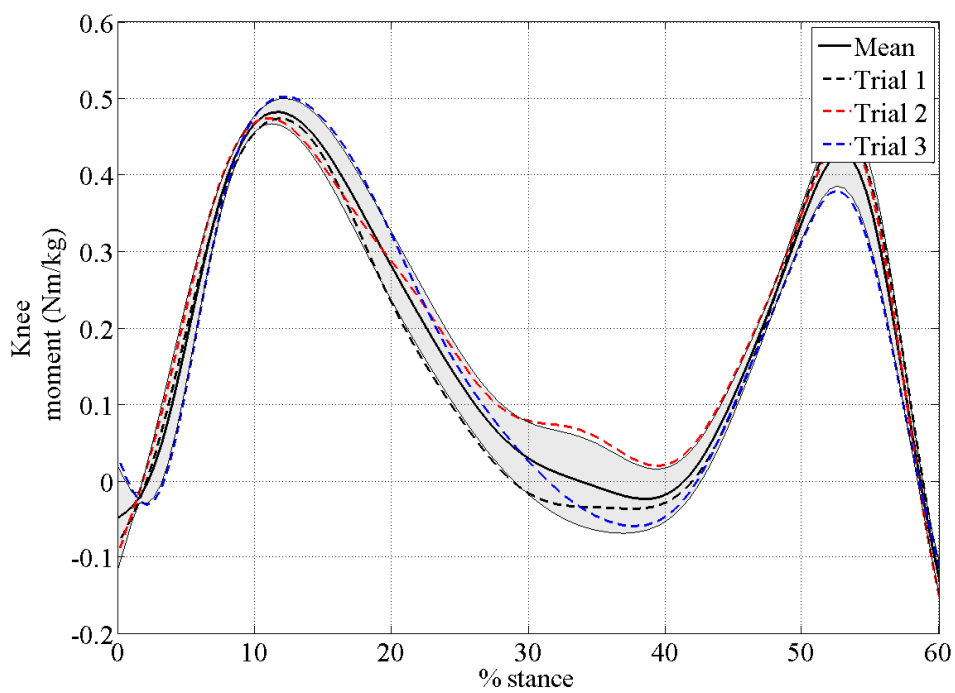


Figure B.16: Subject 4 intra-session knee moment comparison

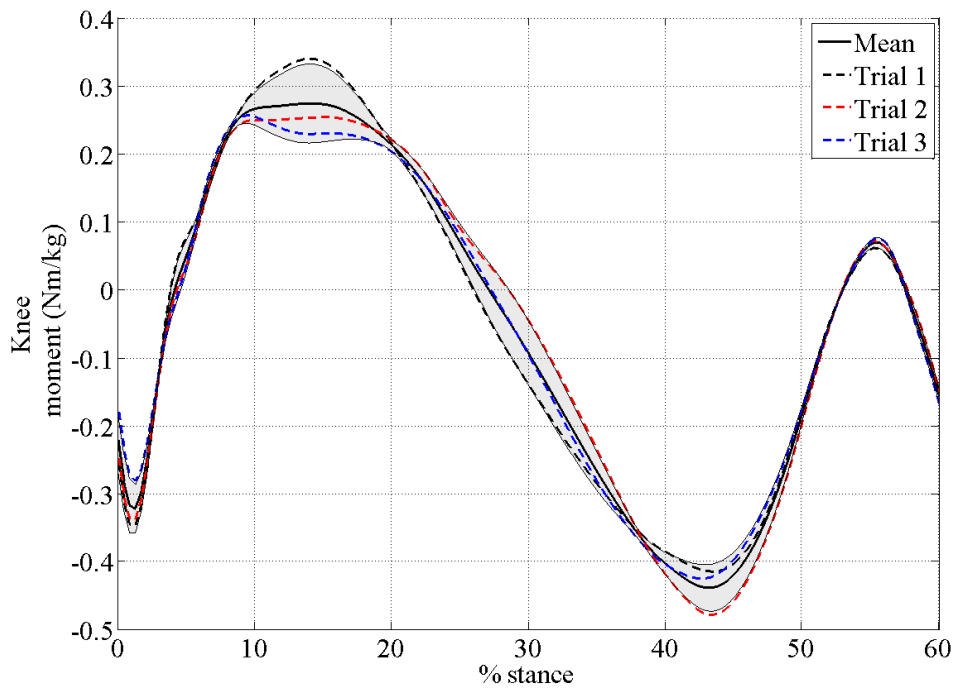


Figure B.17: Subject 6 intra-session knee moment comparison

B.2.3 RRA results

Table B.2: Session one RRA results for the left and right leg trials

Thresholds	Left foot			Right foot		
	Trial 1	Trial 2	Trial 3	Trial 1	Trial 2	Trial 3
Max residual force (N)	10.27	18.74	-12.20	-49.08	-19.85	-74.88
RMS residual force (N)	4.97	7.93	8.24	32.69	15.05	44.55
Max residual moment (Nm)	33.69	-39.43	-44.26	-59.00	-28.08	72.58
RMS residual moment (Nm)	19.05	22.27	20.52	40.28	16.69	59.19
Max positional error (cm)	-2.86	5.87	-4.60	3.24	-4.56	8.11
RMS positional error (cm)	1.51	3.16	3.46	1.70	3.29	3.13
Max positional error (rotation, <i>degrees</i>)	-2.16	-1.83	-1.06	0.98	-2.16	-1.53
RMS positional error (rotation, <i>degrees</i>)	1.26	1.11	0.71	0.77	1.20	1.14

Table B.3: Session two RRA results for the left and right leg trials

Thresholds	Left foot			Right foot		
	Trial 1	Trial 2	Trial 3	Trial 1	Trial 2	Trial 3
Max residual force (N)	-13.54	-22.63	-20.76	-14.20	-20.96	-18.79
RMS residual force (N)	6.26	16.73	13.70	6.66	8.18	8.40
Max residual moment (Nm)	-29.18	-34.85	-38.75	26.11	25.79	25.71
RMS residual moment (Nm)	12.81	13.55	18.44	15.44	15.04	14.79
Max positional error (cm)	-3.44	-4.40	-4.91	-3.35	-4.67	-5.83
RMS positional error (cm)	1.98	3.31	3.68	2.39	3.47	4.37
Max positional error (rotation, <i>degrees</i>)	0.41	-0.28	0.58	0.82	0.88	0.89
RMS positional error (rotation, <i>degrees</i>)	0.21	0.14	0.35	0.51	0.56	0.57

Table B.4: Session 2 left and right foot maximum knee moment and GRF data

Measure	Left			Right		
	Trial 1	Trial 2	Trial 3	Trial 1	Trial 2	Trial 3
Max knee moment (Nm)	25.5797	25.657	25.6938	35.8685	28.7387	26.1255
Max mediolateral force (N)	38.11	34.61	31.00	52.55	48.77	53.90
Max anteroposterior force (N)	127.24	111.19	136.23	132.75	126.11	122.21
Max vertical force (N)	813.23	755.34	776.47	797.15	800.02	779.43

B.2.4 CMC results comparison

Table B. 5: Session 1 CMC results

Thresholds	Left	Right
------------	------	-------

	Trial 1	Trial 2	Trial 3	Trial 1	Trial 2	Trial 3
Max Residual Force (<i>N</i>)	10.40	19.00	-11.84	-48.69	-20.07	-74.21
RMS Residual Force (<i>N</i>)	4.76	9.29	7.75	31.53	15.09	43.11
Max Residual torque (<i>Nm</i>)	34.64	37.47	-40.94	-55.27	27.91	73.12
RMS Residual torque (<i>Nm</i>)	20.03	22.63	18.97	40.30	15.91	60.34
Max positional error (translation, <i>cm</i>)	-0.022	0.020	0.034	-0.028	0.015	0.021
RMS positional error (translation, <i>cm</i>)	0.010	0.013	0.021	0.010	0.007	0.009
Max positional error (rotation, <i>degrees</i>)	-0.92	-1.03	2.24	-3.99	0.87	-3.56
RMS positional error (rotation, <i>degrees</i>)	0.50	0.52	1.55	1.57	0.37	1.41
Max reserve torque (<i>Nm</i>)	-11.78	-14.35	-13.21	16.75	-17.71	12.89
RMS reserve torque (<i>Nm</i>)	2.37	2.57	3.79	4.97	3.72	3.89

Table B.6: Session 2 CMC results

Thresholds	Left			Right		
	Trial 1	Trial 1	Trial 2	Trial 3	Trial 2	Trial 3
Max Residual Force (<i>N</i>)	-14.13	-22.58	-20.65	-14.01	-20.96	-19.15
RMS Residual Force (<i>N</i>)	6.13	17.59	13.59	6.44	7.88	8.40
Max Residual torque (<i>Nm</i>)	-26.19	-34.80	-35.51	26.09	25.83	25.64
RMS Residual torque (<i>Nm</i>)	11.63	13.53	17.87	14.88	15.01	14.50
Max positional error (translation, <i>cm</i>)	0.016	-0.014	0.015	0.040	-0.030	-0.025
RMS positional error (translation, <i>cm</i>)	0.008	0.008	0.010	0.016	0.011	0.008
Max positional error (rotation, <i>degrees</i>)	-0.54	-0.53	-0.78	1.07	-1.85	-1.82
RMS positional error (rotation, <i>degrees</i>)	0.33	0.29	0.40	0.41	1.01	1.02
Max reserve torque (<i>Nm</i>)	-21.85	-17.37	-19.15	11.32	-20.85	-22.69
RMS reserve torque (<i>Nm</i>)	3.52	2.72	3.46	2.45	2.60	2.88

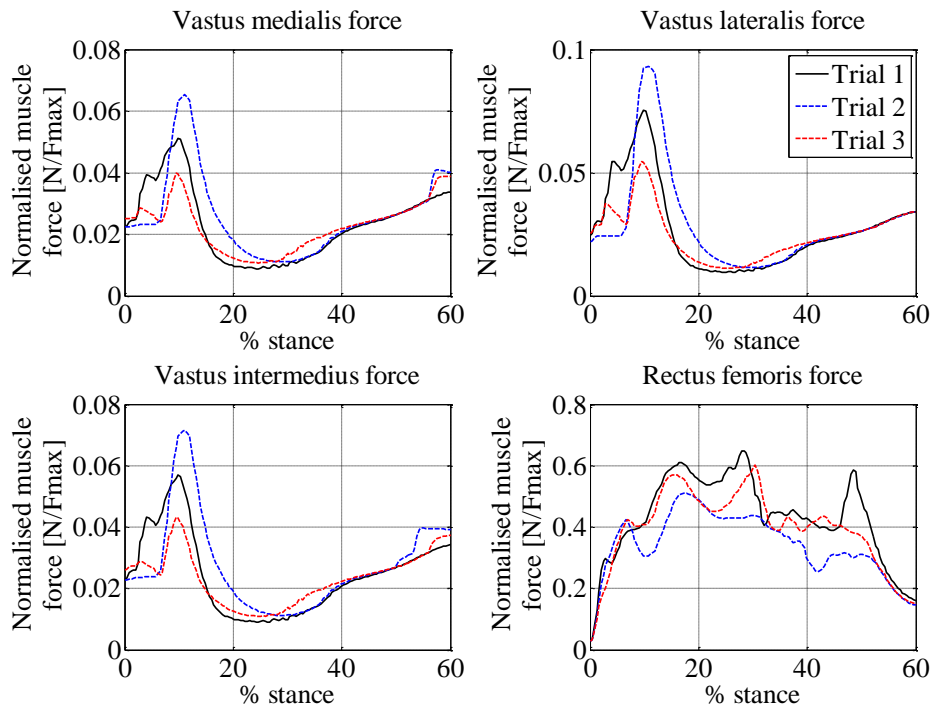


Figure B. 18: Right leg session 2 normalised extensor muscle forces

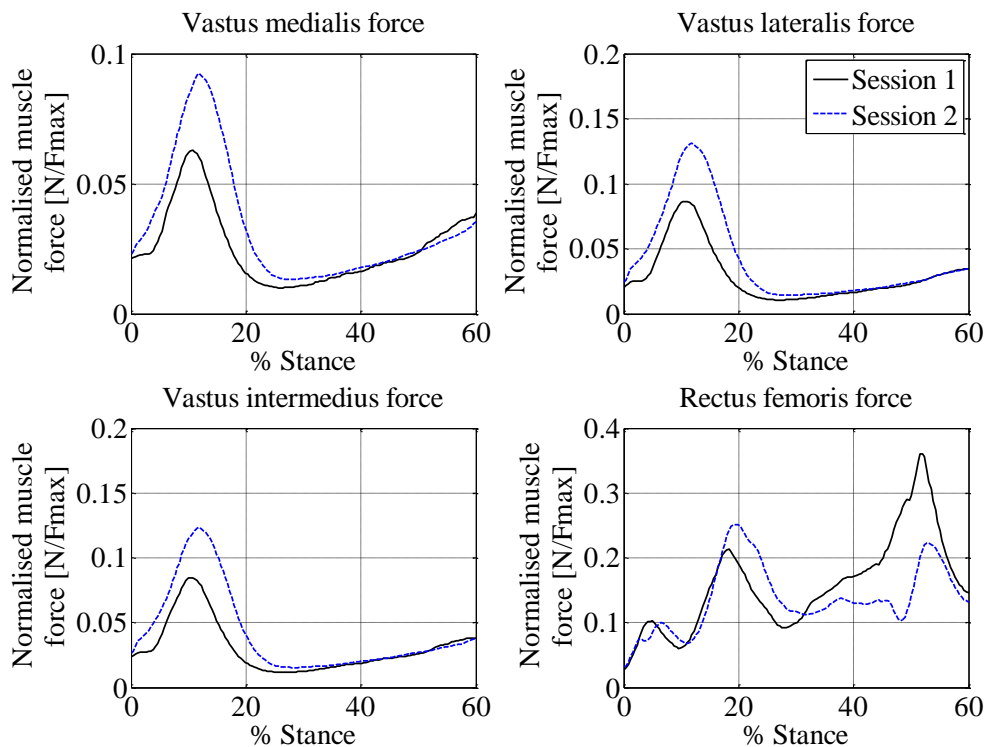


Figure B.19: Normalised left leg extensor muscle forces

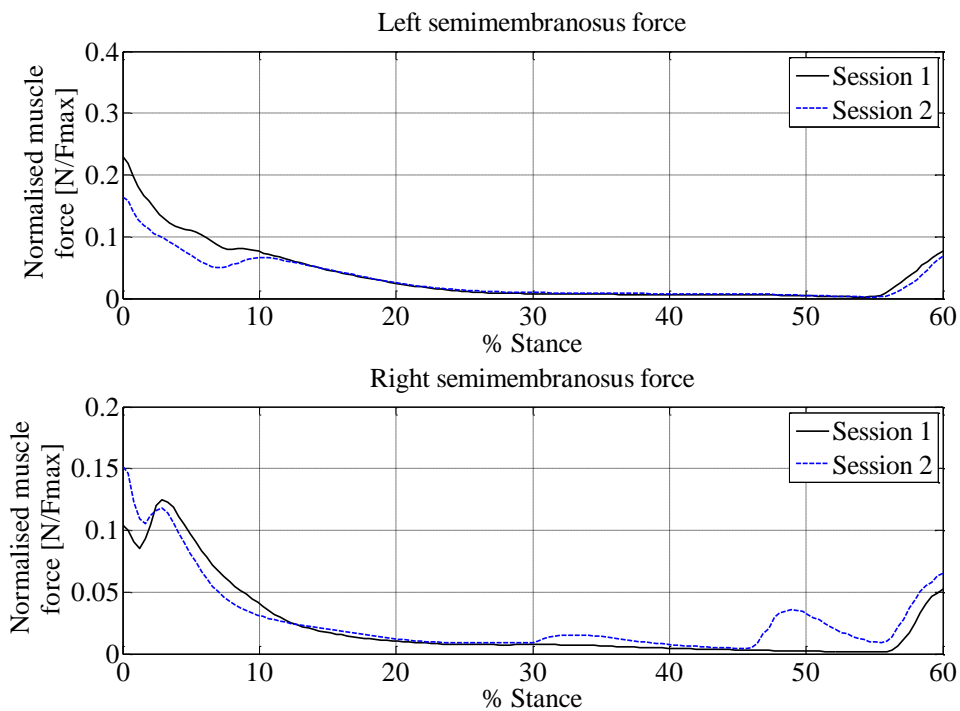


Figure B.20: Normalised semimembranosus force for the left and right leg

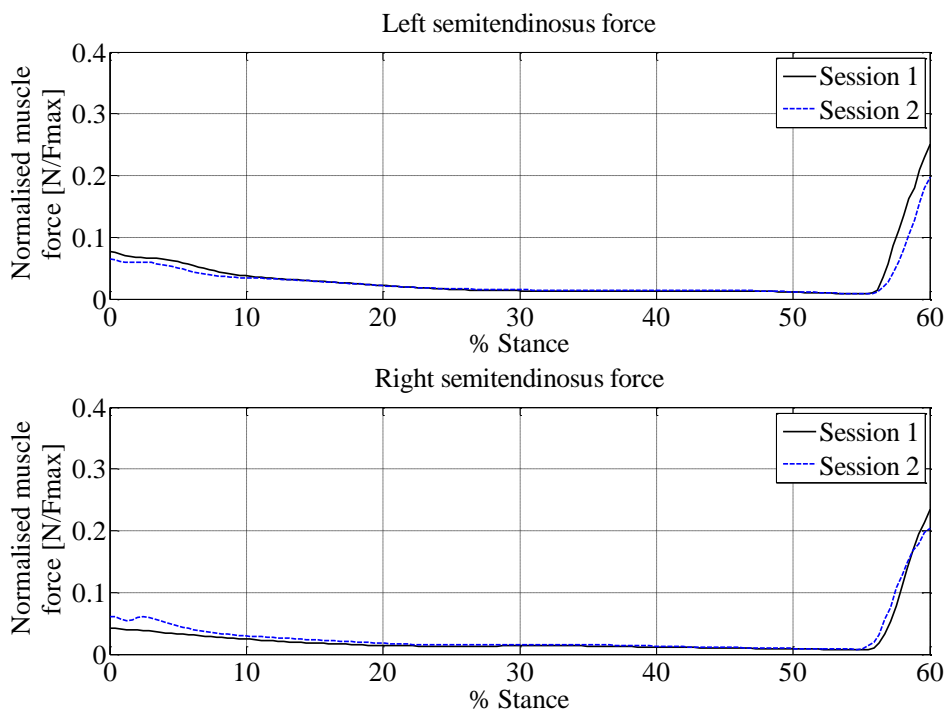


Figure B.21: Normalised semitendinosus force for the left and right leg

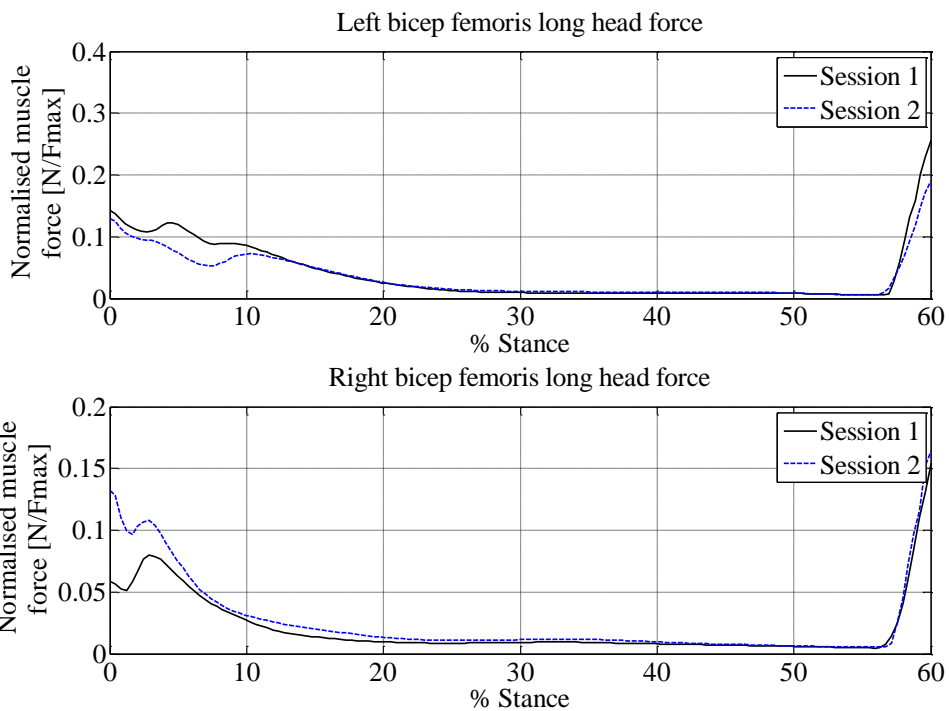


Figure B.22: Normalised bicep femoris long head force comparison for the left and right leg

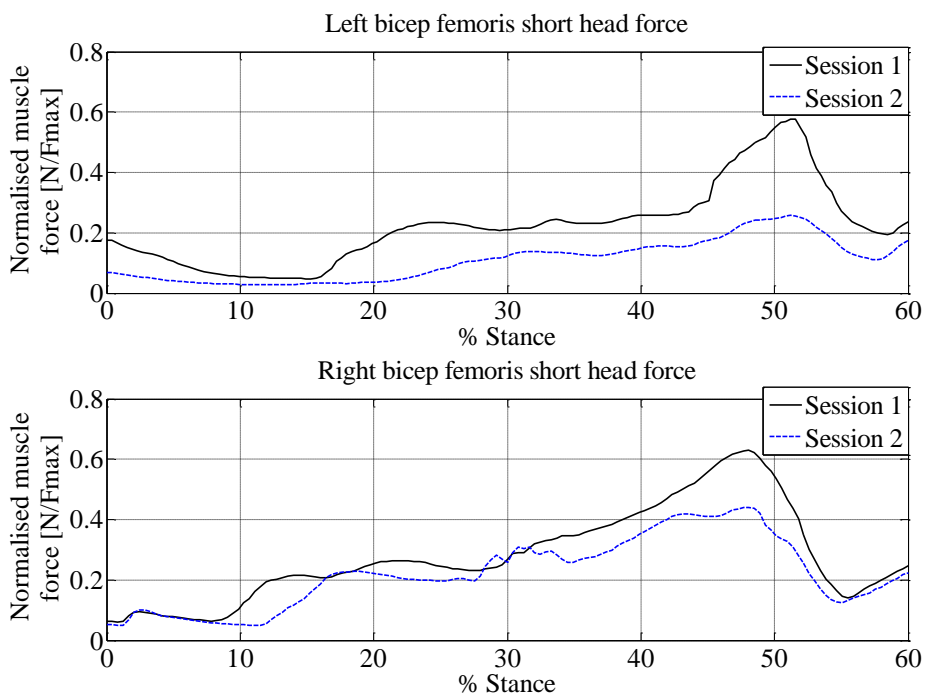


Figure B.23: Normalised bicep femoris short head force comparison for the left and right leg

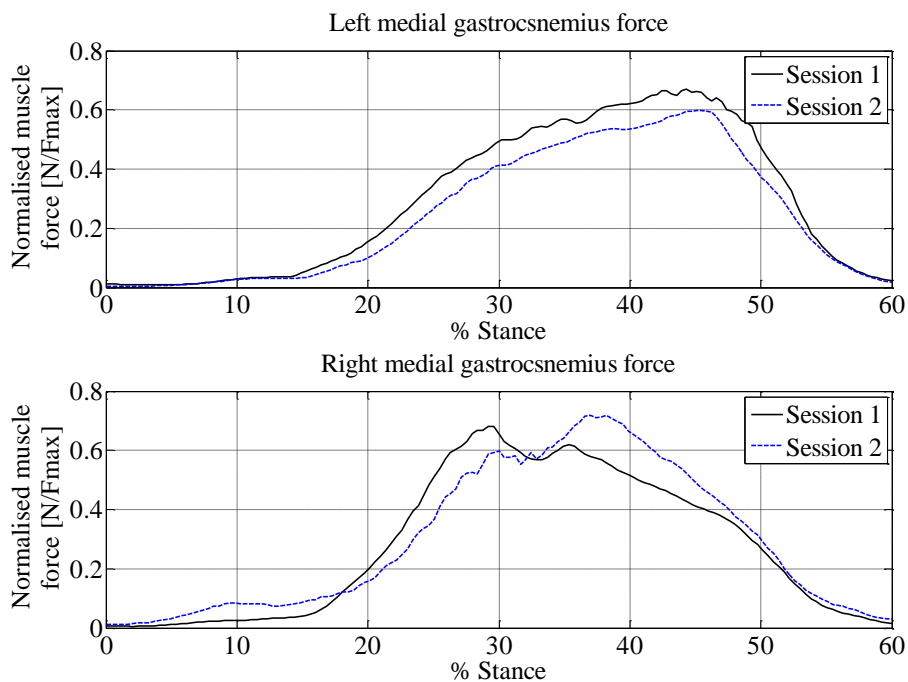


Figure B.24: Normalised medial gastrocnemius force comparison for the left and right leg

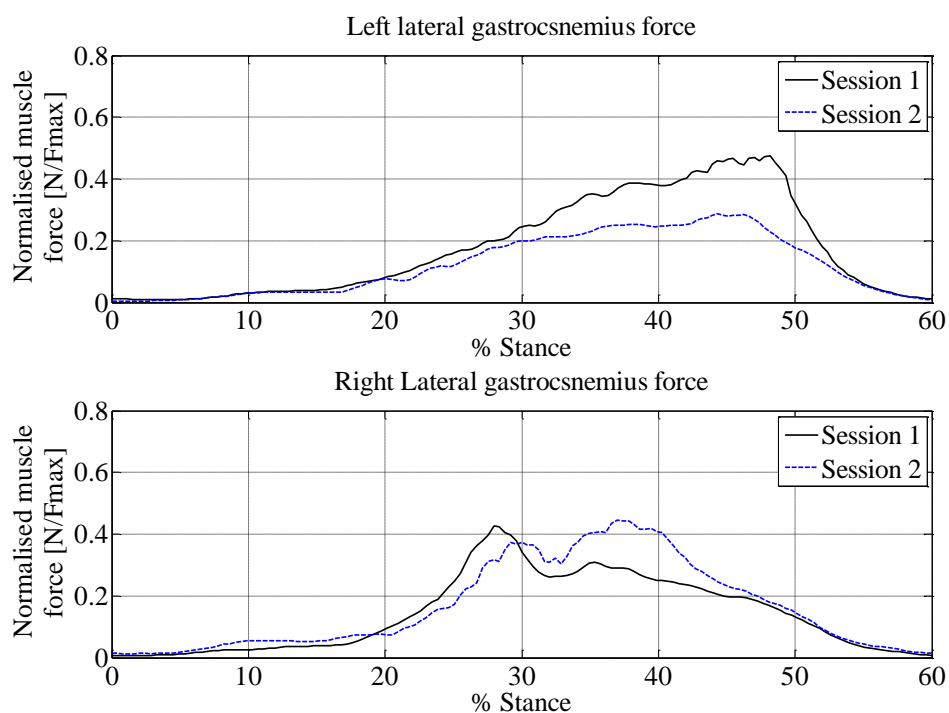


Figure B.25: Normalised lateral gastrocnemius force comparison for the left and right leg

Appendix C: Adams results

C.1. Patellofemoral contact force comparison

Table C.1: Intra-session knee flexion angle comparison

Trial	Session	Correlation coefficient, R [R ²]	RMS error (degrees)	%Max error
1	1	0.995 [0.990]	1.07	3.65
2		0.998 [0.996]	1.27	6.03
3		0.999 [0.998]	0.71	3.66
1	2	0.999 [0.998]	0.86	3.84
2		0.999 [0.998]	0.53	2.26
3		0.998 [0.996]	1.2	4.77

